
Geosynthetic Reinforced Soil for Low-Volume Bridge Abutments

JANUARY 2012

Final Report

CENTER FOR
CEER
EARTHWORKS ENGINEERING
RESEARCH



IOWA STATE UNIVERSITY
Institute for Transportation

Sponsored by
Iowa Highway Research Board
(IHRB Project TR-621)
Iowa Department of Transportation
(InTrans Project 10-380)

About the Center for Earthworks Engineering Research

The mission of the Center for Earthworks Engineering Research (CEER) at Iowa State University is to be the nation's premier institution for developing fundamental knowledge of earth mechanics, and creating innovative technologies, sensors, and systems to enable rapid, high quality, environmentally friendly, and economical construction of roadways, aviation runways, railroad embankments, dams, structural foundations, fortifications constructed from earth materials, and related geotechnical applications.

About the Bridge Engineering Center

The mission of the Bridge Engineering Center (BEC) is to conduct research on bridge technologies to help bridge designers/owners design, build, and maintain long-lasting bridges.

Disclaimer Notice

The contents of this report reflect the views of the authors, who are responsible for the facts and the accuracy of the information presented herein. The opinions, findings and conclusions expressed in this publication are those of the authors and not necessarily those of the sponsors.

The sponsors assume no liability for the contents or use of the information contained in this document. This report does not constitute a standard, specification, or regulation.

The sponsors do not endorse products or manufacturers. Trademarks or manufacturers' names appear in this report only because they are considered essential to the objective of the document.

Non-Discrimination Statement

Iowa State University does not discriminate on the basis of race, color, age, religion, national origin, sexual orientation, gender identity, genetic information, sex, marital status, disability, or status as a U.S. veteran. Inquiries can be directed to the Director of Equal Opportunity and Compliance, 3280 Beardshear Hall, (515) 294-7612.

Iowa Department of Transportation Statements

Federal and state laws prohibit employment and/or public accommodation discrimination on the basis of age, color, creed, disability, gender identity, national origin, pregnancy, race, religion, sex, sexual orientation or veteran's status. If you believe you have been discriminated against, please contact the Iowa Civil Rights Commission at 800-457-4416 or Iowa Department of Transportation's affirmative action officer. If you need accommodations because of a disability to access the Iowa Department of Transportation's services, contact the agency's affirmative action officer at 800-262-0003.

The preparation of this (report, document, etc.) was financed in part through funds provided by the Iowa Department of Transportation through its "Agreement for the Management of Research Conducted by Iowa State University for the Iowa Department of Transportation," and its amendments.

The opinions, findings, and conclusions expressed in this publication are those of the authors and not necessarily those of the Iowa Department of Transportation.

Technical Report Documentation Page

1. Report No. IHRB Project TR-621	2. Government Accession No.	3. Recipient's Catalog No.	
4. Title and Subtitle Geosynthetic Reinforced Soil for Low-Volume Bridge Abutments		5. Report Date January 2012	
		6. Performing Organization Code	
7. Author(s) Pavana Vennapusa, David White, Wayne Klaiber, Shiyun Wang		8. Performing Organization Report No. InTrans Project 10-380	
9. Performing Organization Name and Address Center for Earthworks Engineering Research and Bridge Engineering Center Iowa State University 2711 South Loop Drive, Suite 4600 Ames, IA 50010-8664		10. Work Unit No. (TRAIS)	
		11. Contract or Grant No.	
12. Sponsoring Organization Name and Address Iowa Highway Research Board Iowa Department of Transportation 800 Lincoln Way Ames, IA 50010		13. Type of Report and Period Covered Final Report	
		14. Sponsoring Agency Code	
15. Supplementary Notes Visit www.ceer.iastate.edu for color PDFs of this and other research reports.			
16. Abstract <p>This report presents a review of literature on geosynthetic reinforced soil (GRS) bridge abutments, and test results and analysis from two field demonstration projects (Bridge 1 and Bridge 2) conducted in Buchanan County, Iowa, to evaluate the feasibility and cost effectiveness of the use of GRS bridge abutments on low-volume roads (LVRs). The two projects included GRS abutment substructures and railroad flat car (RRFC) bridge superstructures. The construction costs varied from \$43k to \$49k, which was about 50 to 60% lower than the expected costs for building a conventional bridge. Settlement monitoring at both bridges indicated maximum settlements ≤ 1 in. and differential settlements ≤ 0.2 in transversely at each abutment, during the monitoring phase.</p> <p>Laboratory testing on GRS fill material, field testing, and in ground instrumentation, abutment settlement monitoring, and bridge live load (LL) testing were conducted on Bridge 2. Laboratory test results indicated that shear strength parameters and permanent deformation behavior of granular fill material improved when reinforced with geosynthetic, due to lateral restraint effect at the soil-geosynthetic interface. Bridge LL testing under static loads indicated maximum deflections close to 0.9 in and non-uniform deflections transversely across the bridge due to poor load transfer between RRFCs. The ratio of horizontal to vertical stresses in the GRS fill was low (< 0.25), indicating low lateral stress on the soil surrounding GRS fill material. Bearing capacity analysis at Bridge 2 indicated lower than recommended factor of safety (FS) values due to low ultimate reinforcement strength of the geosynthetic material used in this study and a relatively weak underlying foundation layer. Global stability analysis of the GRS abutment structure revealed a lower FS than recommended against sliding failure along the interface of the GRS fill material and the underlying weak foundation layer. Design and construction recommendations to help improve the stability and performance of the GRS abutment structures on future projects, and recommendations for future research are provided in this report.</p>			
17. Key Words bridge abutments—bridge performance monitoring—geosynthetic reinforced soil—GRS—low-volume roads—railroad flat car bridges		18. Distribution Statement No restrictions.	
19. Security Classification (of this report) Unclassified.	20. Security Classification (of this page) Unclassified.	21. No. of Pages 134	22. Price NA

GEOSYNTHETIC REINFORCED SOIL FOR LOW- VOLUME BRIDGE ABUTMENTS

**Final Report
January 2012**

Principal Investigator

David J. White, Ph.D.
Associate Professor and Director of CEER

Co-Principal Investigators

Pavana KR. Vennapusa, Ph.D.
Research Assistant Professor and Associate Director of CEER

F. Wayne Klaiber, Ph.D.
Professor Emeritus and Faculty Affiliate of BEC

Research Assistants

Shiyun Wang and Heath Gieselman

Authors

Pavana Vennapusa, David White, Wayne Klaiber, and Shiyun Wang

Sponsored by
the Iowa Highway Research Board
(IHRB Project TR-621)

Preparation of this report was financed in part
through funds provided by the Iowa Department of Transportation
through its research management agreement with the
Institute for Transportation and the Center for Earthworks Engineering Research.
(InTrans Project 10-380)

A report from
Center for Earthworks Engineering Research (CEER)

Iowa State University
2711 South Loop Drive, Suite 4600
Ames, IA 50010-8664
Phone: 515-294-7910
Fax: 515-294-0467
www.ceer.iastate.edu

TABLE OF CONTENTS

ACKNOWLEDGMENTS	XI
EXECUTIVE SUMMARY	XIII
INTRODUCTION	1
BACKGROUND	3
Geosynthetic Reinforced Soil Abutment Systems	4
Rail Road Flat Cars for Low-Volume Road Bridges.....	12
LABORATORY AND IN SITU TESTING METHODS	14
Laboratory Test Methods	14
In Situ Testing.....	18
RESULTS AND ANALYSIS FROM FIELD PROJECTS	26
Bridge 1 — Olympic Avenue, Buchanan County, Iowa	26
Bridge 2 — 250th Street, Buchanan County, Iowa	44
Recommendations for Future GRS Bridge Construction Projects	103
KEY FINDINGS, CONCLUSIONS, AND RECOMMENDATIONS	105
REFERENCES	109
APPENDIX A: MIRAFI® 500X TECHNICAL DATA SHEET.....	113
APPENDIX B: VIBRATING WIRE EARTH PRESSURE READINGS FROM UNDER THE FOOTING – BRIDGE 2	114

LIST OF FIGURES

Figure 1. Typical cross-section of GRS-IBS with frictionally connected facing elements (from Adams et al. 2011a)	3
Figure 2. GRS abutment walls with different facings (from Adams et al. 2011b).....	5
Figure 3. Concrete masonry unit facing for a GRS abutment wall (from Adams et al. 2011b)	6
Figure 4. Recommended gradations for well-graded and open-graded granular backfill materials (data from Adams et al. 2011b)	7
Figure 5. Recommended steps for GRS-IBS design (modified from Adams, et al. 2011b).....	8
Figure 6. Performance test results for different compacted geosynthetic reinforced granular backfill materials (from Adams et al. 2011b)	9
Figure 7. Example setup of a performance test: (a) photo of the setup, (b) face view of the setup (from Adams, et al. 2011b)	10
Figure 8. Split mold, steel platen (4 in. diameter), and vibratory hammer for compaction of granular materials.....	15
Figure 9. Sample preparation for triaxial testing: (a) compaction of sample in split mold and (b) lift thickness verification.....	16
Figure 10. Triaxial chamber, load frame, and computer equipment for cyclic triaxial testing	17
Figure 11. Iowa State University truck-mounted rotary drill rig	18
Figure 12. Three 5 ft long inclinometer casings snapped together ready for installation.....	19
Figure 13. Sand used to fill the borehole cavity around the inclinometer	19
Figure 14. (a) Model 3510 semiconductor EPC installation to measure total vertical stresses, and (b) Model 4800 vibrating wire EPC installation to measure horizontal stresses	21
Figure 15. On-site datalogger system installed to continuously record EPC and piezometer readings	23
Figure 16. LWD testing during placement of GRS fill material.....	24
Figure 17. Loaded truck used for live load testing and total station equipment used for bridge deflection measurement under loading.	25
Figure 18. Bridge 1 — Olympic Avenue project location in Buchanan County, Iowa.....	27
Figure 19. Bridge 1 — Schematic of GRS bridge abutment with geosynthetic wrapped sheets flexible facing	28
Figure 20. Bridge 1 — Pictures of the project site after removing the existing bridge abutments (Courtesy of Brian Keierleber)	29
Figure 21. Bridge 1 — Building up of GRS fill material (Courtesy of Brian Keierleber)	30
Figure 22. Bridge 1 — Compaction of GRS fill material (Courtesy of Brian Keierleber).....	31
Figure 23. Bridge 1 — Building up of GRS fill material behind the footing (Courtesy of Brian Keierleber)	32
Figure 24. Bridge 1 — Pictures of north (top) and south abutments built up with flexible wrapped around facing (Courtesy of Brian Keierleber)	33
Figure 25. Bridge 1 — Excavation at the toe to install erosion stone (Courtesy of Brian Keierleber)	34
Figure 26. Bridge 1 — Installation of riprap over the flexible geosynthetic wrapped facing (Courtesy of Brian Keierleber)	35
Figure 27. Bridge 1 — Installing cement grout over riprap facing for scour protection (Courtesy of Brian Keierleber)	36
Figure 28. Bridge 1 — Leveling pad install concrete footing reinforcement (Courtesy of Brian	

Keierleber)	37
Figure 29. Bridge 1 — Installation of reinforced concrete footing (Courtesy of Brian Keierleber)	38
Figure 30. Bridge 1 — Installation of RRFC bridges (Courtesy of Brian Keierleber).....	39
Figure 31. Bridge 1 — Installation of RRFC bridges (contd.) (Courtesy of Brian Keierleber) ...	40
Figure 32. Bridge 1 — Pictures of the completed bridge (7/27/2010)	41
Figure 33. Bridge 1 — Condition of riprap one year after construction (9/8/2011).....	42
Figure 34. Bridge 1 — Abutment settlement readings	43
Figure 35. Bridge 2 — 250 th street project location in Buchanan County, Iowa.....	44
Figure 36. Bridge 2 — Pictures of the existing 250 th street bridge	45
Figure 37. Bridge 2 — Cracks observed on the east abutment wing wall.....	46
Figure 38. Bridge 2 — Plan view of the bridge abutments prepared for installation of the new RRFC bridge	47
Figure 39. Bridge 2 — Cross-sectional view on the east abutment side of the bridge, subsurface soil profile, piezometer locations, details of GRS fill material, and EPC locations in GRS fill material.....	48
Figure 40. Bridge 2 — East and west abutments after removing the existing bridge	49
Figure 41. Bridge 2 — Installation of sheet piles on the north and south sides of each abutment for scour protection	49
Figure 42. Bridge 2 — Excavation of a trench to place GRS fill material to support the bridge concrete footing	50
Figure 43. Bridge 2 — Placement of geosynthetic layer at bottom of excavation and granular fill over the geofabric	52
Figure 44. Bridge 2 — Placement and compaction of granular fill over geosynthetic layer using vibratory plate	53
Figure 45. Bridge 2 — Lift thickness control using laser measurement	54
Figure 46. Bridge 2 — 1 inch thick neoprene pads placed over the footing prior to placement of the flat cars.....	55
Figure 47. Bridge 2 — Placement of RRFCs on the footings	56
Figure 48. Bridge 2 — Picture of all three RRFCs placed on the footings	57
Figure 49. Bridge 2 — W-sections confined with inverted channel sections placed between the footing and the RRFCs.....	57
Figure 50. Bridge 2 — Bolted connections every 5 ft between the RRFCs	58
Figure 51. Bridge 2 — Picture of the completed bridge.....	58
Figure 52. Bridge 2 — Log of boring B-1	61
Figure 53. Bridge 2 — Log of boring B-2	62
Figure 54. Bridge 2 — Piezometer pore pressure readings monitoring in B-3 and B-4.....	64
Figure 55. Bridge 2 — Grain-size distribution curve of GRS fill material in comparison with Adams et al. (2011b) recommended gradation limits	67
Figure 56. Bridge 2 — Proctor compaction test results for GRS fill material.....	67
Figure 57. Bridge 2 — Plot of shear stress versus horizontal displacement (top) and change in sample height versus horizontal displacement (bottom) for three different applied normal stresses for compacted GRS fill material.....	68
Figure 58. Bridge 2 — Mohr-Coulomb failure envelope from direct shear tests for compacted GRS fill material	69
Figure 59. Bridge 2 — Deviator stress versus strain plots from CD tests from shearing phase for granular fill material with and without geosynthetic reinforcement.....	70

Figure 60. Bridge 2 — Mohr-Coulomb failure envelopes from CD tests for granular fill materials test with and without geosynthetic reinforcement	71
Figure 61. Bridge 2 — Mohr circles for stresses applied during repeated loading cyclic triaxial tests	72
Figure 62. Bridge 2 — Results of permanent strain versus loading cycles from cyclic triaxial test	72
Figure 63. Bridge 2 — Cross-sectional view of the GRS fill material and location of semiconductor and vibrating wire EPCs embedded in the fill.....	73
Figure 64. Bridge 2 — Plan view of the concrete footing showing location of vibrating wire and semiconductor EPCs under the footing.....	74
Figure 65. Bridge 2 — In-situ LWD and NG test results of each GRS lift.....	74
Figure 66. Bridge 2 — Inclinometers results for B-1	75
Figure 67. Bridge 2 — Inclinometers results for B-2	76
Figure 68. Bridge 2 — In ground total vertical stresses in PE 1 (at the bottom of the excavation) and PE 2 (at about 2.2 ft below footing) during compaction of GRS fill material in excavation	77
Figure 69. Bridge 2 — In ground total vertical stresses and temperature readings from 9/23/2010 to 11/26/2010 in PE 1 (at the bottom of the excavation), PE 2 (at about 2.2 ft below footing), and PE 3 (at the bottom of the footing).....	78
Figure 70. Bridge 2 — In ground total vertical stresses and temperature readings in PE 1 (at the bottom of the excavation), PE 2 (at about 2.2 ft below footing), and PE 3 (at the bottom of the footing) for the full project period	79
Figure 71. Bridge 2 — In ground total horizontal stresses and temperature readings in vibrating wire EPCs for the full project period	81
Figure 72. Bridge 2 — Abutment elevation monitoring results	82
Figure 73. Bridge 2 — Dimensions of the test truck used for live load testing.....	83
Figure 74. Bridge 2 — North, center, and south lanes divided for load testing	85
Figure 75. Bridge 2 — Center of tandem axle positioned over a desired location along the bridge	85
Figure 76. Bridge 2 — Bridge deflections at center when truck is positioned at the bridge center in north, center, and south lanes (10/29/2010).....	86
Figure 77. Bridge 2 — Bridge deflections at center when truck is positioned at the bridge center in north, center, and south lanes (10/20/2011) – Truck travelling east to west	87
Figure 78. Bridge 2 — Bridge deflections at center when truck is positioned at the bridge center in north, center, and south lanes (10/20/2011) – Truck travelling west to east	88
Figure 79. Bridge 2 — Increase in total vertical stresses in PE 1 (at the bottom of the excavation) and PE 2 (at about 2.2 ft below footing) during static load testing on north, center, and south lanes (10/29/2010).....	90
Figure 80. Bridge 2 — Increase in total vertical stresses in PE 1 (at the bottom of the excavation) and PE 2 (at about 2.2 ft below footing) during static load testing on north, center, and south lanes (10/20/2011).....	91
Figure 81. Bridge 2 — Increase in total horizontal stresses against the excavation walls during static load testing on north, center, and south lanes (10/20/2011).....	93
Figure 82. Bridge 2 — Increase in total vertical stresses in PE 1 (at the bottom of the excavation) and PE 2 (at about 2.2 ft below footing) during dynamic loading at 10 to 40 mph on center lane (10/29/2010)	94
Figure 83. Bridge 2 — Increase in total vertical stresses in PE 1 (at the bottom of the excavation) and PE 2 (at about 2.2 ft below footing) during dynamic loading under husbandry traffic	

and load test vehicle (10/20/2011).....	95
Figure 84. Bridge 2 — Dual tandem axle loaded grain cart passed over the bridge during 10/20/2011 load testing.....	96
Figure 85. Bridge 2 — Bearing capacity failure modes: (a) failure in foundation soil due to stresses at the base of GRS fill material, (b) failure within GRS fill material, and (c) punching shear failure through the GRS fill material and bearing capacity failure in the foundation soil	99
Figure 86. Bridge 2 — Cross-section setup for slope stability analysis	101
Figure 87. Bridge 2 — Global stability analysis for three different water level conditions.....	102

LIST OF TABLES

Table 1. Summary of the load test results on different bridges from Wipf et al. (2003) and (2007)	13
Table 2. Loading sequences following in cyclic triaxial testing.....	17
Table 3. Bridge 1 — Construction costs.....	43
Table 4. Bridge 2 — Construction events and ISU field instrumentation installation/testing timeline	59
Table 5. Bridge 2 — Construction costs.....	59
Table 6. Bridge 2 — Summary of dead loads on the bridge.....	60
Table 7. Bridge 2 — Summary of laboratory test results for GRS fill material	66
Table 8. Bridge 2 — Summary of direct shear test results for compacted GRS fill material.....	69
Table 9. Bridge 2 — Summary of CD test results for compacted GRS fill material with and without geosynthetic	70
Table 10. Bridge 2 — Summary of live load testing at different testing times	83
Table 11. Bridge 2 — Summary of test trucks axle loads and total weights	84
Table 12. Bridge 2 — Comparison of measured and estimated maximum stress increase in GRS fill material due to static live loads	92
Table 13. Bridge 2 — Summary of maximum stresses measured in GRS fill material during dynamic loading and dynamic to static stress ratio	96
Table 14. Bridge 2 — Summary of bearing capacity analysis results for different failure modes	100
Table 15. Bridge 2 — Summary of FS results from slope stability analysis.....	103

ACKNOWLEDGMENTS

The authors would like to thank the Iowa Highway Research Board and Buchanan County for sponsoring this research (TR-621). The authors would also like to acknowledge the support of the Buchanan County Engineer Mr. Brian Keierleber, P.E., for initiating the project, identifying bridge locations for testing, assisting in field testing, and providing helpful insights during the course of this project. Buchanan County Department staff Randy Andrews, Phil Fangman, Jeff White, Chuck Kivell, Dick Lehs, Alex Davis, Tom Reidy, Andy Monaghan, Ron Crawford, Rick Wendling, Jerry Slattery, Brian Donnelly, and Ned Johnson also assisted with the field testing and instrumentation work and their help is greatly appreciated. Heath Gieselman of Iowa State University assisted in performing soil borings and in-situ testing.

EXECUTIVE SUMMARY

The feasibility of using geosynthetic reinforced soil (GRS) abutment systems which involves constructing engineered granular backfill material with closely-spaced alternating layers of geosynthetic reinforcement, for supporting bridge abutments on low-volume roads, is evaluated in this research study. A review of literature on GRS abutment systems along with material specifications, a newly-developed Federal Highway Administration (FHWA)-recommended design methodology and construction considerations, and results from two field demonstration projects are presented in this report. The two projects included GRS abutment substructures and railroad flat car (RRFC) superstructures and were constructed in Buchanan County, Iowa. A woven geosynthetic material was used as the geosynthetic reinforcement in the granular fill material on both projects. Details of the two demonstration projects are provided below.

Bridge 1 – Olympic Avenue

Bridge 1 involved replacing an existing timber back wall abutment, with a GRS bridge abutment with flexible wrapped geosynthetic and grouted riprap facing, to support a 73 ft RRFC bridge on a reinforced concrete spread footing. No instrumentation or testing was performed by the ISU research team on that project. The research team's assessment on project conditions based on review of photos, field visits, and bridge abutment settlement data are provided in this report.

Bridge 2 – 250th Street

Bridge 2 involved replacing a 90+ year old steel bridge supported on concrete abutment with a 68.5 ft RRFC bridge supported on reinforced concrete spread footings founded on GRS fill material. The new bridge was longer, so the existing concrete bridge abutments, along with some existing fill, were left in place to serve as GRS facing. The existing soil under the new footing location was excavated and replaced with GRS fill material to improve the support conditions (e.g., bearing capacity and stiffness). Steel sheet piles were installed on the excavation sides for scour protection. Soil borings, in situ testing, laboratory testing, and instrumentation installation were conducted at this bridge site.

In situ tests included conducting nuclear gauge (NG) density tests and light weight deflectometer (LWD) tests on GRS fill material, live load (LL) tests (with a loaded test truck) monitoring bridge deflections and stresses in the GRS fill material, and bridge abutment settlement monitoring. Instrumentation included installing inclinometers and piezometers in the ground, and semiconductor and vibrating wire earth pressure cells (EPCs) in the GRS fill material and under the footing. Laboratory tests included characterizing the shear strength properties of GRS fill material from direct shear and consolidated drained (CD) triaxial tests on material with and without geosynthetic reinforcement. In addition, repeated load cyclic triaxial tests were conducted on material with and without geosynthetic reinforcement to evaluate differences in their permanent deformation characteristics.

Key Findings and Conclusions

Savings in Construction Costs: The construction costs of Bridges 1 and 2 were about \$49k and \$43k, respectively. These construction costs were about 50 to 60 percent lower than the estimated construction costs for building a conventional bridge with reinforced concrete abutments, piling, and concrete superstructure at these sites. The cost reductions using the GRS substructures with the RRFC superstructures are realized with the ease in construction, shortened construction time (one abutment per day), and reduced material and labor costs.

Laboratory Test Results: CD triaxial test results showed an increase in effective shear strength parameters when the granular material was reinforced with geosynthetic (Figure 3). Cyclic triaxial test results showed a decrease in total permanent strain at the end of 70,000 cycles when the granular material was reinforced with geosynthetic (Figure 4). These improvements in geosynthetic reinforced samples are believed to be due to the lateral restraint effect at the soil-geosynthetic interface in the sample.

Field Test and In-Ground Instrumentation Results:

- Bridge 2: Total vertical stress readings in the EPCs located at about 2.2 and 3.8 ft below the footing indicated that the dead load vertical stress applied under the footing (about 2,120 lbs/ft²) was almost fully transferred down to the bottom of the GRS fill. The horizontal dead load stresses along the excavation walls were about 600 lbs/ft² or less. The horizontal to vertical stress was less than 0.25, thus indicating low lateral stress on the soil surrounding the GRS fill material.
- Bridges 1 and 2: Bridge abutment elevation monitoring since the end of construction to about 1 year after completion of construction indicated maximum settlements of ≤ 0.7 in. with transverse differential settlements of ≤ 0.2 in at each abutment.
- Bridge 2: Static LL tests indicated non-uniform deflections transversely across the bridge at the center span (with a differential deflection of up to 0.8 in.) when the truck was positioned along the edges. This suggests poor load transfer across the RRFCs. A maximum deflection of about 0.9 in. was measured during static LL testing. The maximum measured deflection was close to but less than the AASHTO allowable deflection. However, it must be noted that the AASHTO allowable limits are based on a 72 kip three-axle test truck, while the test truck used in this study weighed about 52 to 53 kips.
- Bridge 2: Peak increase in vertical stresses in the GRS fill material was observed when the test truck was positioned directly above the footing, as expected. Peak increase in horizontal stresses in the excavation at the GRS/existing soil interface was observed when the test truck was positioned either directly above or within 20 ft of the footing. The estimated vertical stress increase under LL using elastic solutions compared well with the measured vertical stress increase values from EPCs. The horizontal stress increase under LL were lower than the estimated values from elastic solutions, as the elastic solutions used do not account for the lateral restraint effect in the reinforced soil layers, which causes a reduction in the horizontal stresses.
- Bridge 2: EPC results indicated that the ratio of vertical stress increase in the GRS fill

due to dynamic (with test truck traveling from 5 to 40 mph) and static loading varied from about 0.8 to 1.2, with an average of about 1.0. The increase in vertical stresses in the GRS fill material under a 1,000 bushel load semi-truck and a loaded grain cart was about 1.3 and 1.6 times higher than the increase in vertical stresses under the loaded test truck, respectively

Bearing Capacity and Slope Stability Analysis Results – Bridge 2:

- Bearing capacity analysis was conducted for three potential failure modes: A – bearing capacity failure within the foundation soil, B – bearing capacity failure within the GRS fill material, and C – punching shear failure through the GRS fill material and bearing capacity failure in the foundation soil. Analysis results indicated lowest factor of safety (FS) values (1.8 to 2.6) for failure mode B and they were lower than the minimum recommended value ($FS_{\text{GRSBearing}} \geq 3.5$) by the FHWA. For failure modes A and C, a case with the water table at the surface of the GRS fill material showed the lowest FS values in case of dead load + live load and were lower than the recommended value ($FS_{\text{Bearing}} \geq 2.5$) by the FHWA.
- The ultimate strength of geosynthetic reinforcement, T_f , plays a critical role in determining the ultimate bearing capacity of the foundations over GRS fill material. The T_f of the geosynthetic product used in this study was about 1,200 lbs/ft, which is lower than the FHWA recommended minimum $T_f = 4,800$ lbs/ft. This resulted in lower FS values than recommended, as indicated above (failure mode B).
- Global stability analysis was conducted using three water table scenarios: A – water level at the base of the GRS fill material, B – water level during flooding, and C – water levels in a rapid draw down condition. The analysis indicated that the FS values for both rapid draw down and flooding cases (1.2 to 1.4) were lower than the recommended minimum ($FS_{\text{Stability}} = 1.5$) by the FHWA. The potential failure surfaces were at the interface of the GRS fill material and the underlying weaker foundation layer.

Recommendations for Future GRS Bridge Construction Projects:

- The T_f of geosynthetic reinforcement must be selected to meet the minimum FHWA requirements. Typically, the T_f values are provided by the manufacturer as part of the product technical data sheets. Consideration must also be given to selecting a geosynthetic product that has good infiltration capacity so that the GRS fill material is easily drained during flooding. As an example, according to the manufacturer, Mirafi® HP570 woven geosynthetic or higher grade has $T_f \geq 4,800$ lbs/ft and also has good permeability (30 gal/min/ft²).
- Bridge 1 construction involved installation of rock fill for erosion protection at the toe of the GRS abutment slopes. The installation of rock fill material at that project site was performed by excavating a trench after the fill slopes were constructed. Excavation at the toe of slopes can contribute to slope instability and must be avoided. Any excavations at the toe of the slope must be performed before the fill layers are constructed, and should be properly backfilled and compacted.

- Neither bridge evaluated in this study included a drainage design. Field observations indicated that flood water levels reached nearly up to the bottom of the superstructure at Bridge 2. Draining the water entered into the GRS fill materials is critical to the long term performance of these structures. Drainage in critical areas, including behind the wall, base of the wall, and locations where a fill slope meets a wall face, must be incorporated into the design.
- Slope stability analysis on the Bridge 2 abutment indicated potential failure surfaces at the interface of the GRS fill material and the underlying weaker foundation layer. Obtaining subsurface soil information prior to bridge construction is recommended, so that excavation depths to determine any weak foundation layers can be determined prior to construction. If soil boring information is not available, at least testing at the bottom of excavation must be conducted to determine if the foundation layers are stable.

Implementation Benefits and Recommendations for Future Research

The primary benefits of using GRS bridge abutments for low volume road bridges include (1) cost savings due to lower material costs than conventional reinforced concrete bridge abutments and piling, less need for highly skilled labor, and less construction time; (2) ease in construction; and (3) less disruption to traffic due to short construction times.

GRS bridge abutments were constructed using existing abutment wall and grouted riprap as facing elements in this research study. In situ test results from the two demonstration projects in this study indicated that the bridges performed well within the monitoring phase of the project. Performance of these structures over a long period must be investigated. Long-term performance of GRS abutments with different facing elements (e.g., sheet piles, concrete masonry units, and timber-faced walls), must be evaluated. Future research should also include an experimental study to evaluate the bearing capacity of GRS fill materials with different granular fill materials used commonly in Iowa and geosynthetic materials (woven and non woven) with varying ultimate strengths. The bearing capacity evaluations must include performance test evaluation with full-scale field testing to failure, to determine the ultimate bearing capacities.

INTRODUCTION

The state of Iowa currently has approximately 25,000 bridges and about 80% of these bridges are on low-volume roads (LVRs). Since many of these bridges are on rural county roads, funding is limited to replace deficient bridges. Performance of *substructure* components (i.e., abutment and foundation soils) is believed to play a major role in the overall performance of the bridges. Most of the previous work in Iowa on LVRs was focused on *superstructure* components (e.g., Wipf et al. 1994, 1997, 1999, 2003, 2004, 2007a, 2007b, Klaiber et al. 2001, 2004, White et al. 2007). A few studies in Iowa have focused on studying the effects of the *substructure* components in LVR bridges (White et al. 2007, Evans et al. 2012). Use of geosynthetic reinforced soil (GRS) abutment systems, which involves constructing engineered granular backfill material with closely spaced alternating layers of geosynthetic reinforcement, can potentially be a cost-effective and structurally efficient alternative for supporting LVR bridge abutments. However, there are no documented case studies with performance monitoring information in Iowa. The feasibility of using this method has to be properly investigated and documented for local conditions and materials with regard to several aspects including internal and external stability during and after construction, construction methods, and performance monitoring.

The primary objectives of this project were to:

- Develop an instrumentation and monitoring plan to evaluate performance of newly-constructed GRS bridge abutment systems.
- Develop a design approach and construction guidelines for GRS bridge abutment systems with shallow spread footings on LVR bridges.
- Document and evaluate the cost and construction aspects associated with construction of GRS bridge abutment systems from detailed field observations on project sites.
- Produce a research report and technology transfer materials that provide recommendations for use and potential limitations of GRS bridge abutment systems.

The following research tasks were developed to meet the above mentioned project objectives:

- Task 1 – Conduct a literature review on GRS bridge abutment systems on their design, construction, and performance monitoring aspects.
- Task 2 – Identify, select, and conduct field reconnaissance at a selected bridge site.
- Task 3 – Conduct in situ testing and install in-ground instrumentation to obtain field long term performance measurements (i.e., in ground stresses, piezometer water levels, settlement, etc.)
- Task 4 – Observe and document field construction operations and equipment
- Task 5 – Conduct performance monitoring
- Task 6 – Conduct detailed data analysis
- Task 7 – Develop a final report and technology transfer materials

A review of literature on GRS abutment systems, material specifications, a newly-developed design methodology by the Federal Highway Administration (FHWA), and construction

considerations are summarized in the Background chapter of this report. A detailed step-by-step procedure for designing GRS abutment systems is summarized in a recently published report by the FHWA (Adams et al. 2011b). A summary of key aspects of the FHWA design procedure, as relevant to this research project is provided in the Background chapter.

Two field demonstration projects were conducted as part of this research study. In both projects, A woven geosynthetic material (Mirafi[®] 500X) was used as the geosynthetic reinforcement in the fill material. The first demonstration project (Bridge 1) commenced prior to initiation of this research project; however, information was provided by the Buchanan County Engineer (including photos during construction and bridge abutment settlement data) and is included in this report. Bridge 1 involved replacing an existing timber back wall abutment with a GRS bridge abutment with flexible wrapped geosynthetic riprap facing to support a 73 ft rail road flat car (RRFC) bridge on a reinforced concrete spread footing. No instrumentation or testing was performed by the Iowa State University (ISU) research team on this project. The research team's assessment of photos taken during construction and bridge abutment settlement data, and field visits, are included in this report.

Bridge 2 involved replacing a 90+ year old steel bridge supported on concrete abutment with a RRFC bridge supported on reinforced concrete spread footings founded on GRS fill material. The new bridge was about 68.5 ft long and the old bridge was about 35 ft long. Taking advantage of the longer span of the new bridge, some of the existing cohesive backfill material and the concrete bridge abutments were left in place as GRS facing, and the existing soil under the proposed new footing location was excavated and replaced with GRS fill material to improve the support conditions (i.e., bearing capacity and stiffness). Soil borings, in situ testing, laboratory testing to characterize the foundation soils and GRS fill material, and instrumentation installation was conducted at this bridge site. The instrumentation included installing inclinometers and piezometers in the ground, and semiconductor and vibrating wire earth pressure cells (EPCs) in the GRS fill material and under the footing. Inclinometers were installed to monitor lateral ground movements during and after construction, and piezometers were installed to monitor pore water pressures in the foundation soils. EPCs were installed to monitor in ground stresses during and after construction under dead loads and live loads. In situ tests involved conducting: (a) compaction tests on the GRS fill material during placement including nuclear density tests and light weight deflectometer (LWD) tests, (b) bridge live load tests shortly after and one year after construction to monitor bridge deflections and stresses in the GRS fill material, and (c) bridge abutment settlement monitoring over time. Laboratory tests were conducted on the GRS fill material to characterize its shear strength properties. The tests included direct shear (DS) tests, and consolidated drained (CD) triaxial tests on material with and without geosynthetic reinforcement, to characterize the effective shear strength parameters of the material (i.e., cohesion, c' , and angle of shearing resistance, ϕ'). In addition, repeated load cyclic triaxial tests were conducted on material with and without geosynthetic reinforcement to evaluate differences in their permanent deformation characteristics. Results from laboratory and field testing and in ground instrumentation were used to assess the internal and external stability of the GRS abutment structure used on Bridge 2.

BACKGROUND

Use of GRS bridge abutments can potentially be a cost-effective and structurally-efficient alternative for supporting LVR bridge abutments. Recently, two LVR bridges were constructed in the State of Iowa as part of the TR-568 project where GRS fill material was used and retained with steel sheet pile abutments (Evans et al. 2012). As part of this research project, two more LVR bridges were constructed in the State of Iowa with RRFC bridges supported on shallow spread footing over GRS abutments/backfill. The FHWA has added GRS technology to their Every Day Counts (EDC) initiative to promote accelerated implementation of this technology by the states and local authorities, and recently produced two manuals that covers the background, design, construction, and performance aspects of GRS with integrated single span bridge systems (IBS) (Adams et al. 2011a,b). A typical GRS-IBS cross section is provided in Figure 1, which is composed of GRS, the abutment with frictionally connected facing elements, and an integrated bridge approach. This chapter presents background information on GRS abutments, its design and construction considerations, and a summary of RRFC bridge studies in Iowa.

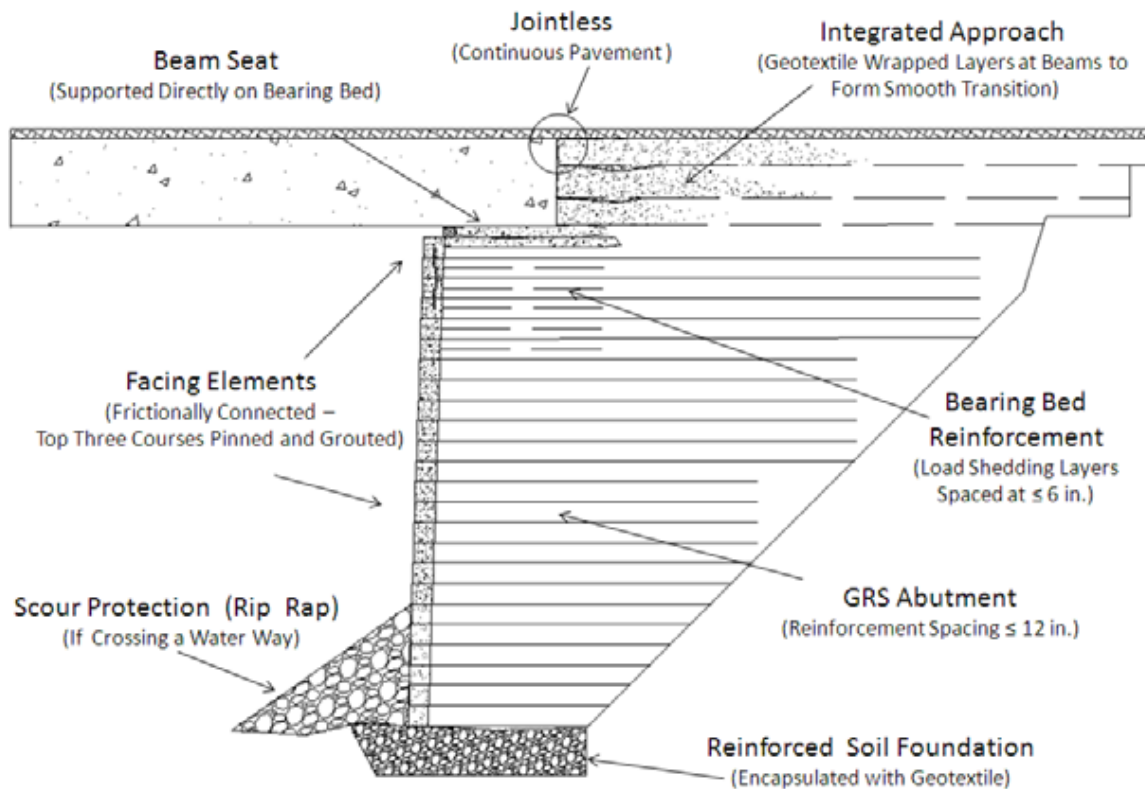


Figure 1. Typical cross-section of GRS-IBS with frictionally connected facing elements (from Adams et al. 2011a)

Geosynthetic Reinforced Soil Abutment Systems

Background

GRS is an engineered fill with closely-spaced alternating layers of compacted granular fill material and geosynthetic reinforcement. Due to the friction developed at the granular soil-geosynthetic interface, the reinforcement restrains lateral deformation of the surrounding soil, increases its confinement, reduces its tendency to dilation, and also increases the strength and stiffness of the soil (Adams et al. 2011a). Sharma et al. (2009) refer to this mechanism as the *lateral restraint effect or confinement effect*. Small scale to large scale test results on reinforced soil systems have been documented by researchers over the past several years demonstrating improvements in the soil bearing capacity, reduction in settlement under static and cyclic loading, and reduction in lateral stresses induced on the surrounding soil (Milligan and Love 1984, Guido et al. 1987, Huang and Tatsuoka 1990, Omar et al. 1994, Adams and Collin 1997, Wu et al. 2006, Adams et al. 2007, Qian et al. 2011).

The main advantages of using GRS bridge abutment systems over conventional reinforced concrete abutments are as follows (Wu et al. 2006):

- GRS abutments are more flexible, hence more tolerant to foundation settlement.
- When properly designed and constructed, GRS abutments are remarkably stable and also have higher ductility (i.e., are less likely to experience a sudden catastrophic collapse) than conventional reinforced concrete abutments.
- When properly designed and constructed, GRS abutments can alleviate differential settlement between the bridge and the approach roadway, thus reducing “the bump at the end of the bridge” problem.
- GRS abutments do not require embedment into the foundation soil for stability. This advantage is especially important when an environmental problem such as excavation into previous contaminated soil is involved.
- The lateral earth pressure behind GRS abutment wall is much smaller than that in a conventional reinforced concrete abutment.
- Construction of GRS abutments is rapid and requires only “ordinary” construction equipment.
- GRS abutments are generally much less expensive to construct than their conventional counterparts.

Facing Elements

The facing elements for GRS abutments can be rigid or flexible (Figure 2). Using pre-cast or cast-in-place concrete walls is considered a rigid facing. Using wrapped geosynthetic sheets, concrete blocks, gabions, or timbers that are not rigidly attached to each other is considered a flexible facing. The facing element is primarily used as a façade to serve as a form for compaction, and protect granular fill from outside weathering. Over the past two decades, GRS has been successfully employed in construction of many earth structures including retaining walls, embankments, slopes, and shallow foundations. Applications of GRS to bridge abutments have gained significant interest over the past few years. Since 1994, Japan Railways has

constructed numerous GRS bridge abutments using rigid facing elements (Tateyama et al. 1994, Tatsuoka et al. 1997). Reportedly, these structures experienced little deformation under service loads and earthquake loads and performed much better than conventional reinforced concrete abutments (Tatsuoka et al. 1997). Construction of rigid facing elements is comparatively more time consuming and expensive than construction of flexible facing elements.

The use of GRS systems in the US was first documented in the 1970s by the U.S. Forest Service (Wu 1994), where it was used to build roads on a steep mountain terrain. Those roads utilized a flexible facing with geosynthetic wrapped around each individual layer and anchored by the overburden of the overlying layer (see top left portion of Figure 2 for an example of wrapped face wall). Reportedly, these roads are still in service (Adams et al. 2011a). GRS bridge abutments with flexible facing have been investigated by Colorado and Ohio DOTs, and the FHWA (Wu et al. 2006). Adams et al. (2011a) reported that as of 2010, 45 bridges were built in the US utilizing GRS abutments, all in areas with relatively shallow scour depth. The most commonly used facing element on these projects included split face concrete masonry unit (CMU) with nominal dimensions of 8 in. x 8 in. x 16 in. (Figure 3) as they are less expensive, lightweight, and easy to install (Adams et al. 2011b).

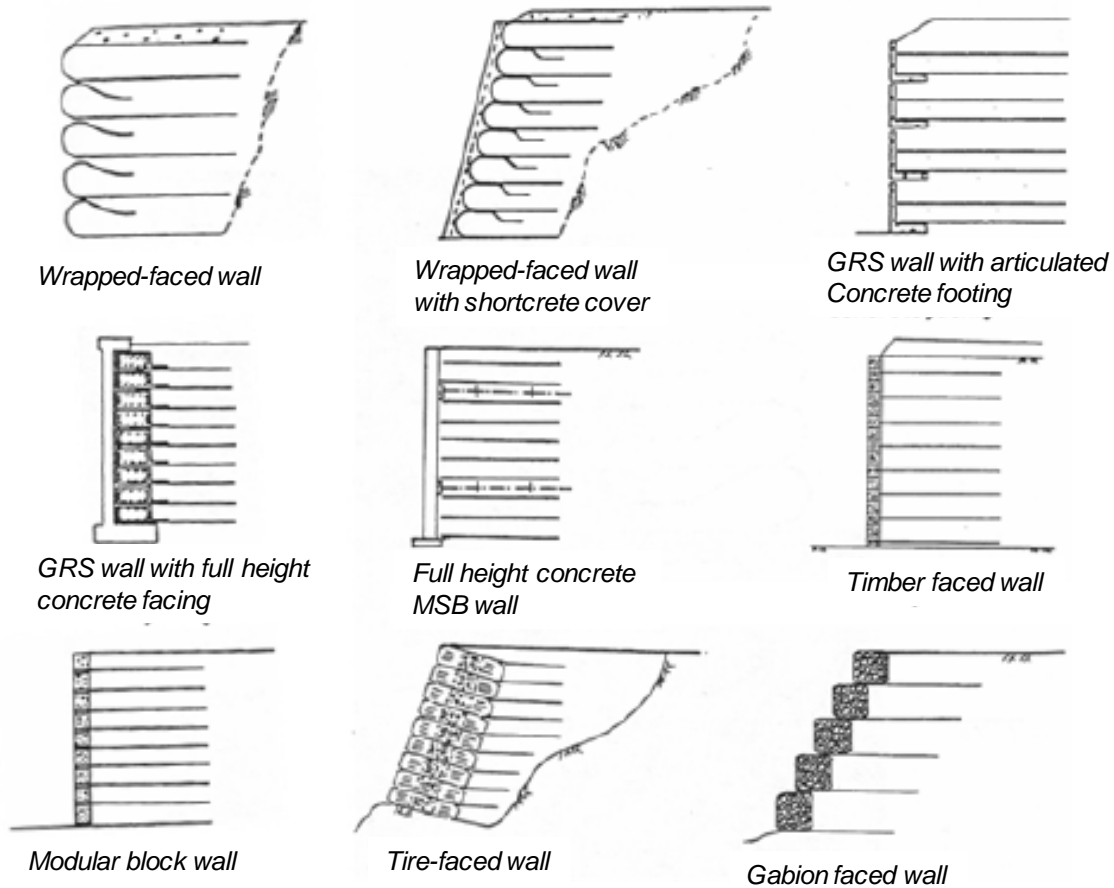


Figure 2. GRS abutment walls with different facings (from Adams et al. 2011b)



Figure 3. Concrete masonry unit facing for a GRS abutment wall (from Adams et al. 2011b)

Backfill Material

The selection of appropriate backfill material is critical to the performance of the GRS abutment system. Adams et al. (2011b) provide the following general guidelines in selecting the backfill material:

- The material should consist of crushed, hard, durable particles or fragments of stone or gravel, that are free from organic matter or deleterious material such as shale or other soft particles that have poor durability.
- The material should meet either well-graded (< 12% passing No. 200 sieve) or open-graded aggregate gradations (shown in Figure 4) or a blend in between the two.
- The maximum particle size should not exceed 2 in (to avoid damaging geosynthetic layers when compacted).
- The material should have angular particles and have an angle of shearing resistance (or friction angle), $\phi' \geq 38^\circ$ (derived from large scale direct shear testing – ASTM D3080).
- The material must have: (a) the ability to ensure compaction, (b) the ability to drain water in case of flooding, and (c) good workability (i.e., easier to spread, level, and compact).

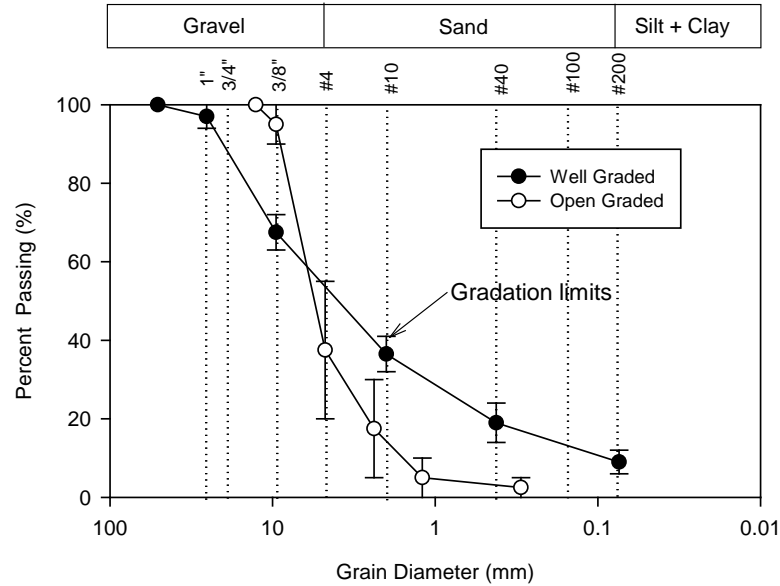


Figure 4. Recommended gradations for well-graded and open-graded granular backfill materials (data from Adams et al. 2011b)

Geosynthetic Material

In the case studies reported by Adams et al. (2011b) with GRS-IBS, biaxial woven polypropylene (PP) geosynthetic material was used for reinforcement. That particular geosynthetic was used for cost, ease of placement, and compatibility reasons. Adams et al. (2011b) indicate that geosynthetic material that meets the following requirements may be used in GRS fill material:

- Ultimate strength of at least 4,800 lb/ft according to ASTM D4595 for geotextiles and ASTM D6637 for geogrids (based on tests conducted at a strain rate of 10%/min).
- Biaxial geosynthetics that has equal strength in both directions (i.e., in machine direction and cross-machine direction) must be used. Uniaxial geosynthetics that has greater strength in the cross-machine direction can be used as they can be rolled out parallel to the wall, but if they have greater strength in the machine direction, the placement must be perpendicular to the wall which can add to the construction time.
- Laboratory tests documenting direct sliding coefficients for various soil types or project specific soils in accordance with ASTM D 5321.
- Follow industry standards on the hydrolysis resistance of polyester, oxidative resistance of PP and high density polyethylene, and stress cracking resistance of HDPE for all components of the geosynthetic, and minimum UV resistance.

Design Methodology

Adams et al. (2011b) provides a detailed step-by-step guidance on the design method for GRS structures (an abutment and wing wall) with a vertical or near vertical face at a height ≤ 30 ft, for

supporting bridges with span lengths of up to 140 ft. The bearing stresses on the GRS fill material should be limited to 4,000 psf, and the reinforcement layer spacing should be limited to 12 inches or less. The performance criterion for GRS-IBS (with single span bridges) consists of a tolerable vertical strain of 0.5% and lateral strain of 1%.

There are nine basic steps in the GRS-IBS procedure (Figure 5), which starts with establishing the project requirements from which the preliminary geometry is determined and then evaluated against external and internal modes of failure. An iterative process is used to assess the geometry and make adjustments as necessary to facilitate construction and assure long-term performance. The external stability in the GRS-IBS design method is similar to checking the external stability of any other abutment systems, i.e., checking for stability against direct sliding at the interface of GRS fill material and foundation soil, bearing capacity of the foundation soils supporting GRS fill material, and global stability (either wedge or rotational) against failure (see Berg et al. 2009). The recommended minimum factor of safety against sliding ($FS_{sliding}$) is 1.5, bearing capacity ($FS_{bearing}$) is 2.5, and global stability ($FS_{stability}$) is 1.5. The internal stability analysis, however, is different from other reinforced soil systems. Internal stability analysis of GRS abutment systems involve evaluating ultimate bearing capacity, deformations, and required reinforcement strength. Both analytical and empirical approaches to analyzing internal stability are provided in Adams et al. (2011b) and are briefly discussed in the following subsections of this chapter.

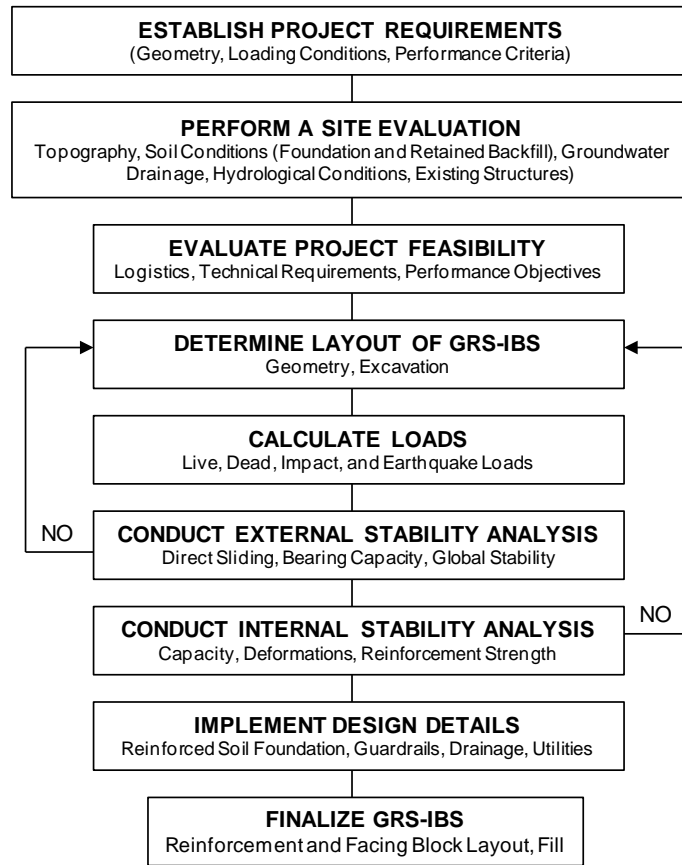


Figure 5. Recommended steps for GRS-IBS design (modified from Adams, et al. 2011b)

Ultimate Bearing Capacity

Both empirical and analytical approaches are presented in Adams et al. (2011b) to determine the ultimate bearing capacity. The empirical approach involves using documented performance test results (Figure 6) on compacted geosynthetic reinforced granular back fill materials of known gradation and shear strength parameters (i.e., c' and ϕ'). The ultimate bearing capacity is defined as the stress at which the GRS fill material in a performance test strains 5% vertically (strain is calculated as deformation divided by the GRS fill material height). If the granular materials fall outside the gradation limits presented in Figure 4, it is recommended that a performance test be conducted to determine the ultimate bearing capacity empirically or analytical procedures can be used.

A detailed description of the performance test is provided in Adams et al. (2011b). In brief, the performance test (or also called as the “mini-pier” test) is a large scale test procedure that involves axially loading GRS fill material while measuring vertical settlement and lateral deformation to monitor performance. The GRS fill material in this test is placed and compacted over a concrete base pad in layers (with facing elements) that matches the field conditions, with at least a base-to-height ratio of 2:1 (base width measured inside the facing elements). An example of this setup from Adams et al. (2011b) is shown in Figure 7, which included an 8 ft tall GRS fill material with segmental retaining wall facing elements. Loading was applied on a 3 ft x 3 ft concrete pad at the surface by applying vertical stresses in increments of 5 psi and lateral and vertical deformations were recorded for each load increment. Ceramic tiles were glued to the concrete pad and facing blocks to create smooth surface for accurate measurements of deformations.

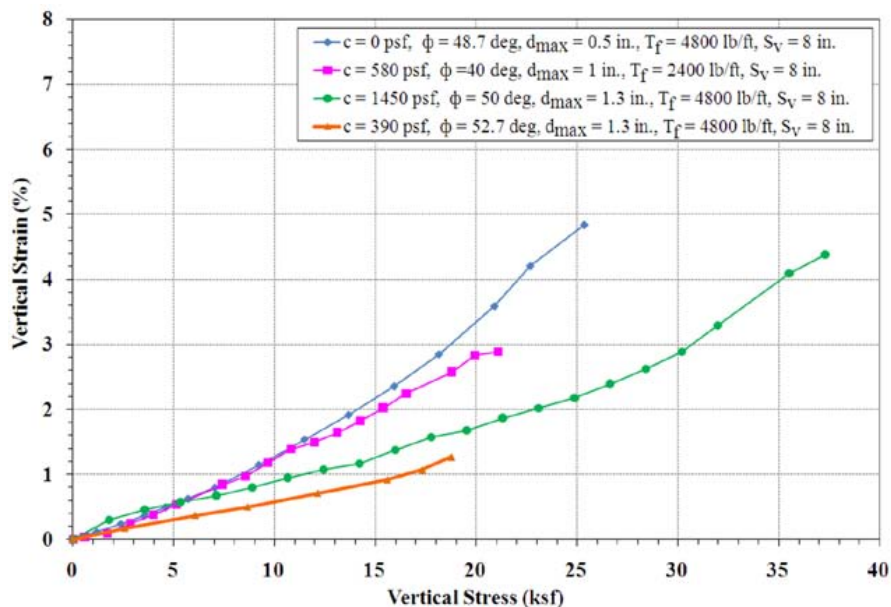


Figure 6. Performance test results for different compacted geosynthetic reinforced granular backfill materials (from Adams et al. 2011b)

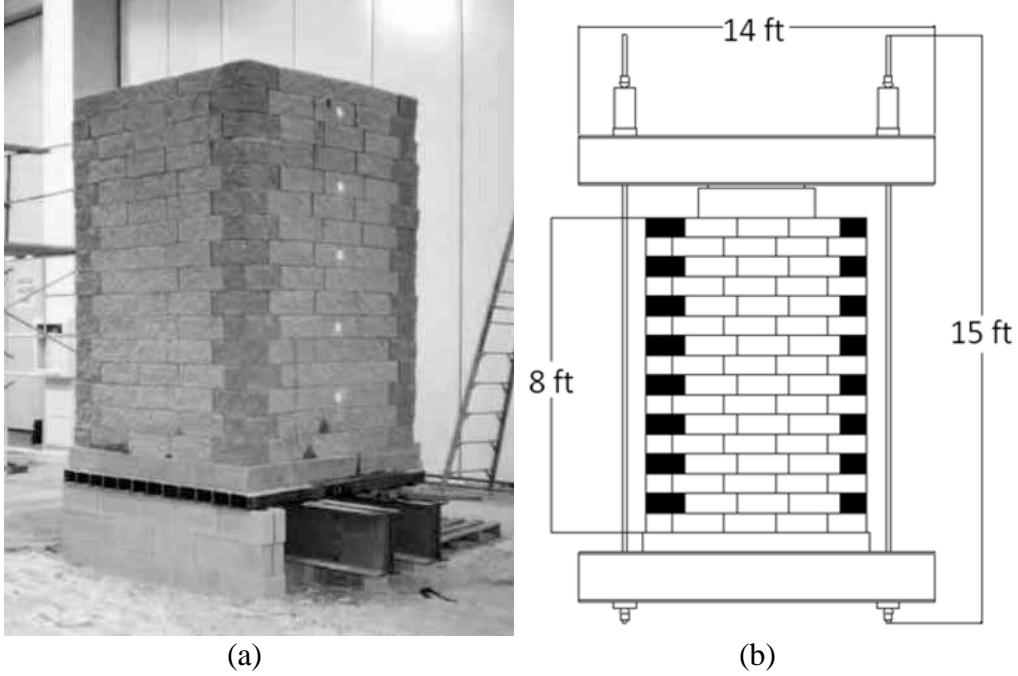


Figure 7. Example setup of a performance test: (a) photo of the setup, (b) face view of the setup (from Adams, et al. 2011b)

The analytical approach involves using Eq. (1):

$$q_{ult} = \left[0.7 \left(\frac{s_v}{6d_{max}} \right) \frac{T_f}{s_v} \right] K_{pr} \quad (1)$$

where, s_v = reinforcement spacing vertically, d_{max} = maximum particle size of the granular backfill material, T_f = ultimate strength of the reinforcement (determined from ASTM D4595 and is typically reported by the manufacturer), and K_{pr} = coefficient of passive earth pressure determined using Eq. (2):

$$K_{pr} = \tan^2 \left(45 + \frac{\phi'_r}{2} \right) \quad (2)$$

where ϕ'_r = angle of shearing resistance of the reinforced fill material. Adams et al. (2011a) report that ultimate bearing capacities estimated using the analytical approach compared well with results obtained from full-scale experiments and in-service GRS structures. The recommended factor of safety against internal bearing capacity ($FS_{GRSbearing}$) = 3.5.

Deformations

Vertical deformation within the GRS fill material is estimated using the stress-strain curve from a performance test. The deformation is calculated as the strain corresponding to the dead load stress multiplied by the height of the GRS fill material. Since the material used in the GRS is granular fill material, it is expected that the settlements occur almost immediately after the bridge is installed and prior to opening the traffic. It is recommended that the vertical strain should be less than 0.5%. The settlement of the underlying foundation soils should be determined using classical consolidation theory taking into account the possible relief of stress due to any excavation of the foundation soil.

Horizontal deformation is estimated as two times the vertical deformation, based on a zero volume change assumption (i.e., volume lost at the top due to settlement is equal to volume gained at the face due to lateral deformation) and represents the worst case scenario (Adams et al. 2002).

Required Reinforcement Strength

The required reinforcement strength (T_{req}) can be determined using Eq. (3), where, σ_h = total lateral stress within the GRS fill material at a given depth and location, which includes contribution from all dead and live loads over the GRS fill material:

$$T_{req} = \left[\frac{\sigma_h}{0.7 \left(\frac{s_v}{6d_{max}} \right)} \right] s_v \quad (3)$$

The T_{req} must satisfy two criteria: (1) it must be less than the allowable reinforcement strength (T_{all}), and (2) it must be less than strength at 2% reinforcement strain. T_{all} is calculated as the ratio of reinforcement ultimate strength, T_f , divided by factor of safety = 3.5.

Hydraulic and Drainage Design Considerations

Adams et al. (2011b) addresses the hydraulic and drainage design aspects of GRS abutment systems, which are vital to consider when bridge abutments are built to span a water channel. This is particularly very important for Iowa conditions where flooding events are possible. It is indicated in Adams et al. (2011b) that GRS-IBS systems have been successfully used to build abutments near rivers and streams, but strongly recommends conducting a thorough hydraulic analysis including an appropriate estimate of the design flow, development of water surface profiles through proposed opening, assessment of scour (abutment, contraction, and long term degradation), and if necessary, the design of counter measures to protect the bridge or stabilize the channel. Section 2.6 (Hydrology and Hydraulics) of the AASHTO LRFD Bridge Design Specifications (AASHTO 2010) provides detailed guidance on how to address the design and construction of foundation systems affected by flooding.

Including drainage features (e.g., drain tiles) in the GRS abutment system in critical areas helps reducing unwanted lateral pressures behind facing elements, erosion of backfill materials, and excess pore pressures within the GRS fill material, when abutments are submerged or partially submerged by flood waters. Critical areas include behind the wall, base of the wall, and any location where a fill slope meets a wall face. The design must include provisions for surface drainage along the fill slopes.

Construction Quality Control/Quality Assurance

A detailed quality control (QC) and quality assurance (QA) program including laboratory and field testing for GRS-IBS is provided in Adams et al. (2011b). Laboratory testing includes gradation, Proctor compaction, and shear strength tests. Large-scale direct shear tests or triaxial tests are the most effective methods for determining shear strength parameters for coarse-grained backfill aggregates. Field testing involves compaction testing on granular back fill material on each layer of fill placed limiting the lift thickness to less than 12 inches. It is recommended that if well-graded granular material is used, the material must be compacted to a minimum of 95% of the maximum standard Proctor density. A method-based specification (e.g., three to five passes with a walk-behind vibratory plate compactor near the wall face) is suggested for compaction of open-graded granular materials, where field density testing may not provide reliable test results. Other items of inspection include geosynthetic reinforcement, wall block placement, and drainage features to ensure these are installed per project design drawings.

Rail Road Flat Cars for Low-Volume Road Bridges

Rail road flat cars (RRFCs) have been used on LVR county bridges in more than 23 states in the US. Oklahoma, Texas, Arkansas, and Montana reported the highest usage of RRFC bridges (Wipf, et al. 1999). Since the late 1990s, several LVR county bridges in the State of Iowa have included RRFCs. The RRFC bridge concept involves using salvaged flatcars as bridge superstructure. RRFC bridges have advantages over conventional bridges including its low cost (less than one half the cost of a conventional concrete bridge structure), ease in installation, variable span length availability (20 to 80 ft), and low maintenance. Additionally, RRFC exhibits reliable structural performance because of its high torsional strength and stiffness in addition to the required flexural strength (Wipf et al. 1999). The viability of using RRFCs as an economical alternative for LVR bridges in Iowa through field testing on full scale projects was investigated in TR-421, TR-444, and TR-498 research projects sponsored by the Iowa DOT (Wipf et al. 1999, Wipf et al. 2003, and Wipf et al. 2007a). A RRFC superstructure bridge was recently incorporated in one of the sheet pile abutment projects (see Evans et al. 2012).

Wipf et al. (2007a) provide the following five criteria to assist in RRFC selection:

- **Structural Element Sizes, Load Distributing Capabilities, and Support Locations:** The RRFC should have a redundant cross-section or exterior girders with the ability to form a proper longitudinal flatcar connection (LFC) and adequate strength and stability at bearing locations.
- **Member Straightness/Damage:** Damaged or deformed members will not adequately

- carry or distribute loads. Visual inspection and string lines should be used to determine member straightness.
- Structural Element Connections: Choose welds over rivets since rivets lose strength over time. Welds must be checked for fatigue cracks.
 - Uniform Matching Cambers: For the transverse connection, the cambers of the two adjacent RRFCs must be within a tolerance of ± 1 in.
 - RRFC Availability: Use easily accessible RRFCs so more bridges can be built without additional design work.

Table 1 summarizes that maximum deflection and stresses in the RRFC bridges due to both dead and live loads (tandem axle test truck weighing around 48 to 53 kips) from Wipf et al. (2003) and (2007a). The deflections are compared with maximum allowable deflection (L/800) per AASHTO specifications (AASHTO 1996). Wipf et al. (2007) determined adjustment factors to correct the deflections measured by the rear tandem axle test truck to AASHTO (1996) specified test truck (HS-20 truck) which is a three axle truck weighing 72 kips with a maximum single axle weight of about 32 kips. The correction factors were based on mid span moments under HS-20 truck and the rear tandem axle test truck used in those studies. The adjusted maximum deflections exceeded the AASHTO allowable limits on three bridges (Table 1). Wipf et al. (2007) suggested that the AASHTO limit is an optional limit and not a strict requirement for legal bridges but is rather guidance.

Table 1. Summary of the load test results on different bridges from Wipf et al. (2003) and (2007)

Bridge Location	Maximum Deflection (in.)	Span Length (ft)	Allowable Deflection (in.)
<i>Wipf et al. (2003)</i>			
280 th Street, Buchanan County	0.37	56.0	0.84
Over North Fork Buffalo Creek, SE of Buffalo Center, Winnebago County	0.63	66.0	0.99
<i>Wipf et al. (2007)</i>			
290 th Street, Buchanan County	0.46*	54.0	0.81
270 th Street, Buchanan County	1.31*	66.2	0.99
460 th Street, Winnebago County	1.27*	66.3	1.00
Over Elk Creek, NE of Greeley, Delaware County	1.15*	66.3	1.00

*adjusted estimated deflections under the AASHTO specified HS-20 truck.

LABORATORY AND IN SITU TESTING METHODS

This chapter describes the laboratory and field testing methods and procedures followed in this research project. For tests where an American Standard for Testing and Materials (ASTM) standard was followed, that standard is simply referenced. Any deviations from the ASTM standard procedures are briefly described. For test methods where no ASTM standard is available or not followed, appropriate references are cited or the test procedure followed is briefly described.

Laboratory Test Methods

Soil Classification

Particle-size analysis tests were conducted on soil samples collected from soil borings in accordance with ASTM D422-63 “*Standard test method for particle-size analysis of soils*”. For the GRS fill material used under the bridge footing, particle-size analysis tests were conducted in accordance with ASTM C136-06 “*Standard test method for sieve analysis of fine and coarse aggregates*”. Atterberg limit tests (i.e., liquid limit—LL, plastic limit—PL, and plasticity index—PI) were performed in accordance with ASTM D4318-10 “*Standard test methods for liquid limit, plastic limit, and plasticity index of soils*” using the dry preparation method. Using the results from particle size analysis and Atterberg limits tests, the samples were classified using the unified soil classification system (USCS) in accordance with ASTM D2487-10 “*Standard practice for classification of soils for engineering purposes (Unified Soil Classification System)*” and American Association of State Highway and Transportation Officials (AASHTO) classification system in accordance with ASTM D3282-09 “*Standard practice for classification of soils and soil-aggregate mixtures for highway construction purposes*”.

Proctor Compaction Test

Standard and Modified Proctor compaction tests were conducted on GRS fill material in accordance with ASTM D698-07 “*Standard test methods for laboratory compaction characteristics of soil using standard effort (12,400 ft-lbf/ft³ (600 kN-m/m³)): Method C*” and ASTM D1557-09 “*Standard test methods for laboratory compaction characteristics of soil using modified effort (56,000 ft-lbf/ft³ (2,700 kN-m/m³)): Method C*”, respectively.

Direct shear (DS) tests were conducted on compacted sand foundation soil specimens from borings and GRS fill material. Tests were conducted in accordance with ASTM D3080-04 “*Standard test method for direct shear test of soils under consolidated drained conditions*”. For GRS fill material, DS tests were conducted in a 4 in. x 4 in. square mold using material passing the No. 10 sieve, per recommendations by Wu et al. (2006). Tests were conducted on compacted samples at three different applied normal stresses (5, 10, and 20 psi). The samples were saturated during the test. DS tests on foundation soils were conducted using a 2.5 in. diameter mold.

Unconfined compression (UC) tests were conducted on undisturbed Shelby tube samples collected from soil borings in accordance with ASTM D2166-06 “*Standard test method for unconfined compressive strength of cohesive soil*”.

Unconsolidated-undrained (UU) triaxial tests were conducted on compacted GRS fill material in accordance with ASTM D2850-03a “*Standard test method for unconsolidated-undrained triaxial compression test on cohesive soils*”. UU tests were conducted using 5 psi confining stress on specimens compacted to a target moisture content and dry unit weight based on field observations (samples were not back-saturated). The samples were compacted using vibratory compaction method as described in AASHTOT-307 (AASHTO 1999) for preparation of granular base/subbase materials. Prior to compaction, materials were moisture-conditioned and allowed to mellow for at least 3 to 6 hours. A 101.6 mm (4 in.) diameter split mold was used to compact the sample (Figure 8) in five lifts of equal mass and thickness using an electric rotary hammer drill and a circular steel platen placed against the material (Figure 9a). Calipers were used to verify consistent compaction layer thicknesses (Figure 9b). AASHTO T-307 procedure requires that the maximum particle size of the material should be 1/5th of the sample diameter, which is approximately 20.3 mm (0.8 in) for a 101.6 mm (4 in) diameter sample. Therefore, material retained over the 3/4” sieve was scalped off.



Figure 8. Split mold, steel platen (4 in. diameter), and vibratory hammer for compaction of granular materials

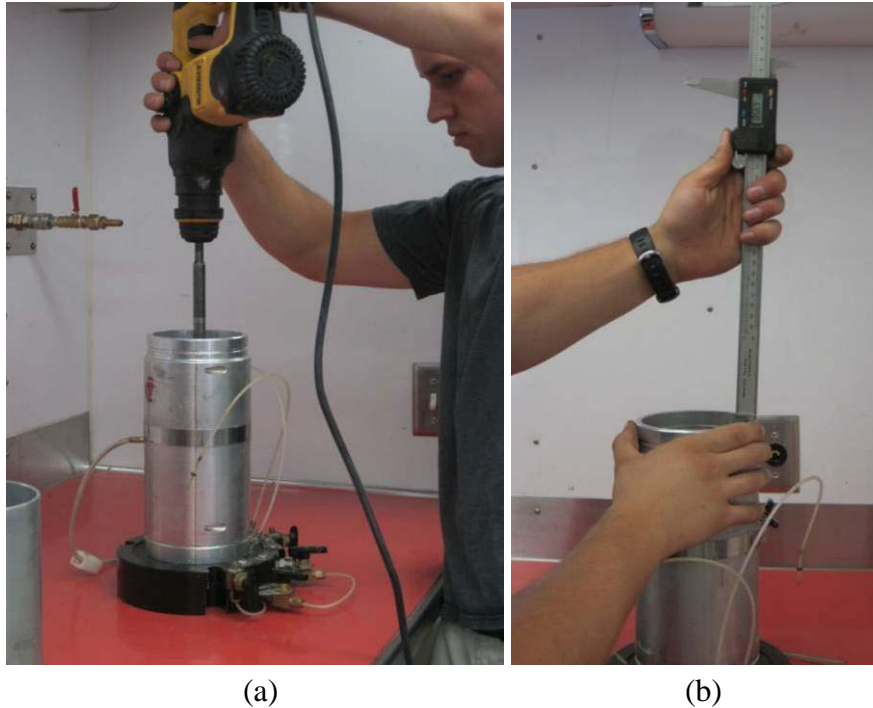


Figure 9. Sample preparation for triaxial testing: (a) compaction of sample in split mold and (b) lift thickness verification

Consolidated-drained (CD) triaxial tests were also conducted on compacted GRS fill material using three different confining stresses (5 psi, 10 psi, and 20 psi). The sample preparation process for CD tests was similar to the procedure described above for UU tests. The samples were compacted to a target moisture and dry unit weight based on field measurements. One set of CD tests were conducted on samples without geosynthetic in the sample, and another set on samples reinforced with one layer of geosynthetic placed at the center of the sample. These tests were conducted to determine the drained shear strength properties of both reinforced and unreinforced granular fill material. During the consolidation phase, a small axial load (about 20 to 30 lbs) was applied on the sample and the samples were allowed to consolidate for about 15 minutes before shearing the sample. The samples were sheared at a strain rate of about 0.4%/minute. Volume-change parameters were not monitored during the CD tests.

Cyclic Triaxial Testing

Repeated loading cyclic triaxial tests (70,000 cycles) were conducted on compacted granular fill material with and without geosynthetic in the sample to compare the permanent deformation behavior of these samples. Samples for this testing were prepared in the same manner as described above for UU and CD tests. Tests were conducted using the Geocomp[®] automated system (Figure 10). The system uses a real-time adjustment of proportional-integral-derivative (PID) controller to adjust the system control parameters as the stiffness of the specimen changes to apply the target loads during the test. The triaxial test chamber used in this study is shown in Figure 10. Two linear voltage displacement transducers (LVDTs) are mounted to the piston rod to measurement axial strains in the sample during the test.

Seven loading sequences, with 10,000 cycles in each sequence as shown in Table 2, were used during testing. Each load cycle consisted of a 0.1 second half-sine-shaped load pulse followed by a 0.9 second rest period. The confining stress was selected based on horizontal stress measurements in the field. The cyclic deviator stresses were selected such that the stress path approaches the static Mohr-Coulomb failure envelope. This is further explained in the Laboratory Test Results chapter of this report.



Figure 10. Triaxial chamber, load frame, and computer equipment for cyclic triaxial testing

Table 2. Loading sequences following in cyclic triaxial testing

Loading Sequence	Confining Stress, psi	Cyclic Deviator Stress, psi	Number of loading cycles
1	3	3	10,000
2	3	6	10,000
3	3	9	10,000
4	3	15	10,000
5	3	20	10,000
6	3	30	10,000
7	3	40	10,000

In Situ Testing

Soil Borings and Sampling

Soil borings were drilled with a truck-mounted rotary drill rig (see Figure 11) equipped with a hydraulic head, using continuous-flight solid-stemmed augers. Thin-walled shelby tube samples and bag samples were obtained from the soil borings. The shelby tube samples were obtained by hydraulically pushing a thin-walled seamless steel tube with a sharp cutting edge into the ground to obtain relatively undisturbed samples of cohesive or moderately cohesive soils. Where sandy soils were encountered, disturbed bag samples were obtained. Field logs were prepared on-site which included visual classifications of materials encountered during drilling as well as driller's interpretation of the subsurface conditions between samples.



Figure 11. Iowa State University truck-mounted rotary drill rig

Inclinometers

Inclinometers were installed in the ground to monitor lateral ground movements. Grooved inclinometer casings (3.34 in. diameter by 5 ft long) supplied by Durham Geo Slope Indicator (DGSI) were used in this study (Figure 12). The casings consisted of built-in couplings that snapped together with adjoining casing. The installation procedure involved: (a) drilling a soil boring, (b) filling the inclinometer casing with water and inserting the casing in the borehole, (c) filling the cavity around the casing with sand (Figure 13), and (d) sealing the top 1 foot of the cavity with cement grout. The inclinometer was filled with water prior to installation to

overcome buoyancy in the hole due to groundwater. DGSI's inclinometer probe was used to measure lateral ground deformations during and after construction. The probe operations and data calculations were performed in accordance with the manufacturer's recommendations.



Figure 12. Three 5 ft long inclinometer casings snapped together ready for installation



Figure 13. Sand used to fill the borehole cavity around the inclinometer

Earth Pressure Cells

Semiconductor and vibrating wire EPCs were used to monitor total vertical and horizontal stresses in the foundation soils. The semiconductor EPCs were used to measure dynamic stresses during construction and load testing by sampling at 100Hz. The semiconductor EPCs were also used to monitor stress in the long-term by obtaining one reading every 10 to 30 minutes. The vibrating wire EPCs were used to monitor stresses in the long-term during and after construction by obtaining one reading every 10 to 30 minutes.

Model 3510 0-60 psi range semiconductor EPCs , Model 4800 0-25 psi vibrating wire EPCs, and Model 4810 0-60 psi vibrating wire EPCs manufactured by Geokon® were used in this study. All the EPCs are 9 in. diameter circular shaped sensors constructed from two stainless steel plates welded together around the periphery with a narrow spaced filled with de-aired hydraulic oil. The hydraulic oil is connected to a pressure transducer where the oil pressure is converted to an electrical signal which is transmitted through a signal cable to the data logger. The Model 3510 and Model 4810 cells are “fat back” cells with thicker plates than found in the Model 4800 cells and are specifically designed to measure soil pressures against structures. All the EPCs were installed with a 2 in. thick layer of sand around the cells (Figure 14).

The semiconductor EPCs used in this study had 0 to 5 volts (V) dynamic readout capability. A gage factor calibration was provided by the manufacturer for the semiconductor EPCs as shown in Eq. 4.

$$\text{Total Stress} = 11.603 \text{ psi/V} \quad (4)$$

The voltage readings in the semiconductor EPCs are sensitive to temperature fluctuations. Therefore, temperatures were monitored using the thermistor equipped on each EPC. The thermistor gives a varying resistance output as the temperature changes. The resistance values were recorded and then converted to temperatures in Centigrade using Eq. 5 per manufacturer recommendations (Geokon 2007).

$$T = \frac{1}{A + B(\ln R) + C(\ln R)^3} - 273.2 \quad (5)$$

where, T = Temperature in °C, lnR = natural log of thermistor resistance, A = 1.4051×10^{-3} , B = 2.369×10^{-4} , C = 1.019×10^{-7} (note A, B, and C are coefficients calculated over the -50 to +150°C span).

After determining the temperatures, the total stress values were corrected using Eq. 6 per manufacturer recommendations (Geokon 2007):

$$\text{Corrected Total Stress, P (psi)} = (V_i - V_0) + K (T_0 - T_i) \quad (6)$$

where, V_i = current voltage reading, V_0 = initial voltage reading, T_0 = initial temperature (before placed in the ground), T_i = current temperature, K = temperature correction constant = 0.69 for cells embedded in fill and 1.38 for contact cells placed under concrete.



(a)



(b)

Figure 14. (a) Model 3510 semiconductor EPC installation to measure total vertical stresses, and (b) Model 4800 vibrating wire EPC installation to measure horizontal stresses

The vibrating wire EPCs used in this study provided a frequency output in Hz. The recorded frequency values were converted to “Digits” using Eq. 7 and then converted to total stress using Eq. 8:

$$\text{Digits, } D = \text{Hz}^2/1000 \quad (7)$$

$$\text{Total stress} = (D_0 - D_i) \times \text{CF} \quad (8)$$

where, D_0 = initial digits reading, D_i = current digits reading, CF = calibration factor. CF’s were provided by the manufacturer for each vibrating wire sensor.

Similar to the semiconductor EPCs, the vibrating wire readings are also sensitive to temperature fluctuations. Therefore, temperatures were monitored using the thermistor equipped on each EPC recording resistance and converting them to temperatures using Eq. 5 as previously described. After determining the temperatures, the total stress values are corrected using Eq. 9, and a temperature calibration factor, K, which is provided for each sensor by the manufacturer (Geokon 2010):

$$\text{Corrected Total Stress, } P \text{ (psi)} = (D_0 - D_i) \times \text{CF} + (T_i - T_0) \times K \quad (9)$$

Piezometers

Vibrating wire piezometer sensors were used to monitor pore water pressures in the foundation soils at different depths, by obtaining one reading every 2 to 30 minutes. Model 4500AL 0-25 psi and Model 4500S 0-51 psi manufactured by Geokon were used in this study. The piezometer utilizes a sensitive stainless steel diaphragm to which a vibrating wire element is connected. When in use, the changing pressures on the diaphragm cause it to deflect, and this deflection is measured as a change in tension and frequency of vibration of the vibrating wire element. The square of the vibration frequency is directly proportional to the pressure applied to the diaphragm (Geokon 2009). The readings and calculations to calculate stress from piezometers are the same as described above for vibrating wire EPCs. Calibration factors for digits and temperature are provided separately for each sensor by the manufacturer. An initial zero reading was established prior to installation of the piezometers following the manufacturer’s recommendations (Geokon 2009). The procedure involved placing the piezometer in a bucket of water for about 15 minutes for the temperature to stabilize, lifting the piezometer out of the water, and then immediately taking the frequency and temperature readings. After establishing the initial readings, each piezometer sensor was carefully wrapped in a cotton rag filled with sand, the cable was zip tied to a plastic tube to ensure vertical installation, and the sensor was then lowered down the borehole to the desired depth. The borehole was backfilled with sand up to about 1.5 to 2 ft above the piezometer depth, and then filled with bentonite chips up to the surface to seal the borehole.

On-Site Data Recording

The semiconductor EPC, vibrating wire EPC, and vibrating wire piezometer readings were recorded using a weather resistant (-15°F to +122°F) Campbell Scientific CR5000 data logger system with piezoelectric and vibrating wire data logging components and 2GB data storage (Figure 15). The datalogger was secured in a weather resistant enclosure and was powered by a battery that was charged through a 70 watt solar panel. A Raven XTV cellular digital modem was attached to the datalogger. The datalogger was programmed to continuously record and store the data, and wirelessly transfer the data to the internet through the cellular phone modem.



Figure 15. On-site datalogger system installed to continuously record EPC and piezometer readings

Nuclear Gauge

A Humboldt nuclear moisture-density gauge (NG) device was used to obtain moisture and dry unit weight measurements during compaction of GRS fill material. Tests were conducted in general accordance with ASTM D6938-10 “*Standard test method for in-place density and water content of soil and soil-aggregate by nuclear methods (shallow depth)*”. All measurements were obtained using a probe penetration depth of about 6 inches.

Light Weight Deflectometer

Light weight deflectometer (LWD) tests were conducted on GRS fill material during compaction of each lift to determine elastic modulus. The LWD used in this study was manufactured by Zorn and was setup with 300 mm diameter plate and 71 cm drop height (Figure 16). The tests were performed following manufacturer recommendations (Zorn 2003) and the elastic modulus values were determined using Eq. 10:

$$E_{LWD} = \frac{(1 - \eta^2) \sigma_0 r}{D_0} \times F \quad (10)$$

where, E_{LWD} = elastic modulus (MPa), D_0 = measured deflection under the plate (mm), η = Poisson's ratio (0.4), σ_0 = applied stress (MPa), r = radius of the plate (mm), F = shape factor depending on stress distribution (assumed as 8/3) (see Vennapusa and White 2009).



Figure 16. LWD testing during placement of GRS fill material

Live Load Testing and Settlement Monitoring

Bridge live load (LL) tests involved driving a loaded test truck with single axle at front and tandem axle in the back of known weight and axle spacing over the bridge and taking EPC readings by placing the truck (Figure 17) at specified locations along the bridge. The data obtained were used in bearing capacity analysis and also to compare with the estimated values. In addition, the loaded truck was placed at the center of the bridge and deflection of the bridge was measured using total station survey equipment. Bridge abutment elevations were also monitored using the total station survey equipment, by using two on-site benchmarks (nail placed on wooden electric poles).



Figure 17. Loaded truck used for live load testing and total station equipment used for bridge deflection measurement under loading.

RESULTS AND ANALYSIS FROM FIELD PROJECTS

Two field demonstration projects were conducted as part of this research study. The first project (Bridge 1) commenced prior to initiation of this research project; however, project information was provided by the Buchanan County Engineer and is included in this report. No instrumentation or testing was performed by the ISU research team on this project. The research team's assessment of photos taken during construction, bridge abutment settlement data, and field visits, are provided in this chapter. Testing at the second project (Bridge 2) involved soil borings, in situ testing during construction, laboratory testing of materials obtained from the project site, instrumentation installation, and bridge LL testing after construction, and performance monitoring. Laboratory and in situ test results from the project, detailed analysis of the results, and findings from the analysis are presented in this chapter.

Bridge 1 — Olympic Avenue, Buchanan County, Iowa

Project Overview

This demonstration project is located on Olympic Avenue about ¼ miles north of 192nd street, north east of Independence, Iowa (Figure 18). Construction of the new bridge was completed by Buchanan County field personnel. The bridge involved replacing the existing timber abutment back wall with a GRS bridge abutment with flexible wrapped geosynthetic facing to support a 73 ft RRFC bridge which was placed on a reinforced concrete spread footing. Pictures taken during construction, construction and material costs, and bridge abutment settlement monitoring data were provided by the Buchanan County Engineer. A summary of the new bridge construction details based on review of photos, discussions with the County Engineer, and field visits, cost information, and the research teams' assessment are provided in the following subsections of this chapter.

New Bridge Construction Details and Cost

A rough cross-sectional view of the new bridge abutment is presented in Figure 19. The bridge construction commenced with removal of the existing timber abutment back wall (Figure 20). The backfill material around the existing abutment was excavated back on each side of the bridge to match with the designed alignment. Excavation was performed using a John Deere 200LC hydraulic excavator.

Mirafi® 500X woven geosynthetic supplied by Northern Iowa Construction Products was used as the geosynthetic reinforcement in the fill material. According to the manufacturer, the geosynthetic material is composed of high-tenacity polypropylene yarns woven into a stable network and is inert to biological degradation and resistant to naturally encountered chemicals, alkalis, and acids (www.tencate.com). The ultimate tensile strength, T_f , of this geosynthetic material is about 1200 lbs/ft in machine direction and 1440 lbs/ft in cross-machine direction, per manufacturer's technical data sheet (see Appendix A). The T_f value of this geosynthetic product is lower than the minimum recommended value by Adams et al. (2011b), which is 4,800 lbs/ft.

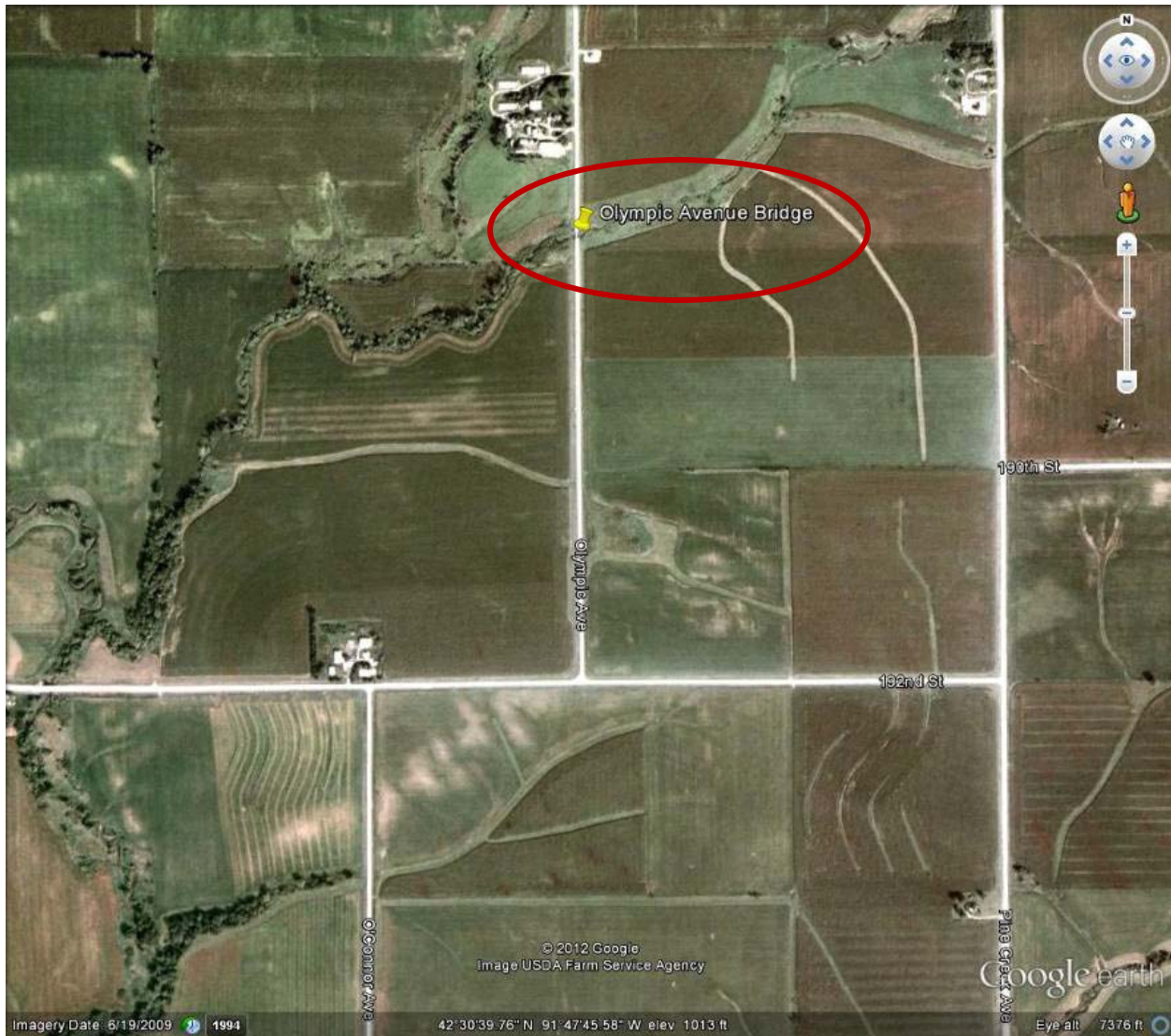


Figure 18. Bridge 1 — Olympic Avenue project location in Buchanan County, Iowa

The geosynthetic was spread in the bottom of the excavation, crushed granular fill material was placed over the geosynthetic, and the fill was compacted using a vibratory plate attached to the excavator. The geosynthetic was installed by rolling out the material in the machine direction perpendicular to the bridge alignment. The geosynthetic was wrapped over the compacted fill, a new geosynthetic layer was placed, and then a new layer of fill was placed over the geosynthetic layers. A GEHL 3935 skid steer loader was used to spread the fill material over the geosynthetic layers. The loose lift thickness was targeted to be about 8 in. and compacted thickness was targeted to be about 7 in. Lift thickness was checked using a laser survey level during placement and compaction. Pictures of the construction operations are shown in Figure 21 and Figure 22. The backfill material behind the concrete footing footprint was also filled with GRS fill material (Figure 23). Pictures of the final wrapped around face slopes of the north and south abutments are shown in Figure 24. Excavation was performed at the toe of the north and south abutment slopes to install a rock fill wall for erosion protection (Figure 25). Rip rap was installed over the geosynthetic wrapped faces as scour protection during flooding (Figure 26) and cement grout

was placed over the rip rap to help seal the voids in the riprap (Figure 27). Reinforcement and form work for a 3 ft wide concrete spread footing was placed over the GRS fill material (Figure 28 and Figure 29). Three 73 ft long RRFC bridges were used for the bridge (Figure 30 and Figure 31). Cranes were used on both abutment sides to install the RRFCs over the footing. 5/8 in. diameter bolts were used to connect the RRFCs at the bottom webs.

About 6 in. of crushed rock was placed over the bridge to finish the road. Steel guard rails were installed on both sides of the bridges. Pictures of the finished bridge are shown in Figure 32. Maximum flood water level during the summer 2010 flooding was at about 6 ft below the road elevation at this bridge location, which is at about the mid height of the GRS abutment (Figure 32). Reportedly, similar flood water elevations were observed during the summer 2011 flooding. Pictures of the abutments taken in September 2011 are shown in Figure 33, which indicated that the riprap facing installed for scour protection was still intact.

A summary of the bridge construction costs is provided in Table 3. The total cost for bridge construction at this site was less than \$50k, and the construction costs of a conventional reinforced concrete abutment system with a concrete bridge at this site would be \$105k to 130k. The cost of this bridge was about 50% to 60% lower than using conventional methods, which presented a significant cost saving to the County.

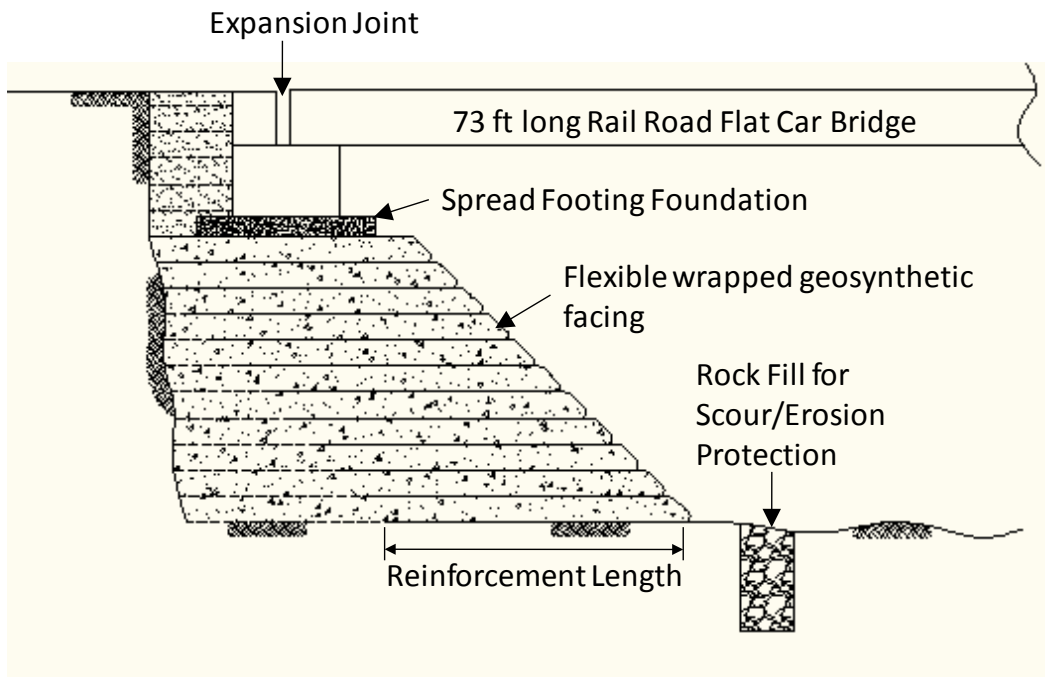


Figure 19. Bridge 1 — Schematic of GRS bridge abutment with geosynthetic wrapped sheets flexible facing



Figure 20. Bridge 1 — Pictures of the project site after removing the existing bridge abutments (Courtesy of Brian Keierleber)



Figure 21. Bridge 1 — Building up of GRS fill material (Courtesy of Brian Keierleber)



Figure 22. Bridge 1 — Compaction of GRS fill material (Courtesy of Brian Keierleber)



Figure 23. Bridge 1 — Building up of GRS fill material behind the footing (Courtesy of Brian Keierleber)



Figure 24. Bridge 1 — Pictures of north (top) and south abutments built up with flexible wrapped around facing (Courtesy of Brian Keierleber)



Figure 25. Bridge 1 — Excavation at the toe to install erosion stone (Courtesy of Brian Keierleber)



**Figure 26. Bridge 1 — Installation of riprap over the flexible geosynthetic wrapped facing
(Courtesy of Brian Keierleber)**



**Figure 27. Bridge 1 — Installing cement grout over riprap facing for scour protection
(Courtesy of Brian Keierleber)**



Figure 28. Bridge 1 — Leveling pad install concrete footing reinforcement (Courtesy of Brian Keierleber)



Figure 29. Bridge 1 — Installation of reinforced concrete footing (Courtesy of Brian Keierleber)



Figure 30. Bridge 1 — Installation of RRFC bridges (Courtesy of Brian Keierleber)



Figure 31. Bridge 1 — Installation of RRFC bridges (contd.) (Courtesy of Brian Keierleber)



Figure 32. Bridge 1 — Pictures of the completed bridge (7/27/2010)



Figure 33. Bridge 1 — Condition of riprap one year after construction (9/8/2011)

Table 3. Bridge 1 — Construction costs

Description	Unit Cost (USD)	Quantity	Total Cost (USD)
Geosynthetic Material	\$400/roll	4	\$1,600.00
Crushed Rock	\$6.95/ton	472.25	\$3,282.18
Rip Rap	\$8.50/ton	26.36	\$224.23
Erosion Stone	\$11.60	12.96	\$150.34
2500 lb Concrete Mix	\$90/yd ³	20	\$1,800.00
Labor (6 crew members) ¹	\$26/hr	16 hrs	\$2,496.00
Railroad flat cars	\$13,000/each	3	\$39,000
Total:			\$48,553

¹Number of crew members and total man hours estimated from information provided for Bridge 2.

Abutment Settlement Monitoring Results

The bridge abutment elevations were monitored by Buchanan County personnel, from shortly after construction (06/24/2010) to about 1 year 2 months after construction (09/06/2011). The elevations were obtained on top of the north and south abutment footings from south west (SW), north west (NW), north east (NE), and south east (SE) corners. The results of change in elevations with time are shown in Figure 34. The results indicate that the maximum settlement is observed at the north abutment. The average settlement of the north abutment footing was about 0.7 in., and the average settlement of the south abutment footing was about 0.4 in. No transverse differential settlement was observed at either abutment at the conclusion of the monitoring phase. Settlements less than 1 in. are considered acceptable for these bridges.

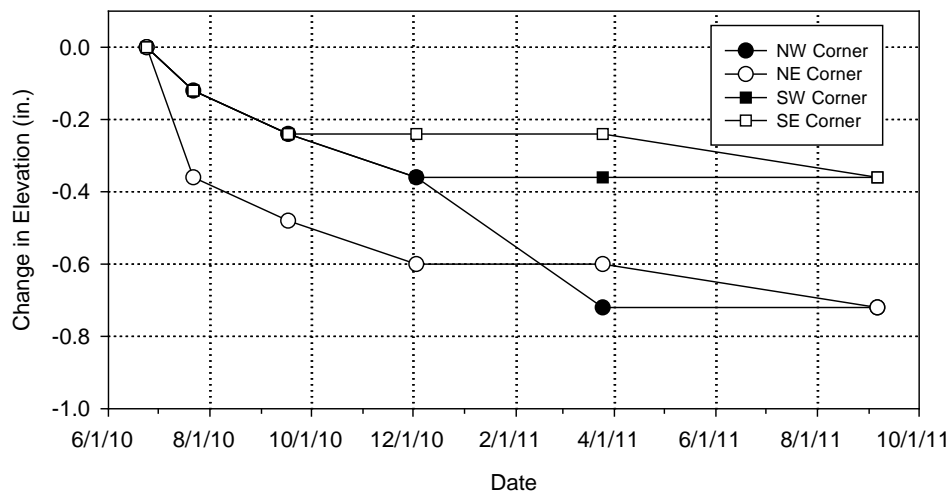


Figure 34. Bridge 1 — Abutment settlement readings

Bridge 2 — 250th Street, Buchanan County, Iowa

Project Overview

This demonstration project is located on 250th street about ¼ mile east of County Road W40 in Buchanan County, Iowa (see Figure 35). The existing bridge at the site was reportedly about 90 years old. The existing steel bridge was about 35 ft long and was supported on concrete abutments. Pictures of the existing bridge are shown in Figure 36. Cracks were observed on the north side of the east abutment (Figure 37). Reportedly, the flood waters reached the bottom of the bridge deck during the summer 2010 flooding. The new bridge was constructed by raising its top surface elevation by about 1.6 ft. RRFCs were used for the new bridge and were supported on concrete footings founded on GRS fill material. Additional details of the new bridge construction are provided in the following section of this report. The new bridge construction was performed by Buchanan County field personnel. The ISU researchers were present on-site during construction to observe construction operations, conduct subsurface exploration using soil borings, and install instrumentation (EPCs, inclinometers, and piezometers). Bridge construction and instrumentation installation activities were performed between September 21, 2010 and October 18, 2010.



Figure 35. Bridge 2 — 250th street project location in Buchanan County, Iowa



Figure 36. Bridge 2 — Pictures of the existing 250th street bridge



Figure 37. Bridge 2 — Cracks observed on the east abutment wing wall

New Bridge Construction Details and Cost

A plan view of the abutments for the new RRFC bridge is presented in Figure 38. On both east and west abutments, at about 11 ft away from the existing concrete abutment wall, about 7.4 ft wide x 4.6 ft deep trench was excavated to install GRS fill material as a foundation to support the new footings. A cross-sectional view on the east abutment side of the bridge is shown in Figure 39. Just prior to excavation, sheet piling was installed on the north and south sides of the excavations as scour protection for the GRS fill material. Excavation was performed using a John Deere 200LC hydraulic excavator. Pictures taken during the sheet pile installation and the excavation process are shown in Figure 40 to Figure 42. The 4.6 ft excavation depth was determined by the Buchanan County engineer to ensure the fill extends down to below frost depth, which is approximately 4 ft in the region (based on frost-depth contour map provided in Bowles 1996).

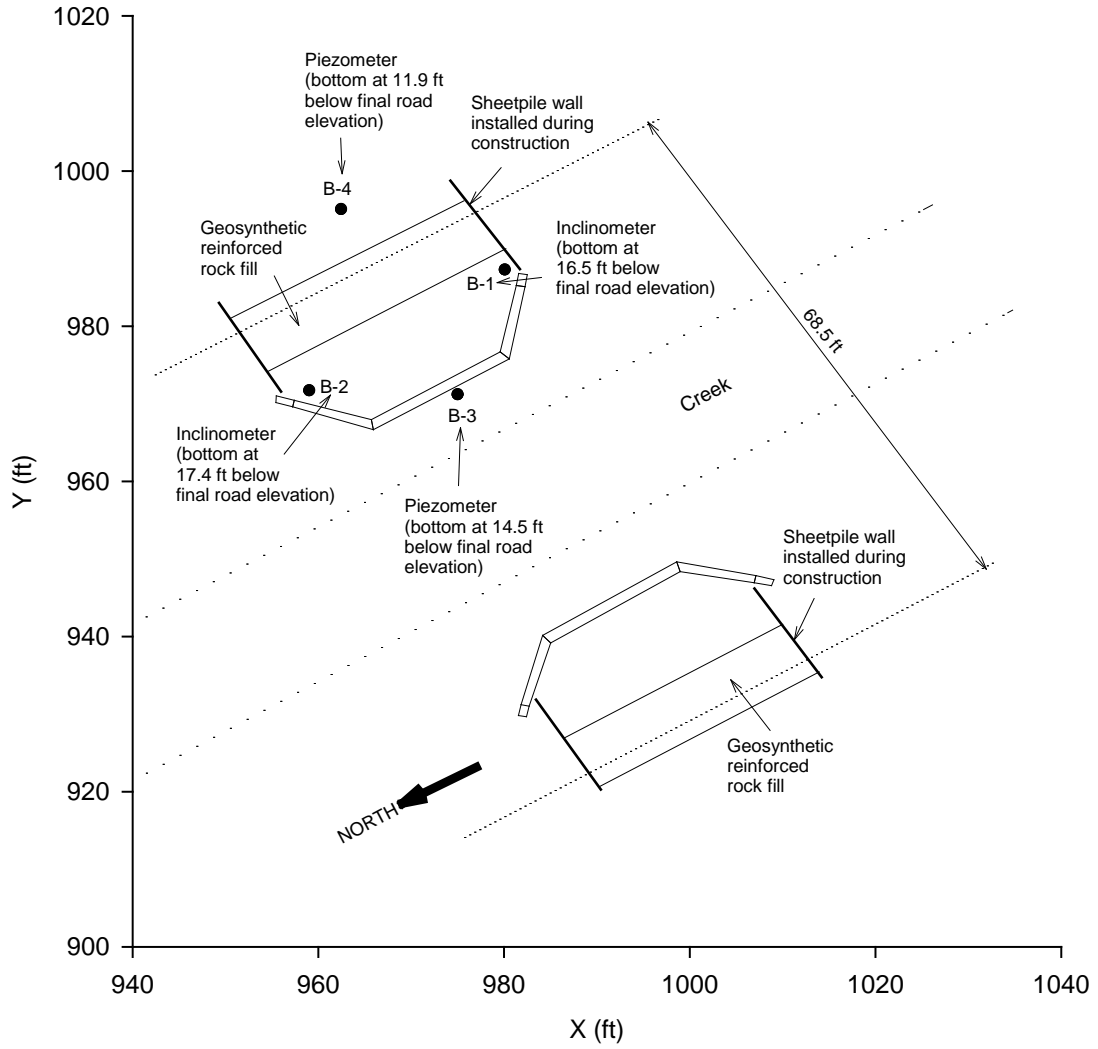


Figure 38. Bridge 2 — Plan view of the bridge abutments prepared for installation of the new RRF bridge

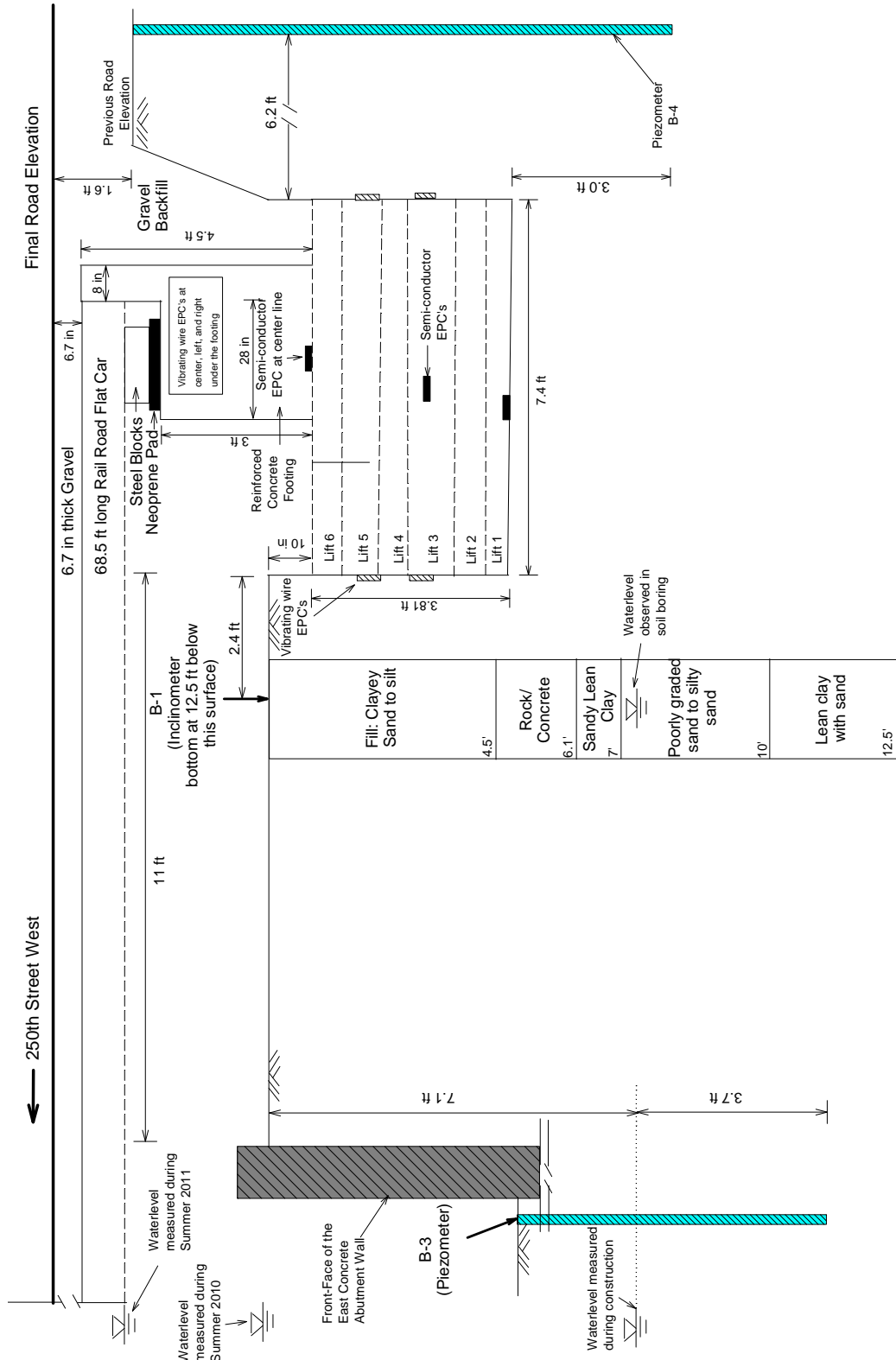


Figure 39. Bridge 2 — Cross-sectional view on the east abutment side of the bridge, subsurface soil profile, piezometer locations, details of GRS fill material, and EPC locations in GRS fill material



Figure 40. Bridge 2 — East and west abutments after removing the existing bridge



Figure 41. Bridge 2 — Installation of sheet piles on the north and south sides of each abutment for scour protection



Figure 42. Bridge 2 — Excavation of a trench to place GRS fill material to support the bridge concrete footing

Mirafi® 500X woven geosynthetic, similar to the one used in Bridge 1, was used as the geosynthetic reinforcement in the fill material on this project. The geosynthetic was spread in the bottom of the excavation, crushed granular fill material was placed over the geosynthetic, and the fill was compacted using a vibratory plate attached to the excavator. The geosynthetic was cut to about 12.5 ft wide x 32 ft long and the excess geosynthetic on the edges was used to wrap over the surface of each lift. The loose lift thickness was targeted to be about 8 in. and compacted thickness was targeted to be about 7 in. Lift thickness was checked using a laser survey level during placement and compaction. Pictures of the construction operations are shown in Figure 43 to Figure 45. The fill was placed in six lifts and the final thickness of the GRS fill material was about 3.8 ft.

A 3 ft wide reinforced concrete spread footing was placed on the GRS fill material. The footing cross-section is shown in Figure 39. The trench behind the footing was backfilled with crushed granular fill material up to the existing surface. About 1 in. thick neoprene pads were placed on the footing to seat the RRFCs (Figure 46). Three 8.6 ft wide x 68.5 ft long RRFCs weighing about 40,000 lbs (email communication with Brian Keierleber, Buchanan County Engineer) each were used for the bridge (Figure 47, Figure 48). Cranes were used each end of the bridge to install the RRFCs on the footings. W-sections were placed under the RRFCs on footings for additional support (Figure 49). Bolts (5/8 in. diameter at approximately 5 ft centers) were used to connect the RRFCs at the bottom webs (Figure 50). About 6.7 in. of crushed rock was placed over the bridge to finish the road, and steel guard rails were installed on both sides of the bridges. A picture of the finished bridge is shown in Figure 51. A summary of the construction event timeline is provided in Table 4, and a summary of the bridge construction cost is provided in Table 5. The total cost of the bridge construction was about \$43k, which is slightly lower than Bridge 1 due to the lower amount of granular fill and geosynthetic materials used at this site.

Instrumentation installation and in situ testing activities during construction was focused on the east abutment side of the bridge. Soil borings were obtained from four locations (B-1 to B-4) and the locations are shown in Figure 38. The instrumentation included installing inclinometers and piezometers in the ground, and semiconductor and vibrating wire EPCs in the GRS fill material. Inclinometers were installed at B-1 and B-2 to monitor lateral ground movements during and after construction, and piezometers were installed in B-3 and B-4 to monitor pore water pressures in the foundation soils.

The self weight of the RRFC, gravel surfacing, guard rail, and reinforced concrete footing were estimated to determine the total dead load stress under the concrete footings (Table 6). The self weight of gravel surfacing was estimated assuming a total unit weight of 130 lb/ft³, guard rail was estimated assuming 100 lb/ft (from Wipf et al. 2007), and the reinforced concrete footing was estimated assuming a total unit weight of 150 lb/ft³. Using these values, the total contact stress under the footing due to dead load is estimated at 2,120 psf.

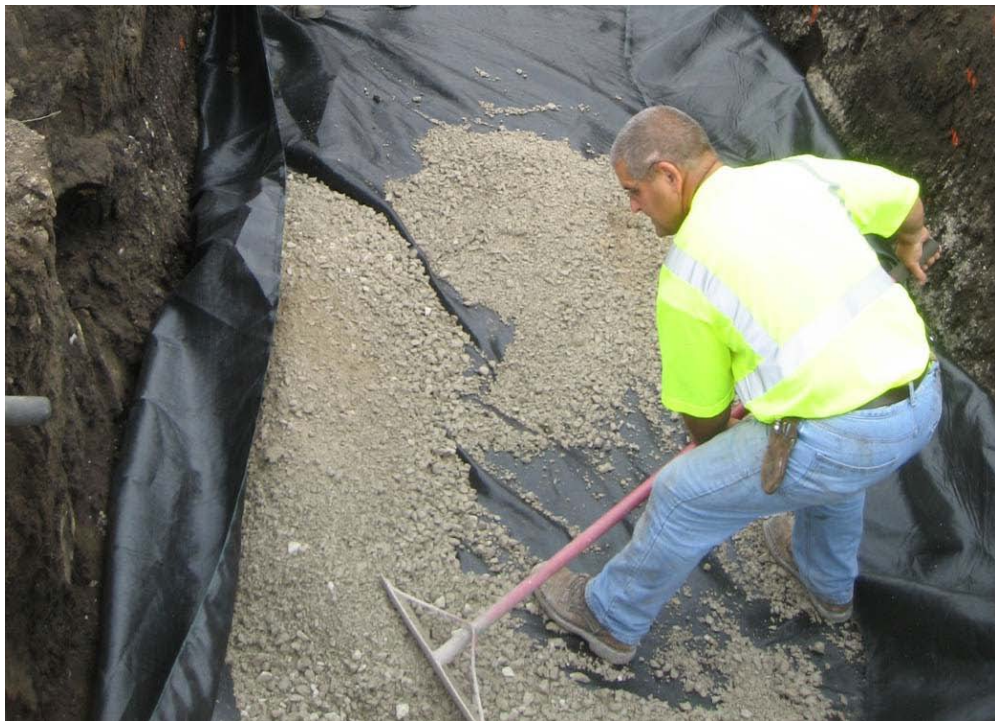


Figure 43. Bridge 2 — Placement of geosynthetic layer at bottom of excavation and granular fill over the geofabric



Figure 44. Bridge 2 — Placement and compaction of granular fill over geosynthetic layer using vibratory plate



Figure 45. Bridge 2 — Lift thickness control using laser measurement



Figure 46. Bridge 2 — 1 inch thick neoprene pads placed over the footing prior to placement of the flat cars



Figure 47. Bridge 2 — Placement of RRFCs on the footings



Figure 48. Bridge 2 — Picture of all three RRFCs placed on the footings



Figure 49. Bridge 2 — W-sections confined with inverted channel sections placed between the footing and the RRFCs



Figure 50. Bridge 2 — Bolted connections every 5 ft between the RRFCs



Figure 51. Bridge 2 — Picture of the completed bridge

Table 4. Bridge 2 — Construction events and ISU field instrumentation installation/testing timeline

Event	Date(s)
Removal of existing bridge	9/20/2010
Sheetpile installation, excavation, and GRS fill material placement in excavation on West Abutment	9/21/2010
Soil borings, and inclinometers/piezometers installation, and inclinometer readings	9/22/2010
Sheetpile installation and excavation on East Abutment ¹	
Fill placement in East Abutment, EPC installation and data recordings in GRS fill material, and inclinometer readings	9/23/2010
Datalogger installation on-site	9/28/2010
EPC installation under footing	10/06/2010
Concrete footing installation and backfill placement	10/07/2010
Backfill placement and installation of RRFCs and inclinometer readings	10/15/2010
Aggregate surfacing on the bridge, road leveling, guard rail placement	Intermittently from 10/16/2010 to 10/29/2010
Bridge live load testing, abutment settlement monitoring, inclinometer readings	10/29/2010
	12/10/2010
	10/20/2011

¹Fill placement could not be completed due to instrumentation installation and inclinometer data recordings

Table 5. Bridge 2 — Construction costs

Description	Unit Cost (USD)	Quantity	Total Cost (USD)
Geosynthetic Material	\$0.70/yd ²	533.3 yd ²	\$373.00
Crushed Rock (for excavation)	\$7.00/ton	156 tons	\$1,088.60
Labor (6 crew members) ¹	\$26/hr	16 hrs	\$2,496.00
Railroad flat cars	\$12,500/each	3	\$37,500.00
Crushed Rock (for backfill + road surfacing ²)	\$7.00/ton	160 tons	\$1,120.00
Total:			\$42,577

¹Number of crew members and total man hours were provided by Buchanan County Engineer

²Estimated assuming gravel surfacing over the bridge plus extending 20 ft on both sides of the bridge

Table 6. Bridge 2 — Summary of dead loads on the bridge

Description	Total Load (kips)
Railroad flat cars ¹ = 40,000 lbs each x 3	120.0 kips
Guardrail ² = 100 lbs/ft x 68.5 ft x 2	13.7 kips
Concrete Footings ³ (2) = 2 x 150 lb/ft ³ x (3 ft x 3 ft + 0.67 ft x 1.5 ft) x 27 ft	81.0 kips
Gravel Surfacing ⁴ = 130 lb/ft ³ x (0.56 ft x 25.8 ft x 68.5 ft)	128.6 kips
Total dead load under the footing = (120.0 + 13.7 + 81.0 + 128.6) kips/2	171.7 kips
Total contact stress under footing = 171.7 kips/(3 ft x 27 ft)	2.120 ksf

¹Measured values provided by Buchanan County Engineer

²From Wipf et al. (2007)

³Reinforced concrete unit weight assumed as 150 lb/ft³

⁴Gravel total unit weight assumed as 130 lb/ft³

Subsurface Soil Conditions and Water Level Observations

A total of four soil borings (B-1 to B-4) were drilled on the east abutment side of the bridge. Boring logs and samples were obtained only from B-1 and B-2. B-3 and B-4 borings were drilled to a desired depth only to make a cavity in the ground to install piezometers. A plan view of the boring locations is shown in Figure 38.

B-1 and B-2 are located on the south and north sides of the east abutment, respectively, within about 1 to 3 ft of the excavation limits. These borings were drilled prior to sheet pile installation and excavation. After soil sampling from these borings, inclinometers were installed. Logs of B-1 and B-2 are shown in Figure 52 and Figure 53, respectively. The logs show the soil layers encountered in the borings, type of samples taken from different depths (ST – shelly tube, B – bag sample, PA – power auger), laboratory test results including USCS soil classification (from grain size analysis and Atterberg limits) and visual soil classification, moisture content, dry unit weight, unconfined compressive (UC) strength, Atterberg limits (LL – liquid limit, PI = plasticity index), effective cohesion (c'), and effective angle of shearing resistance (ϕ').

Existing fill consisting of dark brown to clayey sand to silt was encountered from the existing grade to about 4.5 to 5 ft below grade. Dry unit weight and moisture content measurements from undisturbed ST samples indicated that the fill material was non-uniform with moisture contents varying from about 20% to 26%, dry unit weight varying from about 83 pcf to 103 pcf, and UC strength varying from about 515 psf to 3152 psf. A layer of rock or concrete was encountered below the fill layer to about 6 to 6.1 ft below grade. This layer is likely the foundation beneath the existing concrete abutment wall.

LOG OF BORING NO. 1											
CLIENT		Iowa DOT/Buchanan County		PROJECT NAME		GRS for LVR Bridge Abutments					
SITE		250th Street		PROJECT NUMBER		TR621					
Depth, ft	Boring located on the south side of the east abutment.	DESCRIPTION	USCS SYMBOL	NUMBER	TYPE	RECOVERY, in.	SPT-N BLOWS / ft.	WATER CONTENT, %	DRY UNIT WEIGHT, pcf	UNCONFINED STRENGTH, psf	OTHER
			4.5	FILL: CLAYEY SAND TO SILT, Dark Brown to Brown	SC	1	ST	12		20.1	102.6
	SC	2	ST		16		20.6	102.6	1839	NP	
	ML	3 4	ST		16		26.1 21.8	82.9 98.9	515 797		
5		ROCK/CONCRETE			PA						
6.1											
7		SANDY LEAN CLAY, Brown	CL	5	ST	16	24.0	100.0	564		
			SP	6							
10		POORLY GRADED SAND TO SILTY SAND, Dark Brown to Brown	SM	7	B					c' = 196 psf, ϕ' = 44° (*)	
10											
12.5		LEAN CLAY WITH SAND, Brown Gray (with occasional sand seams)	CL	8	ST	12		20.1	107.5	2875	
			CL	9	B						
15		BOTTOM OF BORING									
		* Sample compacted to dry density = 114 pcf and saturated									
The stratification lines represent the approximate boundary lines between soil and rock types; in-situ, the transition may be gradual.							c' = Effective Cohesion and ϕ' = Effective Friction Angle, LL = Liquid Limit, PI = Plasticity Index				
		WATERLEVEL OBSERVATIONS, ft			BORING STARTED		09/22/10	LOGGED BY		PV	
		WL \simeq 7.5 ft			BORING COMPLETED		09/22/10	RIG		ISU DRILL RIG	
					DRILLED BY		HG	APPROVED BY		PV	

Figure 52. Bridge 2 — Log of boring B-1

LOG OF BORING NO. 2											Page 1 of 1		
CLIENT		Iowa DOT/Buchanan County			PROJECT NAME		GRS for LVR Bridge Abutments						
SITE		250th Street			PROJECT NUMBER		TR621						
Depth, ft	Boring located on the north side of the east abutment.												
	DESCRIPTION			USCS SYMBOL	NUMBER	TYPE	RECOVERY, in.	SPT-N BLOWS / ft.	WATER CONTENT, %	DRY UNIT WEIGHT, pcf	UNCONFINED STRENGTH, psf	OTHER	
5	5	FILL: CLAYEY SAND TO SILT, Dark Brown to Brown			SC	1	ST	16		24.9	95.5	2604	
					SC	2	ST	16		24.2	101.3	3152	
					ML		B			22.1			LL = 49, PI = 18
6	6	ROCK/CONCRETE											
7	7	SANDY LEAN CLAY, Brown			CL	3	ST	12		23.4	98.0	654	c' = 305 psf, φ' = 15° (*)
10	10.5	CLAYEY SAND TO SILTY SAND, Dark Brown to Brown					PA						
					SC	4	B			21.0			LL = 36, PI = 18
					SM	5	B			21.5			
13	13	LEAN CLAY WITH SAND, Brown Gray (with occasional sand seams)			ML	6	B			20.2			LL = 24, PI = 7
							PA						
15	15	BOTTOM OF BORING											
			* Sample compacted to dry density = 100.1 pcf and saturated										
The stratification lines represent the approximate boundary lines between soil and rock types; in-situ, the transition may be gradual.								LL = Liquid Limit, PI = Plasticity Index					
		WATERLEVEL OBSERVATIONS, ft			BORING STARTED		09/22/10	LOGGED BY		PV			
		WL ∇ 8.0 ft			BORING COMPLETED		09/22/10	RIG		ISU DRILL RIG			
					DRILLED BY		HG	APPROVED BY		PV			

Figure 53. Bridge 2 — Log of boring B-2

Below the rock/concrete layer, a layer of sandy lean clay with sand seams was encountered to a depth of about 7 ft. UC test of one undisturbed sample obtained from this layer indicated an undrained strength of about 564 psf. This value was considered low due to predominant amount of sand seams present in the sample and the effect of no confinement during UC testing. Therefore, a direct shear test was conducted on a sample compacted to about 100 pcf at its natural moisture content to determine c' and ϕ' . The c' and ϕ' values for the sandy lean clay layer are summarized in the B-2 boring log.

Below the sandy lean clay layer, clayey sand to poorly graded sand to silty sand layers were encountered down to about 10 to 10.5 ft below grade, underlain by lean clay with sand down to the boring termination depths of about 12.5 to 13 ft below grade. The sand layers were wet with moisture contents varying from about 21% to 24%. Direct shear test was conducted on one sample by compacting the specimen at its natural moisture content to determine c' and ϕ' . The compacted dry density of the specimen was about 114 pcf. Results of direct shear test results on the sand soil are presented in B-1 boring log.

Groundwater levels were encountered at about 7.5 ft and 8.0 ft below grade in B-1 and B-2, respectively, at the time of drilling. Piezometers were installed at B-3 and B-4 to provide a better indication of the long-term fluctuations in the water pore pressures. The cross-sectional view showing the locations and depths of B-3 and B-4 relative to the excavation is shown in Figure 39. Piezometer B-3 is located just in front the existing east concrete abutment wall close to the creek. B-3 extended down to about 10.8 ft below the existing surface and 6.2 ft below the bottom of the excavation, which is within the lean clay layer located from 10 to 12.5 ft below grade in B-1. Piezometer B-4 is located about 6.2 ft east of the east wall of the excavated trench. B-4 extended down to about 4 ft below the bottom of the excavation, which is within the sand layers encountered from about 7 to 10 ft depth in B-1.

Piezometer pore pressure readings monitored from October 2010 to December 2011 are shown in Figure 54. Readings show a spike in pore pressures during mid to late February of 2011. Pore pressures in B4 at that time indicate a water head level at about 8 ft above the bottom of boring B-4, which is close to the footing base level. At other times, the water head levels in B-4 fluctuated between 2 and 5 ft above the bottom of boring B-4, which is about 2 ft below and 1 ft above the bottom of the excavation. Piezometer readings from B3 showed much lower water head levels, likely because the piezometer is embedded in the stiff lean clay layer and there was a downward flow from the creek water at the surface to the ground water table. Reportedly, maximum water levels in the creek were observed at about 1.6 ft below the final road surface during the 2011 summer flooding.

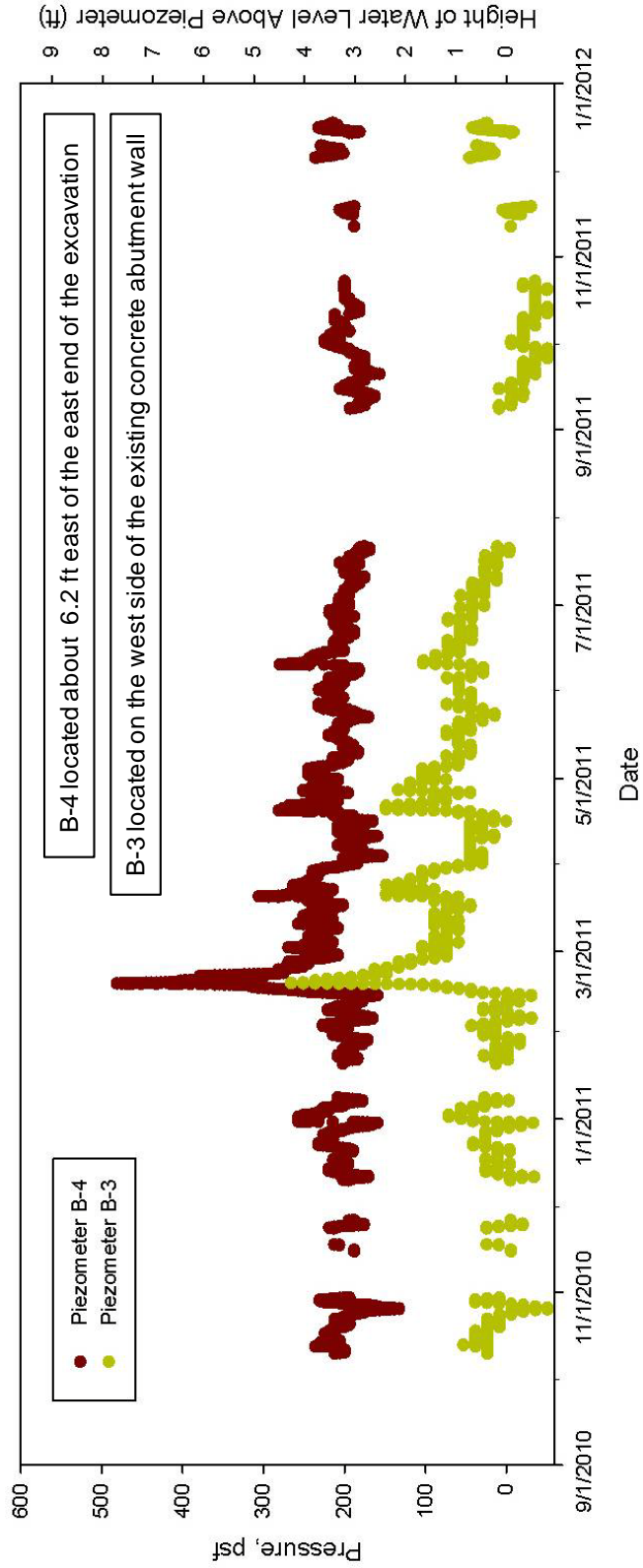


Figure 54. Bridge 2 — Piezometer pore pressure readings monitoring in B-3 and B-4

Laboratory Characterization of GRS fill material

This section of the report presents laboratory test results of the granular fill used in GRS fill material. The laboratory test results include: (a) soil index properties (i.e., grain-size analysis test results, Atterberg limits test results, and soil classification), (b) laboratory Proctor compaction test results, (c) DS and CD shear strength test results, and (d) cyclic triaxial test results.

A summary of the laboratory test results is provided in Table 7. The grain-size distribution curves from particle-size analysis tests are shown in Figure 55. The GRS fill material used in this study met the gradation limits recommended by Adams et al. (2011b) (Figure 55). The GRS fill material was classified as well-graded gravel with sand (GW) according to USCS classification system and A-1-a according to the AASHTO classification system. Moisture versus dry unit weight relationships obtained from standard and modified Proctor tests are shown in Figure 56. The standard Proctor maximum dry unit weight (γ_{dmax}) and optimum moisture content (w_{opt}) were about 133.9 pcf and 8.2%, respectively. Also shown in Figure 56 are field moisture-dry unit weight measurements, which indicate that the field dry unit weights were on average about 94% standard Proctor γ_{dmax} and about 2.1% dry of w_{opt} .

DS tests were conducted on material passing the #10 sieve in accordance with recommendations on laboratory testing on GRS fill materials from Wu et al. (2006). The samples were compacted at a moisture content of about 6.1% to match the values observed in the field, and to about 118 pcf dry unit weight which was lower than the average field dry unit weight of about 125 pcf (note that a high compaction effort similar to standard Proctor test was not used in the direct shear test box). Shear stress versus horizontal displacement and vertical versus horizontal displacement plots at three different normal stresses (5, 10, and 20 psi) are shown in Figure 57. Using the maximum shear stress and the corresponding applied normal stress values, Mohr-Coulomb failure envelope is plotted Figure 58 which showed $c' = 2.8$ psi (403 psf) and $\phi' = 34.2^\circ$. A summary of the DS test results are shown in Table 8.

CD tests were conducted on compacted granular fill material with and without geosynthetic in the sample using material passing the 3/4 in. sieve (note that grain-size results show 99% of the material passing the 3/4 in. sieve). All samples were compacted to a target dry unit weight of 125.0 pcf at 6.1% moisture content, to match with the field measurements. Deviator stress versus strain plots for samples with and without geosynthetic at three different confining pressures (5, 10, and 20 psi) are shown in Figure 59. The stress-strain plots indicate a higher shear stress at failure in sample with geosynthetic. Furthermore, it can be seen that the failure strain (ϵ_f) for the sample with geosynthetic is higher than the sample without geosynthetic at all confining stresses. The higher failure shear stress and failure strain in the reinforced sample are believed to be due to friction force developed at the soil-reinforcement interface. Sharma et al. (2009) explained this behavior as the *confinement effect* or *lateral restraint effect*. A summary of the CD test results with shear stresses and strains at failure are shown in Table 9. Mohr's circles from the CD test results along with Mohr-Coulomb failure envelopes for both samples with and without geosynthetic are presented in Figure 60. Results indicate an improvement in the effective shear strength parameters in the sample with geosynthetic with ϕ' increasing from 34.4° to 41.9° .

Table 7. Bridge 2 — Summary of laboratory test results for GRS fill material

Parameter	Granular Fill
Grain-Size Analysis Results	
Gravel Content (%) (> 4.75mm)	56
Sand Content (%) (4.75mm – 75 μ m)	44
Silt + Clay Content (%) (<75 μ m)	0
D ₁₀ (mm)	0.84
D ₃₀ (mm)	2.75
D ₆₀ (mm)	7.51
Coefficient of Uniformity, c_u	8.94
Coefficient of Curvature, c_c	1.20
Atterberg Limits Test Results	Non-Plastic
AASHTO Classification	A-1-a
USCS Classification	GW
USCS Soil Description	Well-graded gravel with sand
Standard Proctor Test Results (ASTM D698)	
Maximum dry unit weight, γ_{dmax} (pcf)	133.9
Optimum moisture content, w_{opt} (%)	8.2
Modified Proctor Test Results (ASTM D1557)	
Maximum dry unit weight, γ_{dmax} (pcf)	141.2
Optimum moisture content, w_{opt} (%)	6.9
Direct Shear Test Results (on material passing #10 sieve) ¹	
Effective cohesion, c' (psi)	2.8
Effective angle of shearing resistance, ϕ' (°)	34.2
Consolidated-Drained (CD) Triaxial Test (on material passing ¾" sieve) ²	
Effective cohesion, c' (psi) [with no geosynthetic]	13
Effective angle of shearing resistance, ϕ' (°) [with no geosynthetic]	34.4
Effective cohesion, c_r' (psi) [with geosynthetic]	10
Effective angle of shearing resistance, ϕ' (°) [with geosynthetic]	41.9

¹compacted to a target 118 pcf dry unit weight at 6.1% moisture content

²compacted to a target 125 pcf dry unit weight at 6.1% moisture content

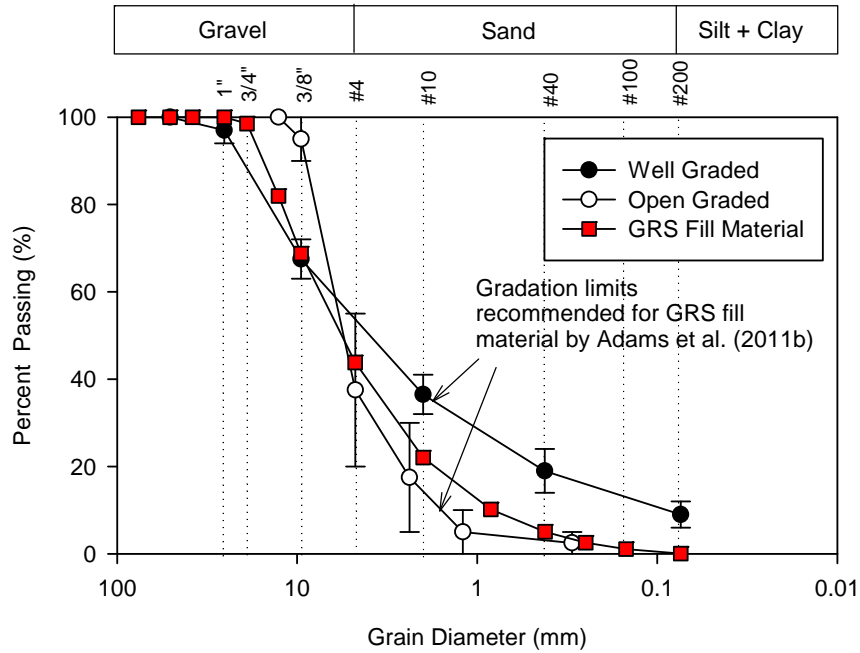


Figure 55. Bridge 2 — Grain-size distribution curve of GRS fill material in comparison with Adams et al. (2011b) recommended gradation limits

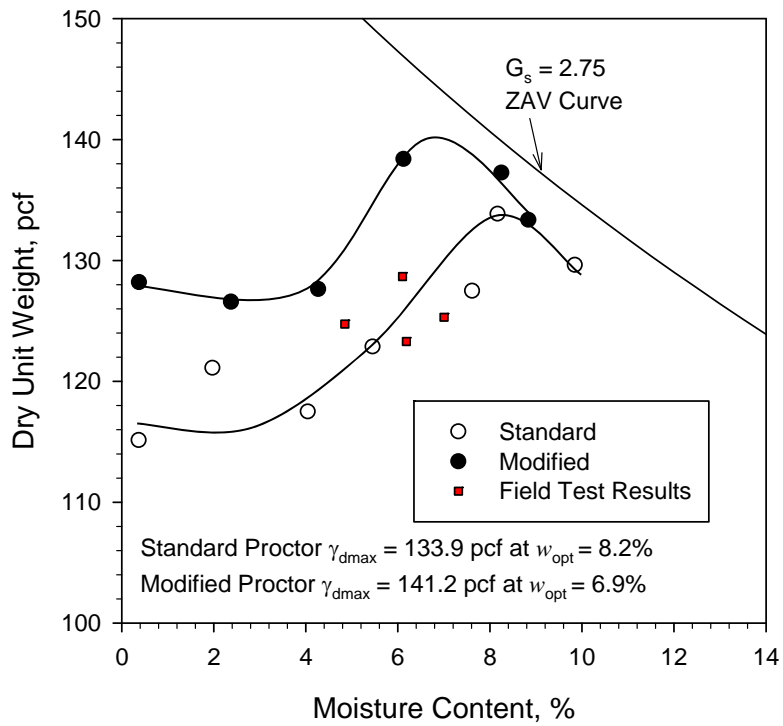


Figure 56. Bridge 2 — Proctor compaction test results for GRS fill material

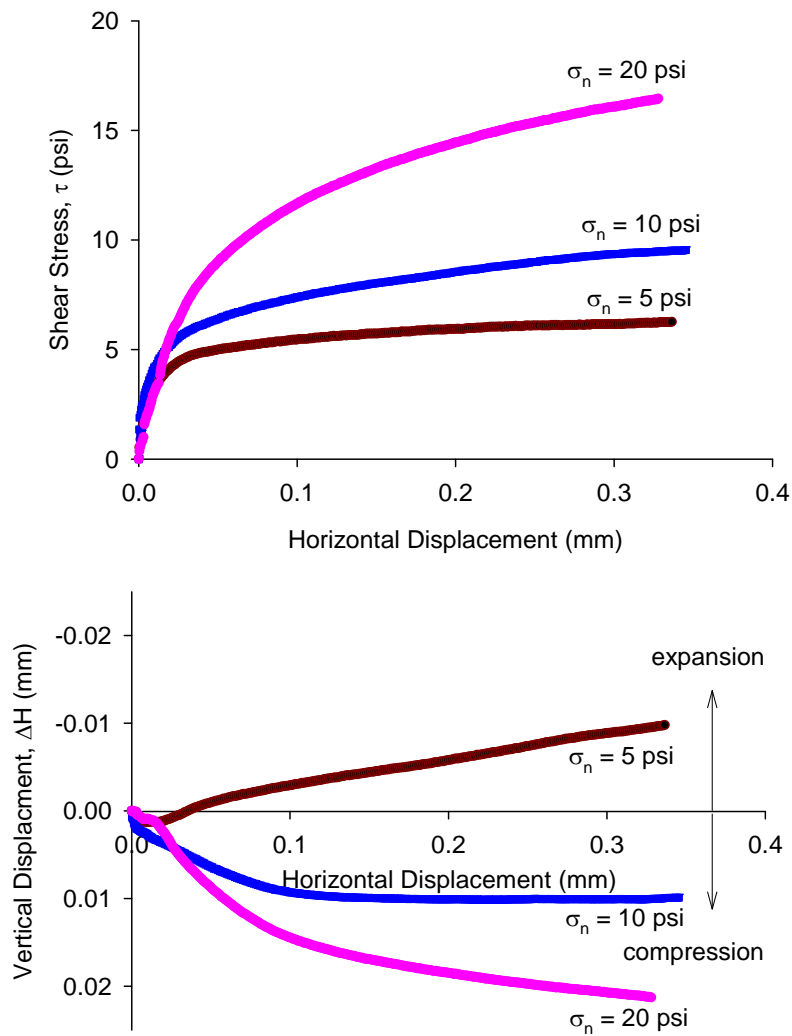


Figure 57. Bridge 2 — Plot of shear stress versus horizontal displacement (top) and change in sample height versus horizontal displacement (bottom) for three different applied normal stresses for compacted GRS fill material

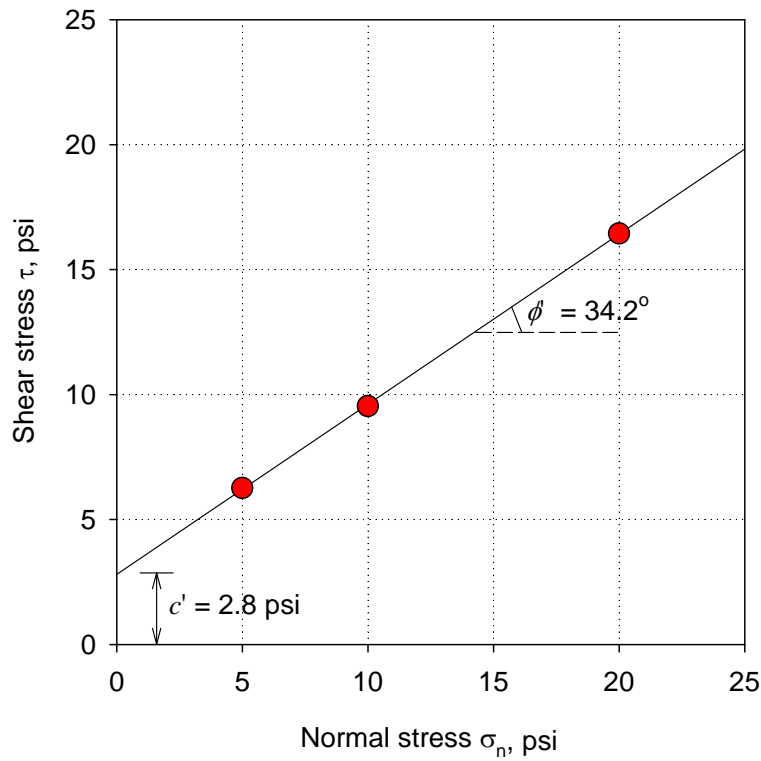


Figure 58. Bridge 2 — Mohr-Coulomb failure envelope from direct shear tests for compacted GRS fill material

Table 8. Bridge 2 — Summary of direct shear test results for compacted GRS fill material

Parameter	Specimen A	Specimen B	Specimen C
Normal Stress, σ_n (psi)	5.0	10.0	20.0
Moisture Content, w (%)	6.1	6.1	6.1
Dry unit weight, γ_d (pcf)	118.0	118.0	118.0
Maximum shear stress, τ_f (psi)	43.2	65.8	113.4
Shear displacement at failure (in)	0.367	0.346	0.328
Vertical displacement at failure (in)	0.049	0.076	0.084

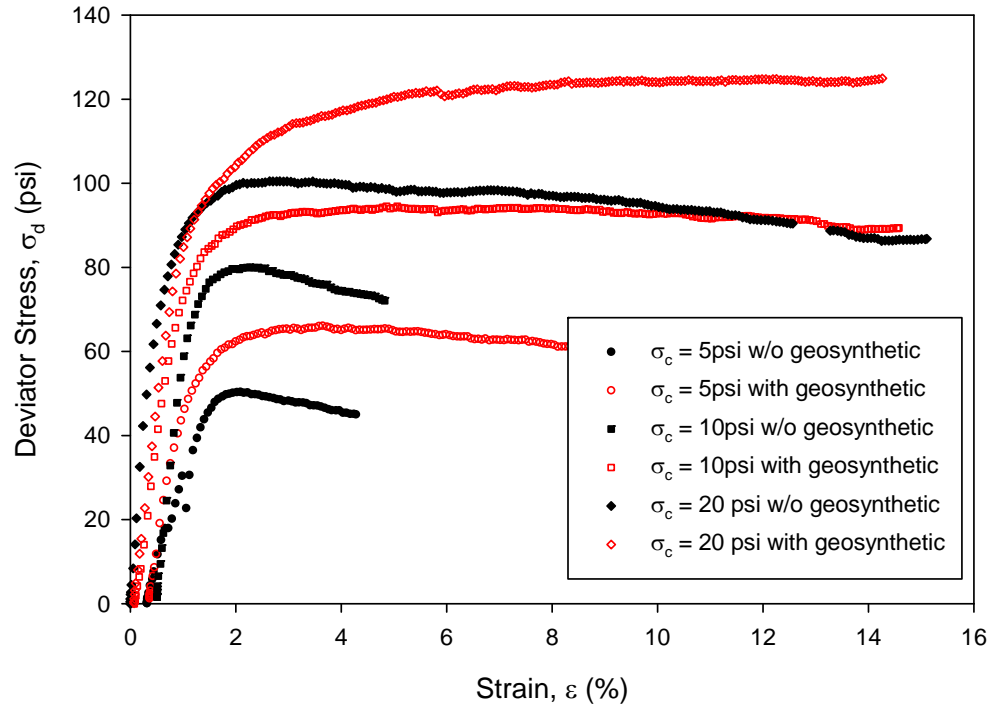


Figure 59. Bridge 2 — Deviator stress versus strain plots from CD tests from shearing phase for granular fill material with and without geosynthetic reinforcement

Table 9. Bridge 2 — Summary of CD test results for compacted GRS fill material with and without geosynthetic

Parameter	Without Geosynthetic			With Geosynthetic		
	5.0	10.0	20.0	5.0	10.0	20.0
Confining stress, σ_c (psi)	5.0	10.0	20.0	5.0	10.0	20.0
Moisture content, w (%)	6.2	6.4	6.1	6.5	6.1	6.6
Dry unit weight, γ_d (pcf)	125.8	125.5	125.9	125.5	125.9	125.3
Peak deviator stress, σ_{df} (psi)	50.3	80.0	100.5	66.1	94.9	124.8
Vertical strain at peak deviator stress, ϵ_f (%)	1.9	2.2	2.6	3.6	5.0	12.0

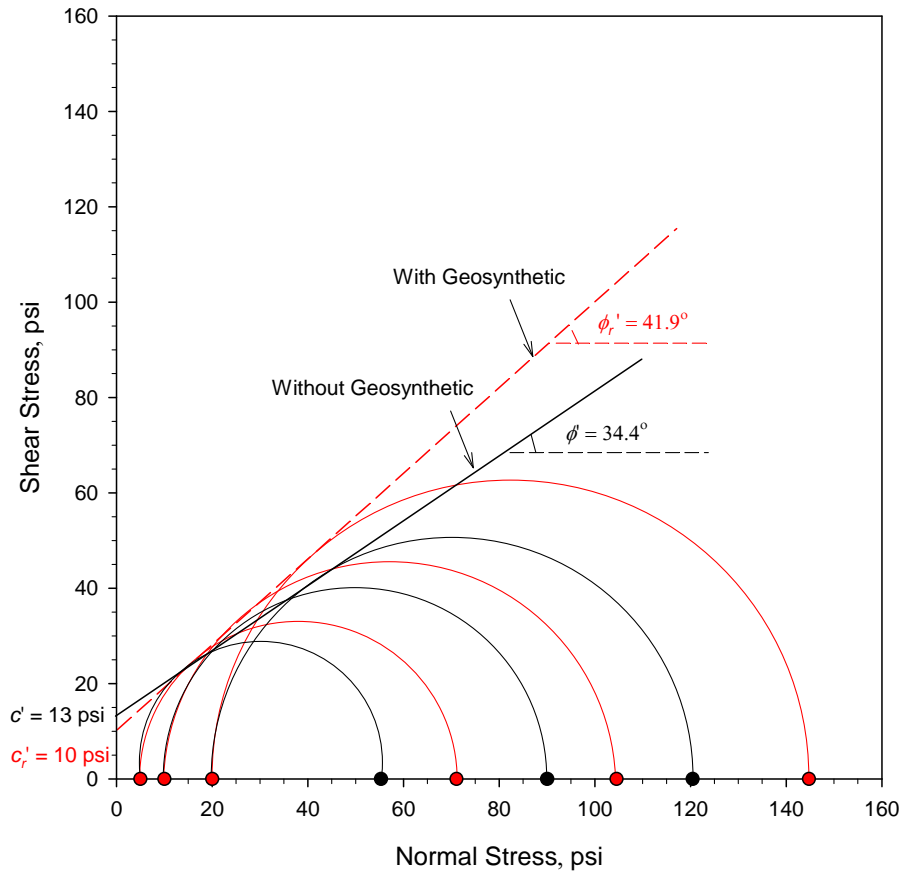


Figure 60. Bridge 2 — Mohr-Coulomb failure envelopes from CD tests for granular fill materials test with and without geosynthetic reinforcement

Cyclic triaxial tests were conducted on compacted GRS fill material with and without geosynthetic. Similar to CD tests, the samples were compacted to a target dry unit weight of 125.0 pcf at 6.1% moisture content, to match with the field measurements. The loading sequences followed during testing were explained earlier in the Laboratory and Field Test Methods Chapter of this report. In brief, seven loading sequences with a constant confining stress (3 psi) and increasing cyclic deviator stress from 3 psi to 40 psi were used for cyclic loading. Each sequence included 10,000 loading cycles. The cyclic deviator stresses were selected such that the stress path increases gradually towards the failure line as depicted in Figure 61. The confining stress of 3 psi was selected based on field horizontal stress measurements. Permanent strain results versus loading cycles for samples with and without geosynthetic are presented in Figure 62. These results indicate that permanent strain up to sequence 5 (with cyclic deviator stress of 20 psi) was about the same for both samples (< 0.5%), but was greater in the sample without geosynthetic for sequences 6 and 7. The permanent strain at the end of the test in the sample with geosynthetic was about 3% and without geosynthetic was about 8%. The reduced permanent strain in the reinforced sample is due to the lateral restraint effect at the soil-reinforcement interface due to tensile forces developed in the geosynthetic material. These test results demonstrates the improved performance of geosynthetic reinforced soils to permanent deformation under cyclic loading.

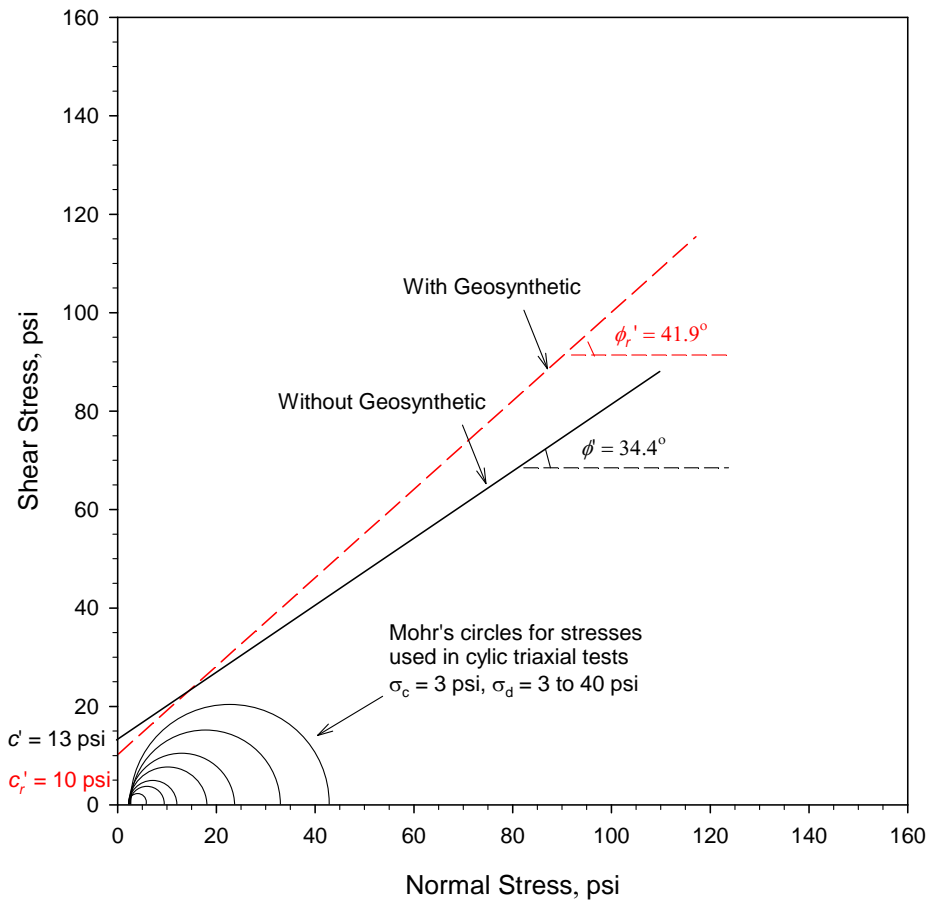


Figure 61. Bridge 2 — Mohr circles for stresses applied during repeated loading cyclic triaxial tests

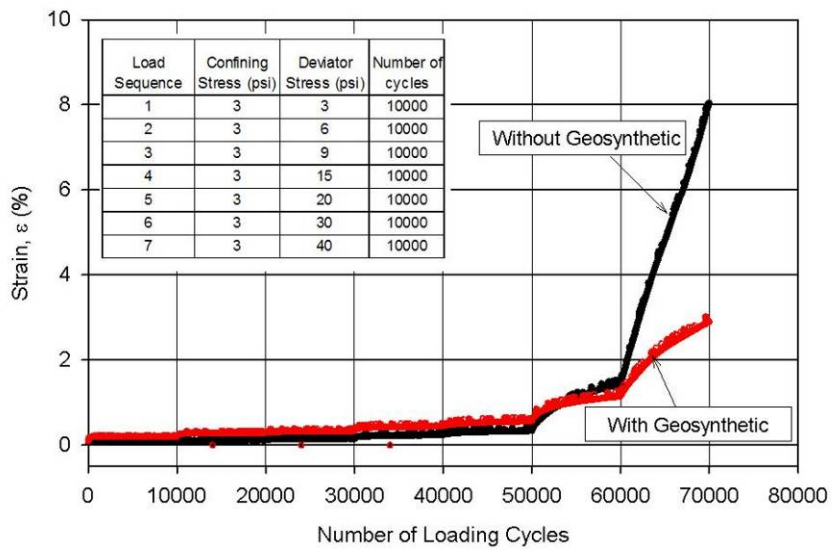


Figure 62. Bridge 2 — Results of permanent strain versus loading cycles from cyclic triaxial test

Instrumentation Installation and In Situ Testing Details

The instrumentation included installing inclinometers and piezometers in the ground, and semiconductor and vibrating wire EPCs in the GRS fill material. Inclinometers were installed at B-1 and B-2 (Figure 38), which are located within about 1 to 3 ft of the excavation limits, just prior to sheet pile installation and excavation. The main purpose of the inclinometers was to monitor lateral ground movements during and post-construction. Inclinometer readings were obtained before and after sheet pile installation, before and after excavation, after GRS fill material placement/compaction, and after bridge installation. The dates/timeline of inclinometer readings are summarized in Table 4.

A cross-section view of the GRS fill material foundation layers and concrete footing showing locations of EPCs is presented in Figure 63. Elevations of each lift at the corners and elevation of EPCs were obtained using a total station survey system. Semiconductor EPCs were installed at the bottom of the excavation on the geosynthetic at about 3.8 ft below the footing (PE 1), within lift 3 at about 2.2 ft below the below the footing (PE 2), and directly below the footing (PE 3). All semiconductor EPCs were installed at the center of the footing. Vibrating wire (VW) Model 4800 EPCs were installed at four locations in the excavation with two each against the west and east side trench walls to measure the lateral stresses at the interface of GRS fill material and the existing abutment fill. VW 1 and VW 2 were installed at about 2.1 ft below the footing against the west and east side walls, respectively. VW 3 and VW 4 were installed at about 1.1 ft below the footing against the west and east side walls, respectively. Along with PE 3, three vibrating wire “fat back” EPCs were installed directly beneath the footing, at center and at about 2 to 3 ft from the edge of the footing (VW 5, VW 6, and VW 7). A plan view of the footing and locations of EPCs under the footing are shown in Figure 64.

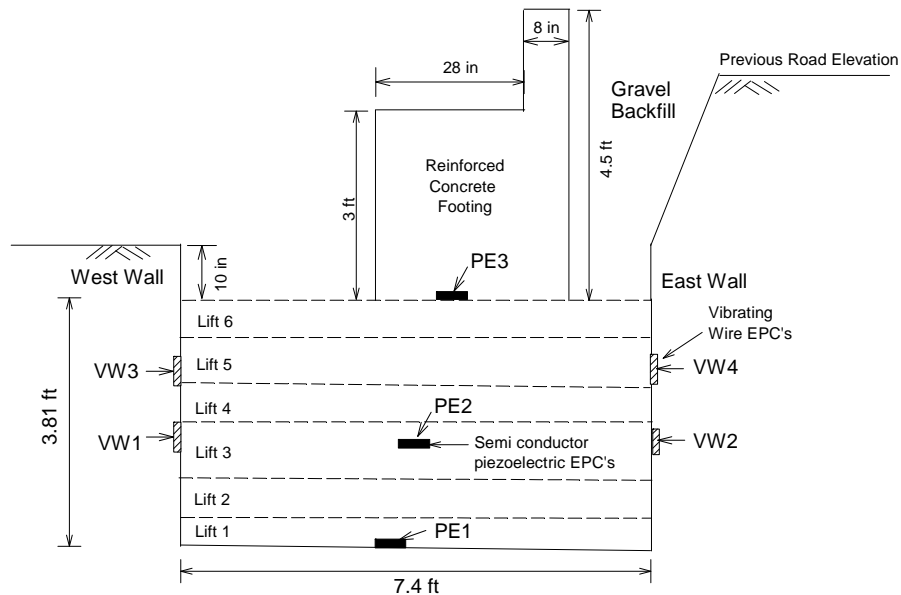


Figure 63. Bridge 2 — Cross-sectional view of the GRS fill material and location of semiconductor and vibrating wire EPCs embedded in the fill

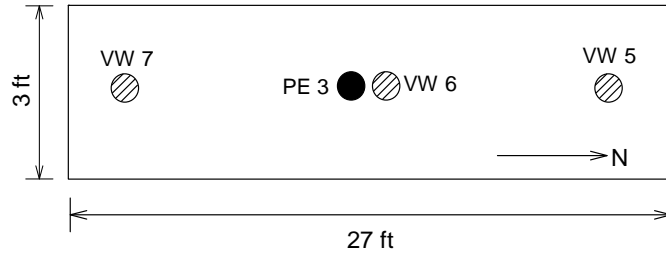


Figure 64. Bridge 2 — Plan view of the concrete footing showing location of vibrating wire and semiconductor EPCs under the footing

In situ testing involved conducting NG and LWD tests during fill compaction. Tests were conducted in the middle of lift 1, and on top of lifts 3, 5, and 6, after compaction.

In Situ Test and Instrumentation Results

Nuclear Gauge and Light Weight Deflectometer Test Results

NG dry unit weight and moisture content measurements and LWD modulus measurements obtained from lift 1, and on top of lifts 3, 5, and 6, are shown in Figure 65. LWD modulus increased from about 1690 psi (~12 MPa) in lift 1 to over 7200 psi (50 MPa) on lifts 3, 5, and 6. These results indicate that the bottom of the excavation was relatively soft, and the reinforced fill layers aided in bridging the soft underlying foundation layer. As indicated earlier when describing the laboratory Proctor test results, field measurements showed an average dry unit weight of 125 pcf (94% standard Proctor γ_{dmax}) and an average moisture content of 6.1% (about 2% dry of standard Proctor w_{opt}).

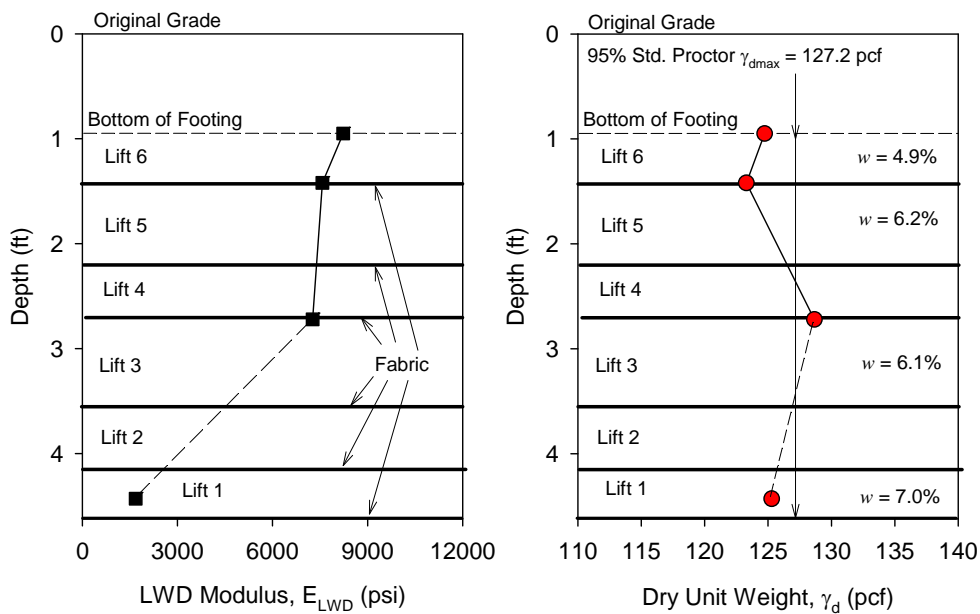


Figure 65. Bridge 2 — In-situ LWD and NG test results of each GRS lift

Inclinometer Readings

Results of lateral ground movements from inclinometers installed in B-1 and B-2 are shown in Figure 66 and Figure 67, respectively. Results indicate the inclinometer casing in B-1 showed more movements compared to B-2. Note that B-1 was located closer to the excavation (about 1 ft away from the excavation) compared to B-2 (about 3 ft away from the excavation). Measurements in B-1 are not considered reliable; as it appears that the bottom of the boring did not extend into a stiff layer. Measurements in B-2 showed very minimal movements (< 0.2 in), during the 1 year measurement period following bridge construction.

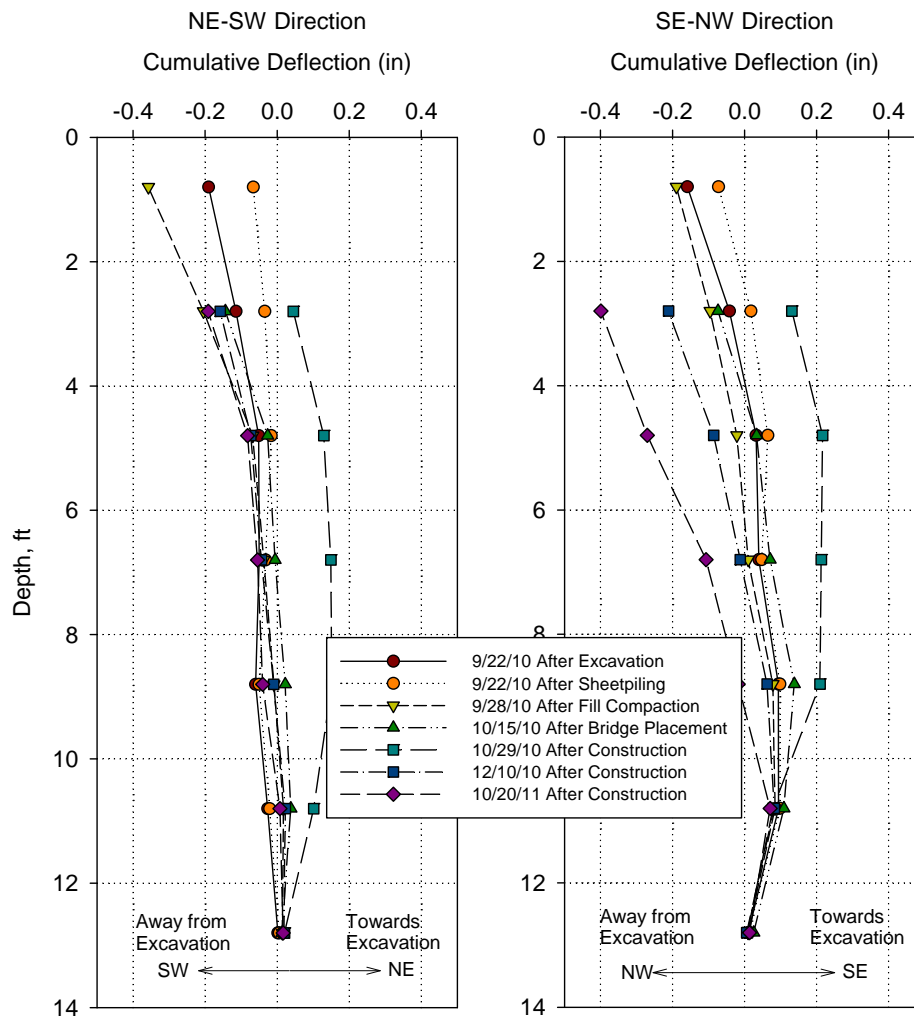


Figure 66. Bridge 2 — Inclinometers results for B-1

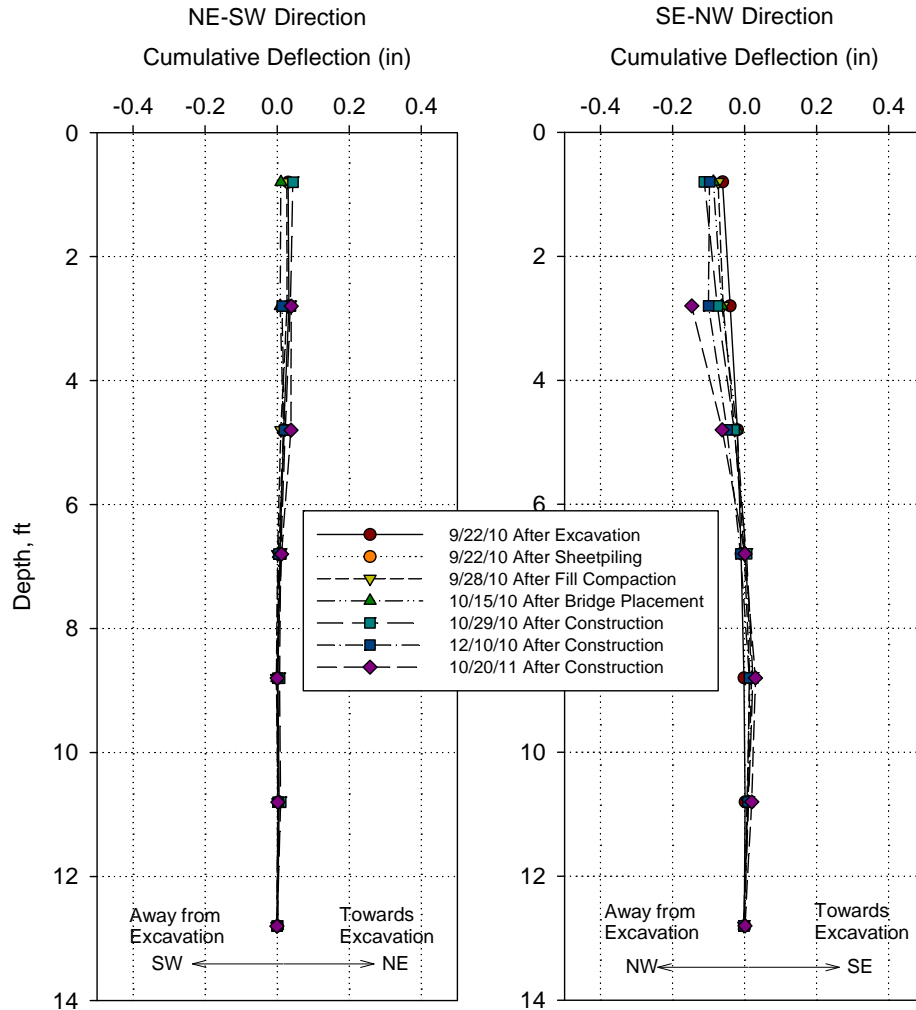


Figure 67. Bridge 2 — Inclinerometers results for B-2

In Ground Stresses Measurements During and After Construction

Total dynamic vertical stress readings during placement and compaction of GRS fill material (on 09/23/2010) from PE 1 and PE 2 EPCs placed at the bottom of the excavation and at about 2.2 ft below the bottom of the footing (within lift 3), respectively, are shown in Figure 68. Note that all EPC readings are corrected for temperature as explained in the Laboratory and Field Test Methods Chapter of this report. As expected, results showed an increase in total vertical stress with lift placement. The maximum increase in total vertical stress under vibratory compaction was recorded at about 3800 psf in PE 2 during compaction of lift 5. EPC total stress and temperature readings from 9/23/2010 to 11/26/2010 from PE 1, PE 2, and PE 3 are shown in Figure 69, depicting the various construction operations and time periods (i.e., the time of fill placement of compaction, footing placement, RRFC bridge placement, gravel road placement, and guard rail placement). EPC total stress and temperature readings for the full project period (9/23/2010 to 12/15/2011) from PE 1, PE 2, and PE 3 are shown in Figure 70.

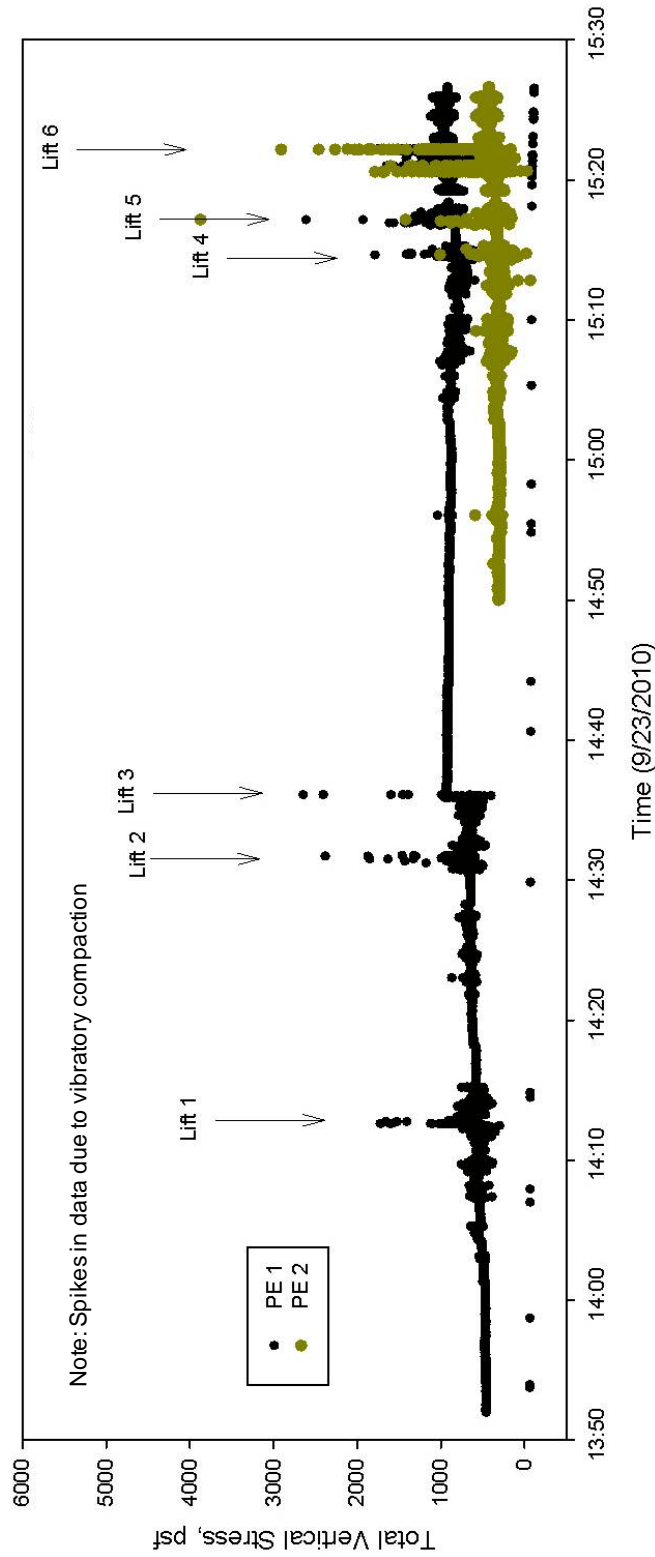


Figure 68. Bridge 2 — In ground total vertical stresses in PE 1 (at the bottom of the excavation) and PE 2 (at about 2.2 ft below footing) during compaction of GRS fill material in excavation

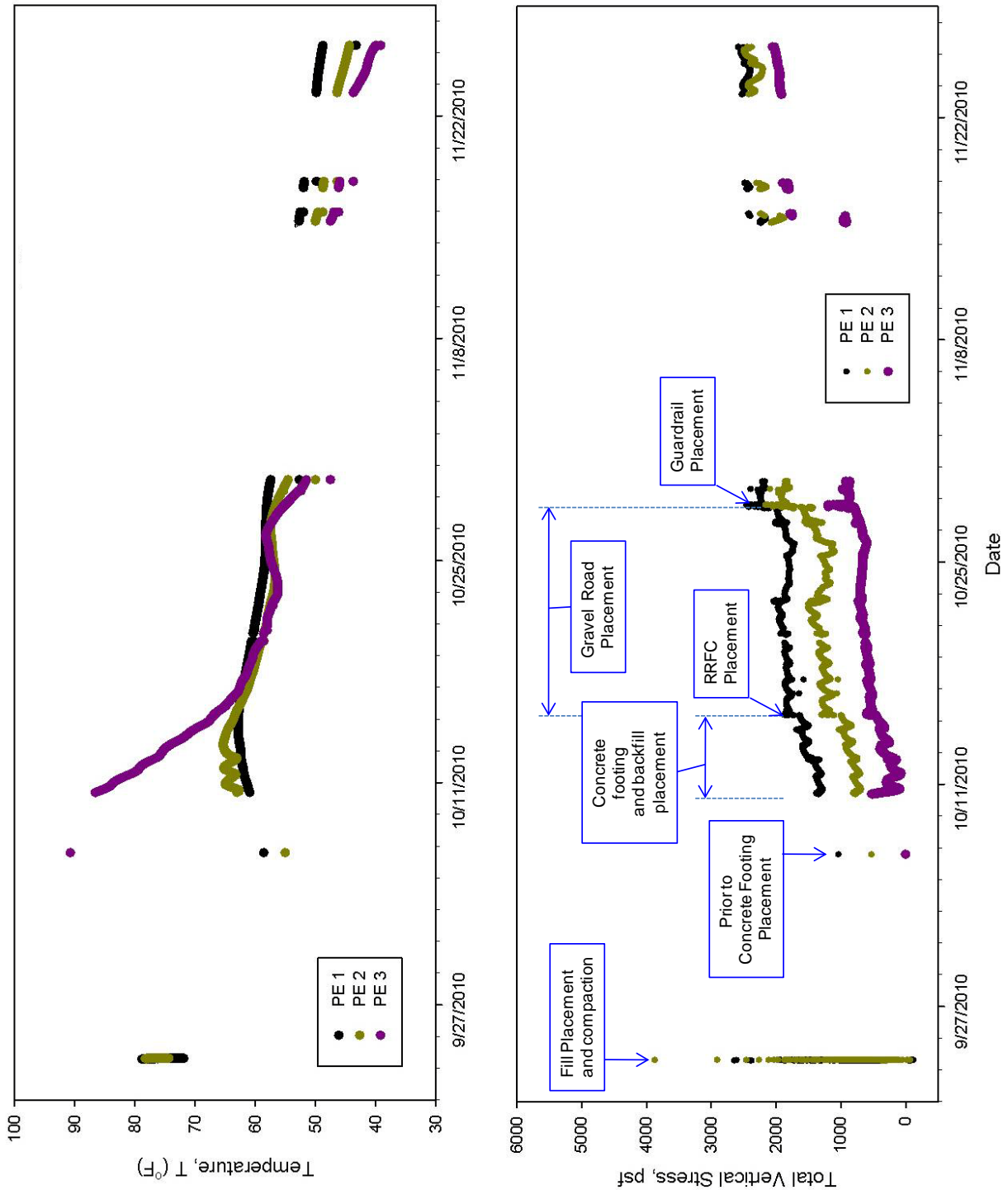


Figure 69. Bridge 2 — In ground total vertical stresses and temperature readings from 9/23/2010 to 11/26/2010 in PE 1 (at the bottom of the excavation), PE 2 (at about 2.2 ft below footing), and PE 3 (at the bottom of the footing)

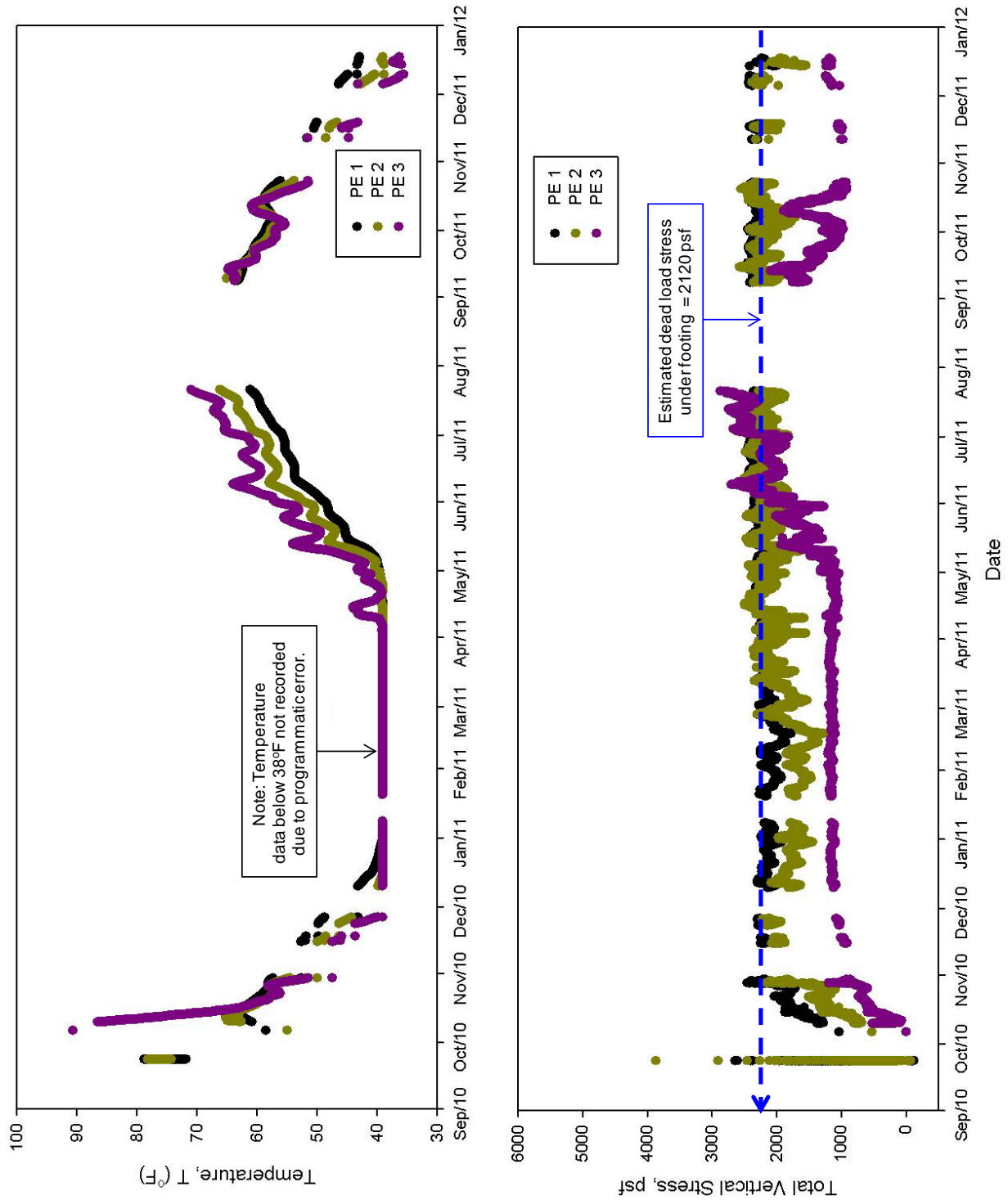


Figure 70. Bridge 2 — In ground total vertical stresses and temperature readings in PE 1 (at the bottom of the excavation), PE 2 (at about 2.2 ft below footing), and PE 3 (at the bottom of the footing) for the full project period

The temperature readings from mid December 2010 to mid April 2011 did not drop below about 38°F due to a programmatic error, which was fixed later during the course of the project. The gaps seen in the data (for e.g. during August and September 2011) were due to battery power issues. Although the EPC readings were corrected for temperature, PE 3 readings appear to be influenced by temperature fluctuations from May to Dec 2011. The PE 1 and 2 readings did not show significant fluctuations during that period. The estimated dead load stress under footing is about 2120 psf and is confirmed with the measured stresses in PE 1 and PE 2. The stress readings also illustrate that the vertical stress applied under the footing is almost fully transferred down to the bottom of the GRS fill material. These are important observations to demonstrate and must be considered in evaluating the bearing capacity of the GRS fill material and the underlying foundation layers.

The temperature and total horizontal stress readings from vibrating wire EPCs for the full project period are shown in Figure 71. The EPC readings indicate that the horizontal stresses in VW4, which is located against the east wall at about 1.1 ft below footing base, were generally higher compared to horizontal stresses in other EPCs. The reason for this is attributed to VW 4 EPCs closer proximity to the footing compared other EPCs. The horizontal stresses against the excavation walls were about 600 psf (4 psi) or less and on average at about 430 psf (3 psi) in the VW 4 EPC. The horizontal to vertical stress ratio is low (< 0.25), which validates the lateral restraint or confinement effect seen in the laboratory CD and cyclic triaxial test results on reinforced samples.

The vibrating wire EPCs installed under the concrete footing did not show reliable results; therefore the results are not discussed in this chapter. The results are however presented in Appendix B. The reason for the unreliable readings is likely because of disturbance during the footing installation. The ISU research team was not present at the time concrete was poured over these sensors. The PE 3 semiconductor EPC readings also showed some unusual variations in the data (Figure 71); therefore, the EPC readings obtained under the footing are not considered for further analysis or interpretation in this report.

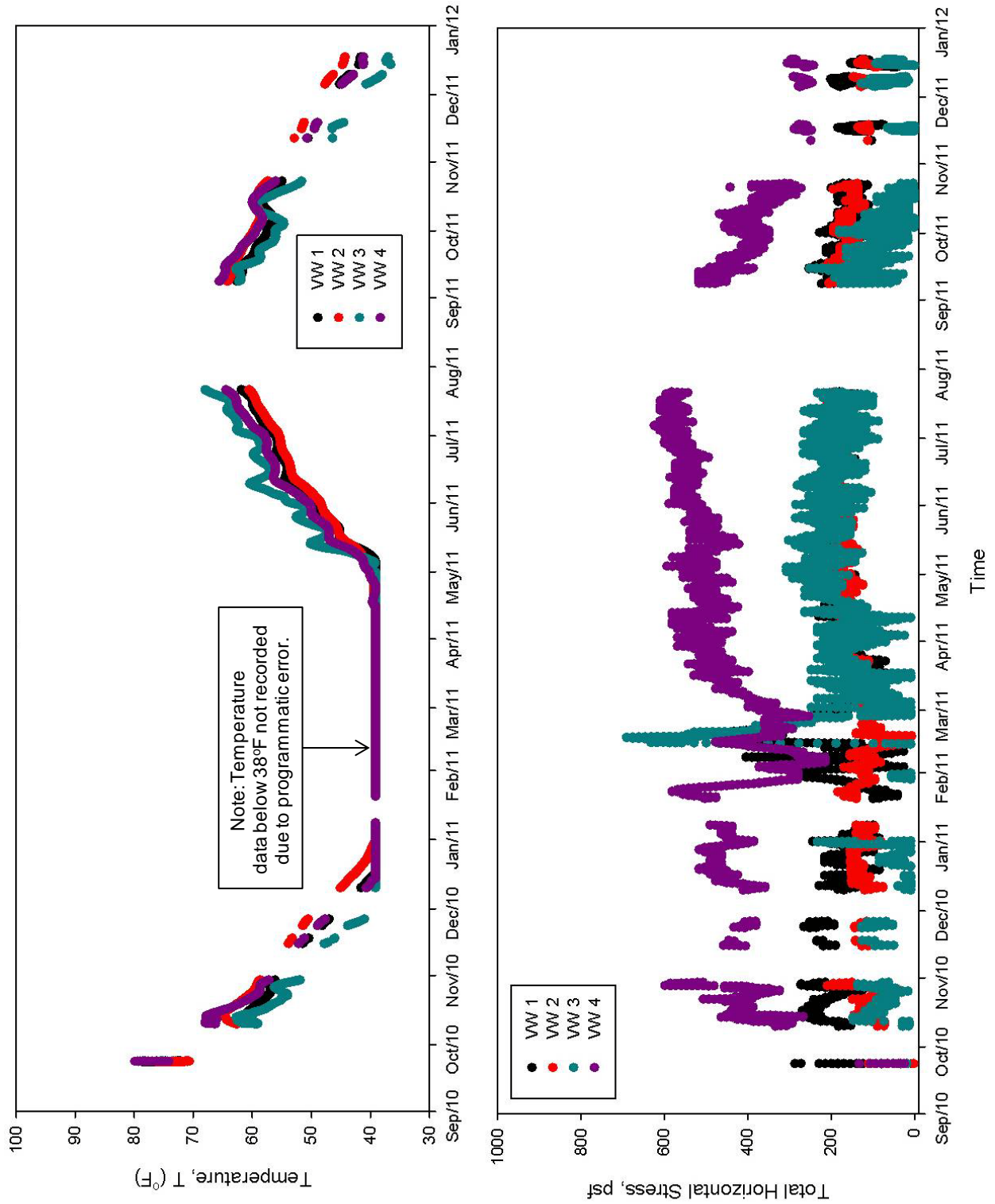


Figure 71. Bridge 2 — In ground total horizontal stresses and temperature readings in vibrating wire EPCs for the full project period

Bridge Abutment Settlement Monitoring

The bridge abutment elevations were monitored in the period after completion of construction (10/15/2010) to about 1 year after construction (10/20/2011). The elevations were obtained on top of the east and west abutment footings from SW, NW, NE, and SE corners. The results of change in elevations are shown in Figure 72. The results indicate that a maximum settlement of about 0.5 in is observed at the SW corner of the bridge (on west abutment footing), which is considered acceptable. The average settlement of the west abutment footing was about 0.4 in. with a transverse differential settlement of about 0.2 in. The SE corner readings on the east abutment footing indicated positive readings suggesting heave under the footing, which is unusual. The readings indicate that most of the settlement occurred within the first two months after completion of construction.

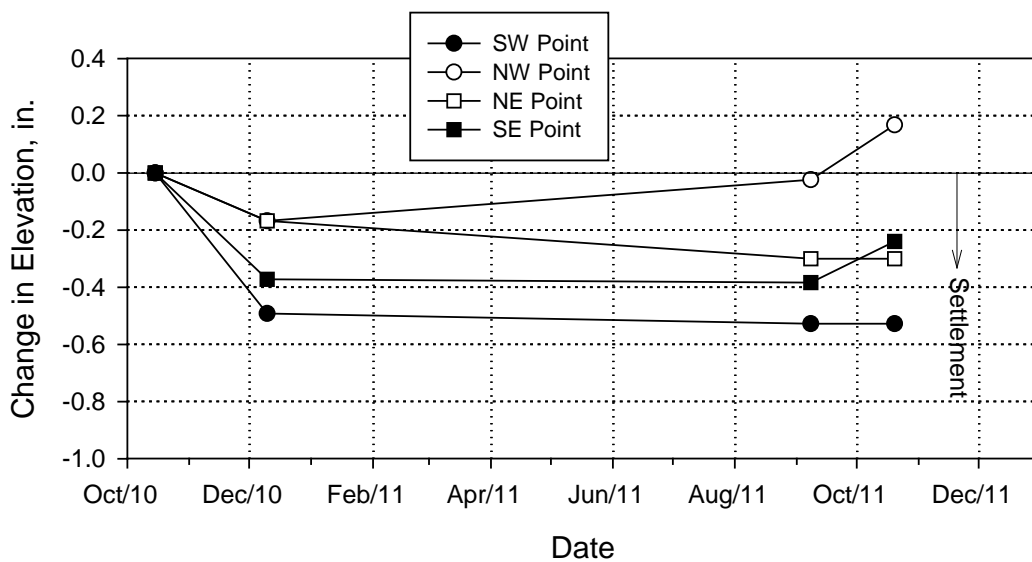


Figure 72. Bridge 2 — Abutment elevation monitoring results

Bridge Live Load Testing

Bridge LL tests were conducted using a loaded test truck to evaluate the structural performance of the bridge and also measure changes in ground stresses in the GRS fill material under LLs. Specifically, the following measurements were obtained during live load testing:

- Bridge deflections under static LL — bridge center of the span deflections were obtained when the tandem axle was placed at the bridge center.
- Increase in vertical stresses under static LL — increase in total vertical stresses in the GRS fill material were obtained from semiconductor EPCs (PE 1 and PE2) when test truck is positioned at several locations across the bridge.
- Increase in horizontal stresses under static LL — increase in horizontal stresses against the east and west walls of the excavation were obtained from vibrating wire EPCs (VW 1 to VW4) when the test truck is positioned at several locations across the

- bridge.
- Increase in vertical stresses under dynamic LL — increase in total vertical stresses in the GRS fill material were obtained from semiconductor EPCs (PE 1 and PE2) when test truck was travelling at 5 to 40 mph speed.

LL testing was conducted at three times during the course of this project. The first load test was conducted on 10/29/2010 which was shortly after bridge construction was completed, second load test was conducted on 12/10/2010, and third load test was conducted on 10/20/2011 approximately one year after bridge construction. A summary of test measurements obtained from each testing time is shown in Table 10. Dimensions of the test truck are shown in Figure 73. A summary of the test truck axle loads and total weights are shown in Table 11.

Table 10. Bridge 2 — Summary of live load testing at different testing times

Measurements	Testing Date		
	10/29/2010	12/10/2010	10/20/2011
Bridge deflections under static live load	■		■
Increase in vertical stresses under static live load	■		■
Increase in horizontal stresses under static live load			■
Increase in vertical stresses under dynamic live load		■	■

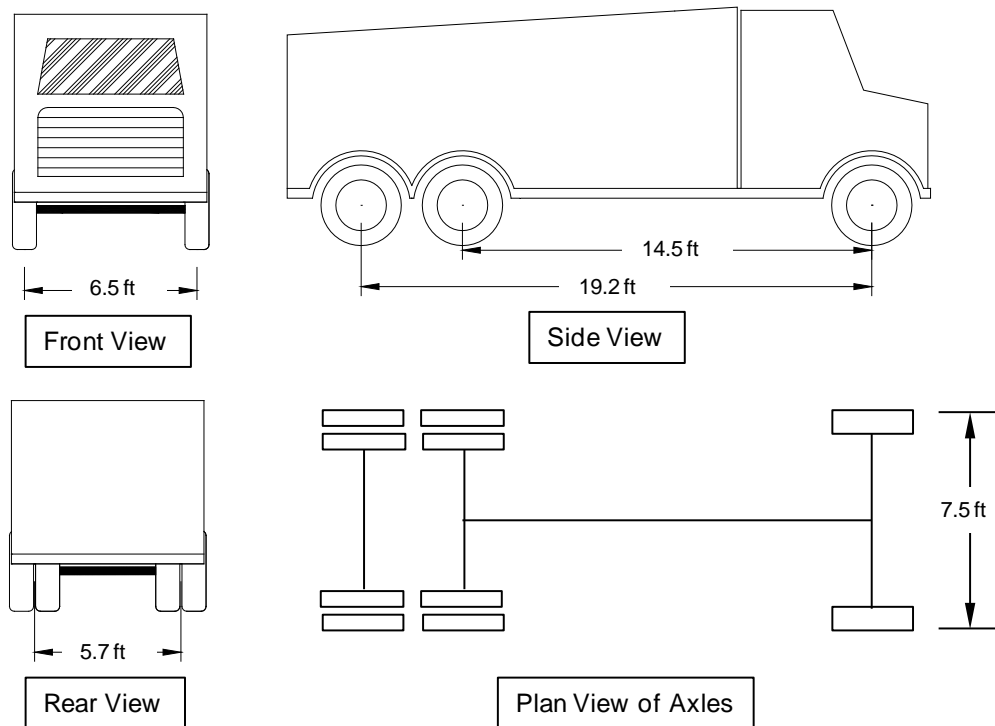


Figure 73. Bridge 2 — Dimensions of the test truck used for live load testing

Table 11. Bridge 2 — Summary of test trucks axle loads and total weights

Description	Load (lbs)		
	10/29/2010	12/10/2010	10/20/2011
Front axle weight	17,180	15,400	16,760
Tandem axle weight	34,960	37,400	35,200
Total weight	52,140	52,800	51,960

The bridge was divided into three lanes: north, center, and south. Each lane was about 8.6 ft wide, which is equal to the width of the RRFCs (Figure 74). The test truck was about 7.5 ft wide (Figure 73); therefore, the truck was effectively on only one RRFC when positioned in a lane. Bridge deflection testing under static live loads was conducted by positioning the center of the tandem axle (Figure 75) at bridge center span, along all three lanes. Bridge deflection measurements were obtained on the north and south sides of the bridge at the center span, before and during loading.

Deflection measurements from the 10/29/2010 testing are shown in Figure 76 which indicate that the bridge showed non-uniform deflections on the north and south sides, when the test truck was positioned on the north and south lanes. When the test truck was positioned in the north lane, about 0.8 in. deflection was measured on the north side while only about 0.2 in. deflection was measured on the south side. Similarly, when the test truck was positioned in the south lane, about 0.6 in. deflection was measured on the south side while no deflection was measured on the north side. All of these measurements were obtained in east to west travel direction. The influence of test truck travel direction (east to west (E-W) and west to east (W-E)) on bridge deflections was evaluated during the 10/20/2011 testing. Results for E-W and W-E travel directions are shown separately in Figure 77 and Figure 78, respectively. There were few changes in the deflections with change in travel directions, which is likely due to change in the position of the center of gravity of the vehicle. The maximum deflection observed during this testing was about 0.9 in. on the south side, when the test truck was positioned on the south lane. Similar to observations from the 10/29/2010 testing, results from this testing also showed non-uniform deflections on the north and south sides of the bridge, when the test truck was positioned on the north and south lanes.

According to AASHTO (1996) specifications, the maximum allowable superstructure deflection under LL is about 1/800 of the length of the span. Using that criteria, the maximum allowable deflection for this bridge is about 1 in. (i.e., $L/800 = 68.5\text{ft}/800 = 0.085\text{ ft} = 1\text{ in}$). The maximum measured deflection was about 0.9 in. which is close to but less than the allowable deflection. However, it must be noted that the AASHTO (1996) allowable limits are based on a HS-20 three axle test truck weighing 72 kips with a maximum single axle weight of about 32 kips. The test trucks used in this study weighed about 52 to 53 kips with a tandem axle weight of about 35 to 37 kips. Further, the non-uniform deflections observed across the bridge suggest poor load transfer across the RRFCs.

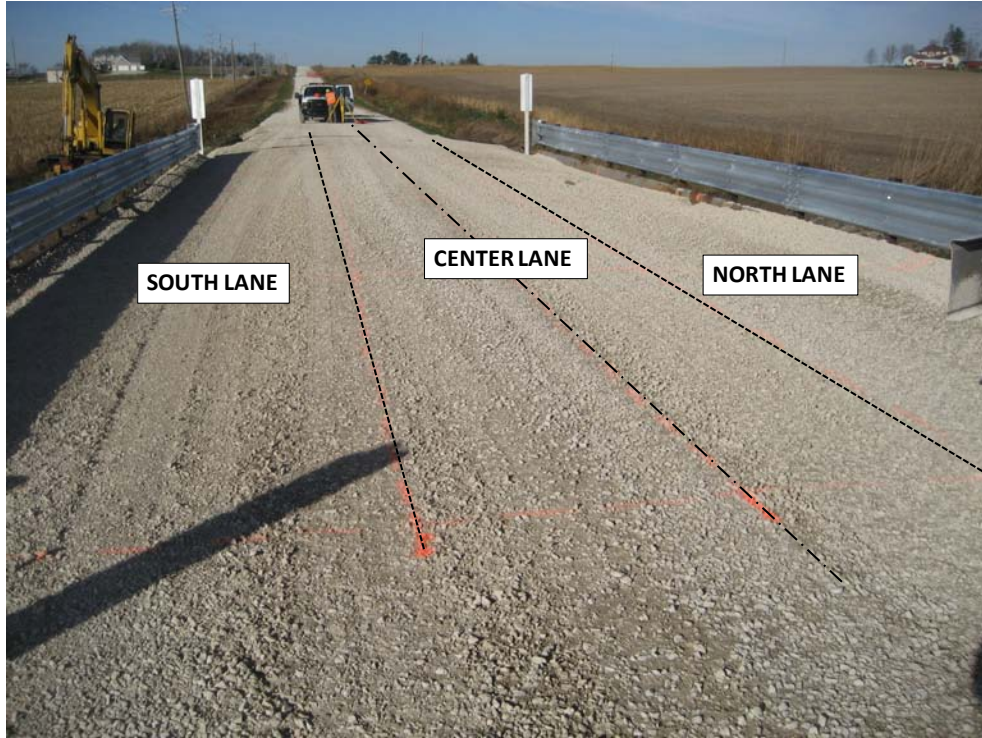


Figure 74. Bridge 2 — North, center, and south lanes divided for load testing



Figure 75. Bridge 2 — Center of tandem axle positioned over a desired location along the bridge

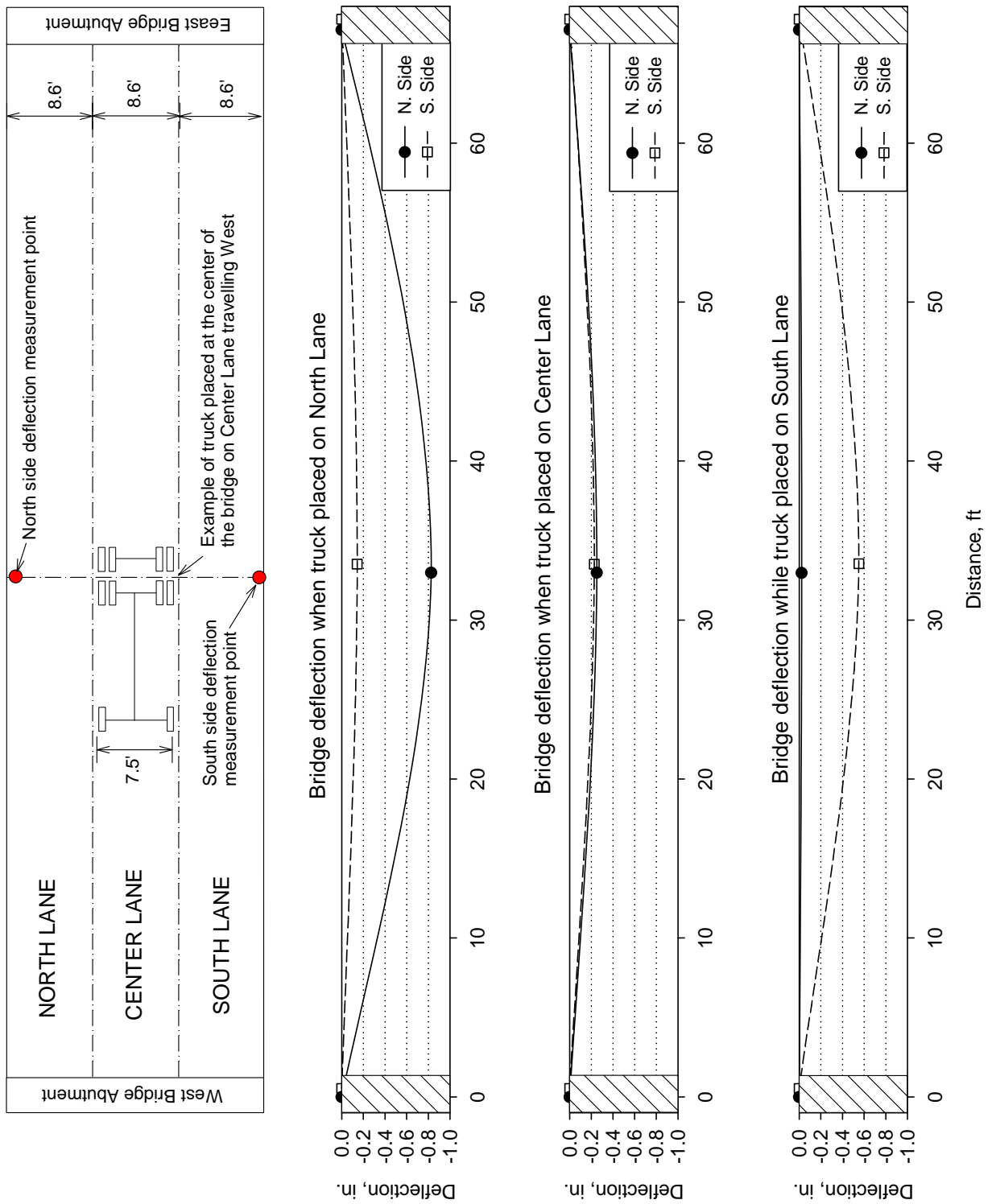


Figure 76. Bridge 2 — Bridge deflections at center when truck is positioned at the bridge center in north, center, and south lanes (10/29/2010)

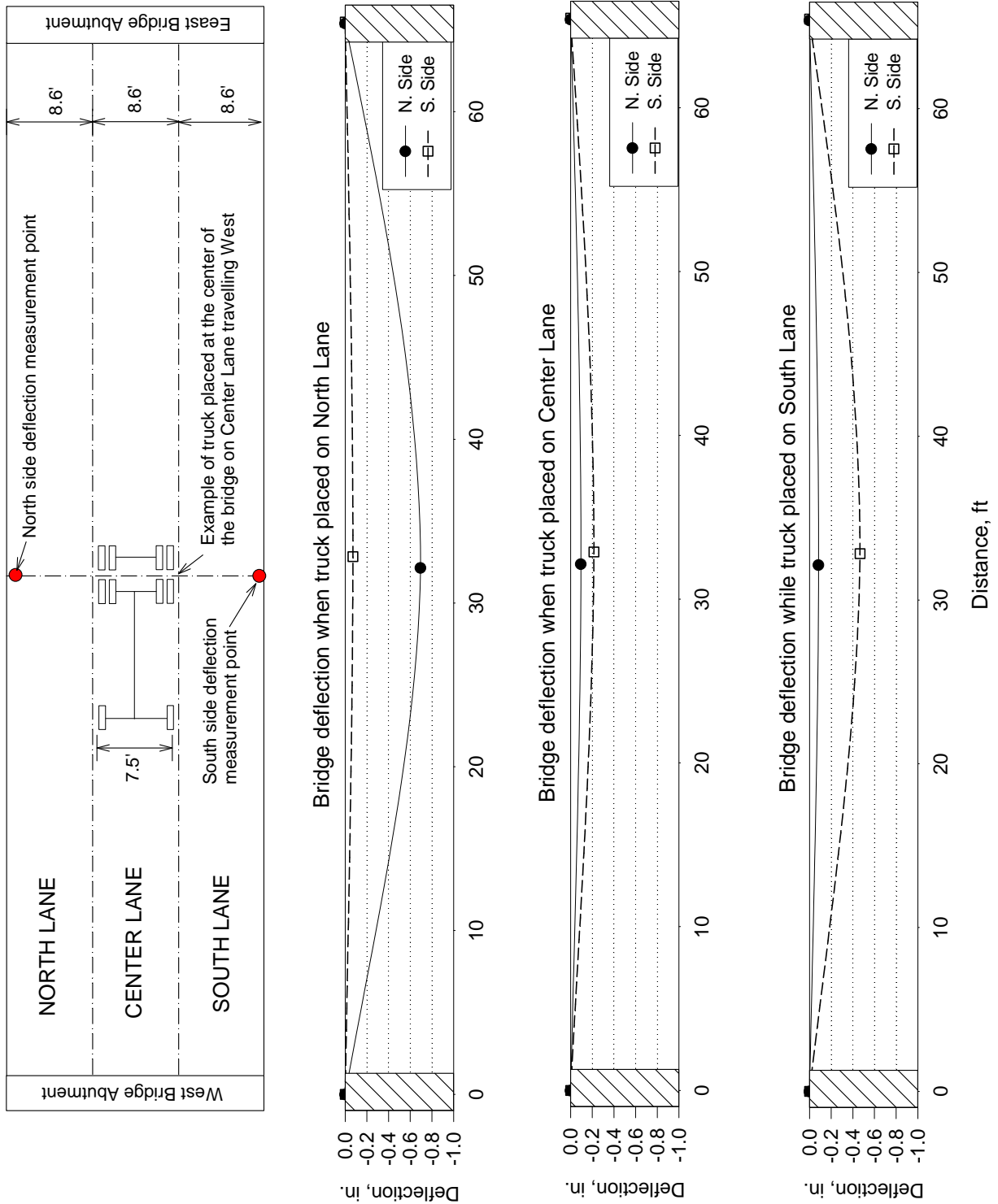


Figure 77. Bridge 2 — Bridge deflections at center when truck is positioned at the bridge center in north, center, and south lanes (10/20/2011) – Truck travelling east to west

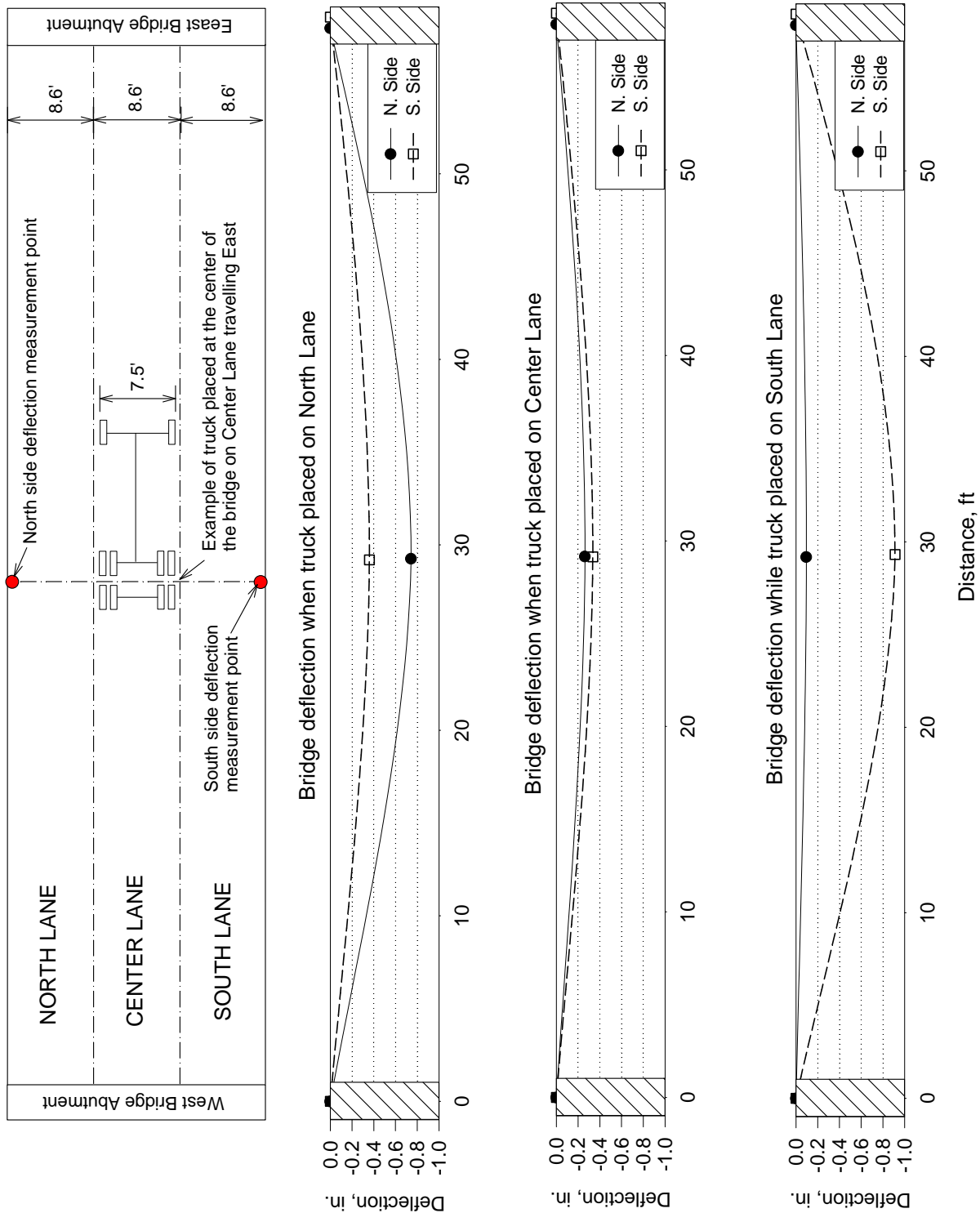


Figure 78. Bridge 2 — Bridge deflections at center when truck is positioned at the bridge center in north, center, and south lanes (10/20/2011) – Truck travelling west to east

Vertical stresses under static live loads were measured using the EPCs (PE 1 and PE 2) in the GRS fill material by positioning the test truck at 8 different locations along and outside the bridge span, on the north, center, and south lanes. This testing was performed with truck traveling in W-E direction. These positions are labeled A through H and indicates the position of the center of the truck tandem axle with reference to the bridge footings as described below:

- A — center of tandem axle at about 40 ft east of the center of east side footing
- B — center of tandem axle at about 20 ft east of the center of east side footing
- C — center of tandem axle directly above the center of east side footing
- D — center of tandem axle at about 17.13 ft west of the center of east side footing
- E — center of tandem axle at about 34.25 ft west of the center of east side footing (i.e., at about center span)
- F — center of tandem axle at about 51.38 ft west of the center of east side footing
- G — center of tandem axle directly above the center of west side footing
- H — center of tandem axle at about 20 ft west of the center of west side footing

Vertical stress measurements during static live loading in PE 1 and PE 2 are shown in Figure 79 and Figure 80 for 10/29/2010 and 10/20/2011 testing, respectively. As expected, results indicated that the stresses in PE 2 (located at about 2.2 ft below footing base) are higher than in PE 1 (located at about 3.8 ft below footing base). Peak increase in stresses were observed when the test truck was at position C (i.e., directly above the footing) and in the center lane. EPC readings showed very similar (but slightly lower) increase in stresses when the truck was in the north lane. However, vertical stresses were lower when the truck was in south lane. This difference in stresses measured when truck was positioned in different lanes was consistent during both 10/29/2010 and 10/20/2011 testing.

A summary of maximum stress increase in PE 1 and PE 2 EPCs under static live loading from the 10/29/2010 and 10/20/2011 testing along with estimated stress increase values is provided in Table 12. The estimated stress increase values were calculated using elastic solutions for the case of uniform loading over a strip footing of width = 3 ft (Poulos and Davis 1974). Influence factors were estimated based on the location of the EPCs relative to the footing location. The contact stress under the footing was estimated using total weight of the truck (i.e., about 52 kips) and dividing that by the area of the footing (3 ft x 27 ft), which was about 640 psf. The estimated values compared well with the measured values and were within 50 psf.

Horizontal stresses were measured from vibrating wire sensors (VW 1 to VW 4) located along the east and west walls of the excavation, during the 10/20/2011 LL testing. Results from VW 1 to VW 4 EPCs are presented in Figure 81. VW 4 EPC located closer to the footing base than other EPCs (see Figure 63 for EPC locations) showed the highest increase in horizontal stress when the truck was either positioned directly over or near the footing. A comparison of the estimated and the maximum measured horizontal stress increase values is provided in Table 12. The estimated horizontal stress increase values were calculated using elastic solutions, similar to the procedure followed for vertical stress increase as described above. The estimated values were lower than the measured values, as the elastic solutions used do not account for the lateral restraint effect in the reinforced soil layers which causes a reduction in the horizontal stresses.

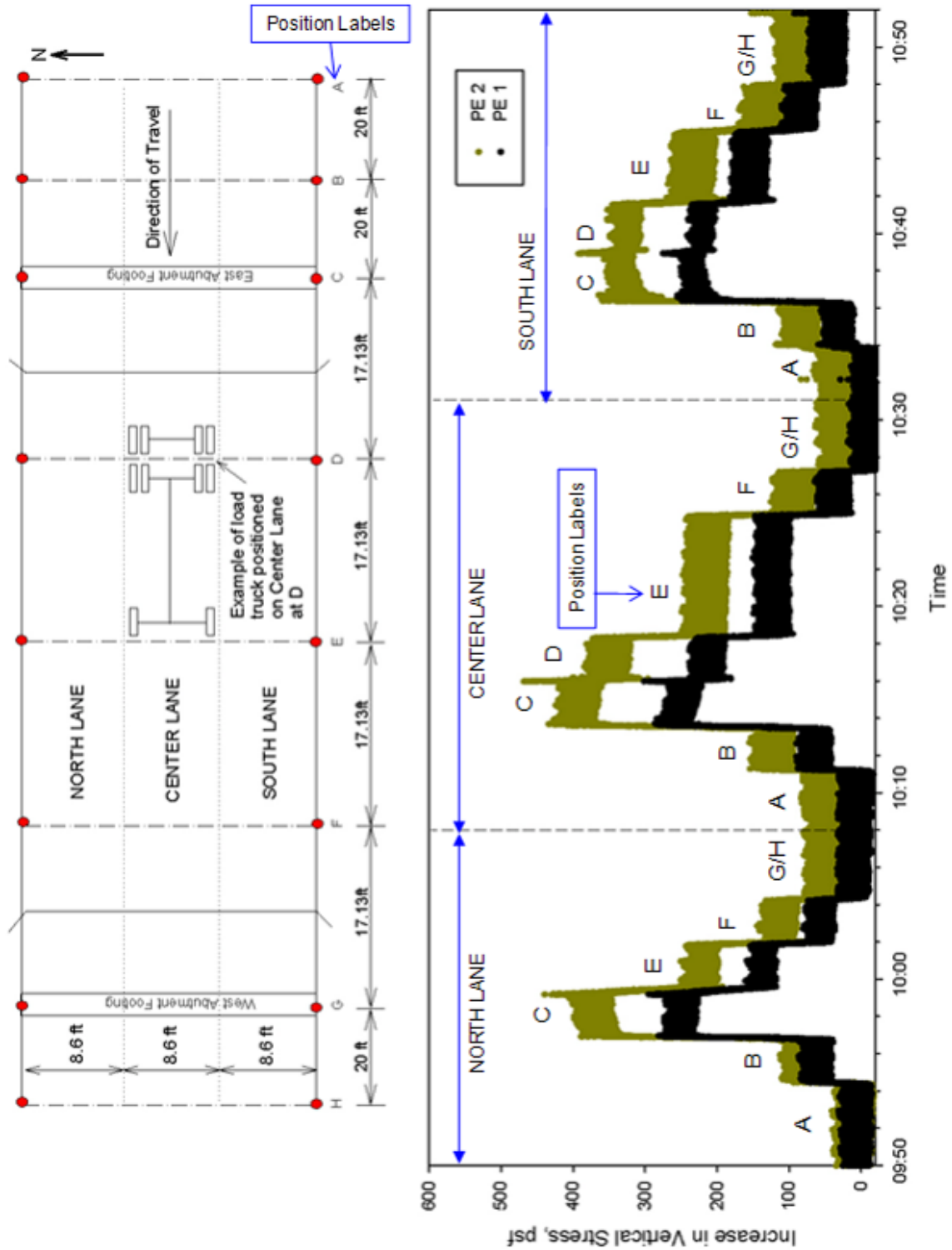


Figure 79. Bridge 2 — Increase in total vertical stresses in PE 1 (at the bottom of the excavation) and PE 2 (at about 2.2 ft below footing) during static load testing on north, center, and south lanes (10/29/2010)

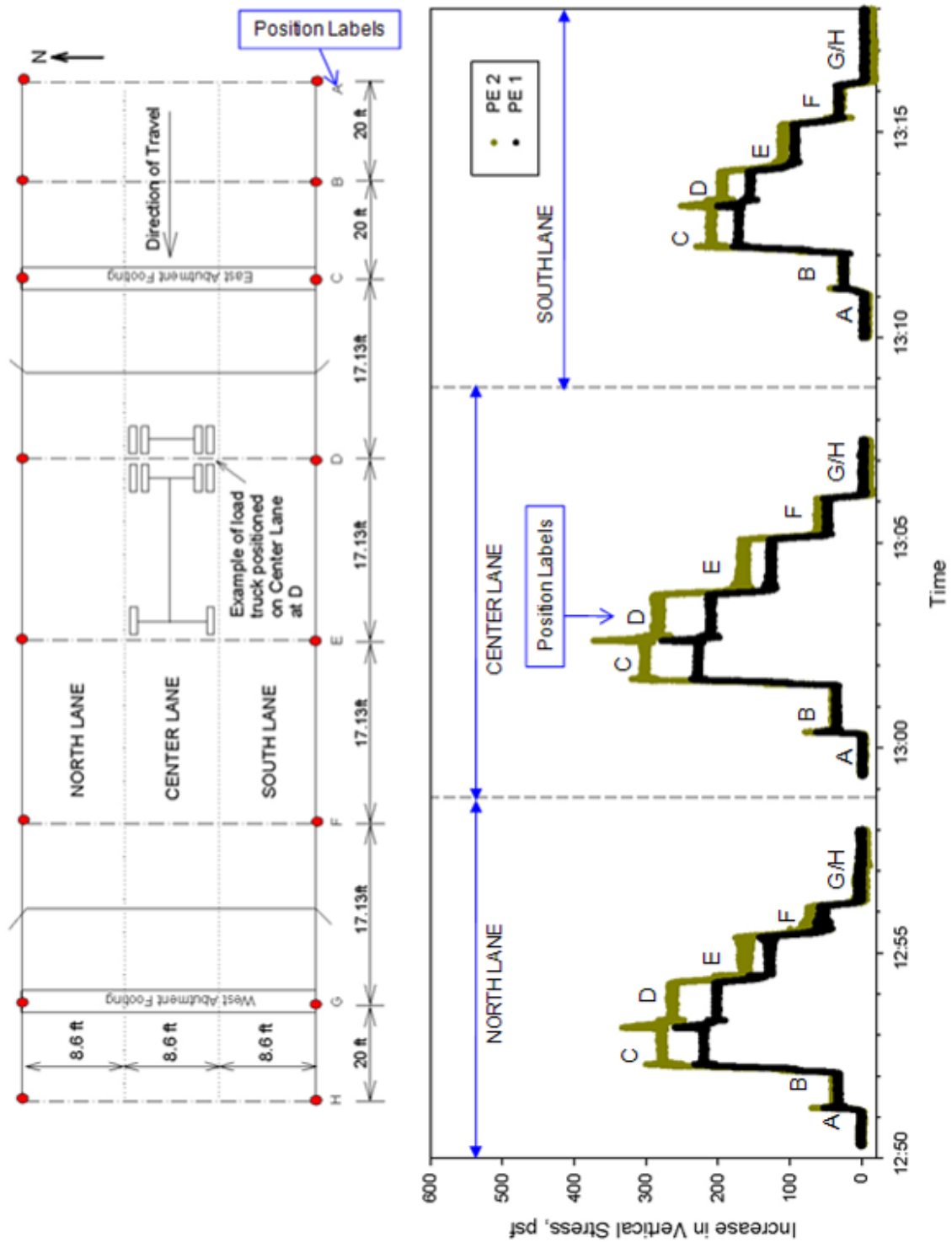


Figure 80. Bridge 2 — Increase in total vertical stresses in PE 1 (at the bottom of the excavation) and PE 2 (at about 2.2 ft below footing) during static load testing on north, center, and south lanes (10/20/2011)

Table 12. Bridge 2 — Comparison of measured and estimated maximum stress increase in GRS fill material due to static live loads

Sensor ID and Location	V or H	10/29/2010 testing		10/20/2011 testing	
		Estimated ¹ (psf)	Measured ² (psf)	Estimated ¹ (psf)	Measured ² (psf)
PE 1 – 3.8 ft below footing base	V	254	250	254	235
PE 2 – 2.2 ft below footing base	V	369	390	369	310
VW 1 – 2.1 ft below footing base (West wall of excavation)	H	76	Not Measured	76	0
VW 2 – 2.1 ft below footing base (East wall of excavation)	H	109		109	29
VW 3 – 1.1 ft below footing base (West wall of excavation)	H	77		77	15
VW 4 – 1.1 ft below footing base (East wall of excavation)	H	179		179	39

V – Vertical; H - Horizontal

¹Estimated assuming influence factors determined from elastic solutions for uniform loading over strip footing (Poulos and Davis 1974)

²Stress measured in EPCs when test truck was placed in position C (directly over the footing)

Increase in vertical stresses in PE 1 and PE 2 EPCs under dynamic LL from test truck traveling at 5 to 40 mph speeds from the 12/10/2010 and 10/29/2011 testing are shown in Figure 82 and Figure 83, respectively. During the 12/10/2010 testing, the test truck was used to apply dynamic loads at 10, 20, 30, and 40 mph driving speeds traveling along the center lane. During the 10/20/2011 testing, the test truck was used to apply dynamic loads at 5, 10, and 20 mph driving speeds traveling along the center, north, and south lanes. A summary of peak vertical stress increase under dynamic loads and a ratio of dynamic to static stresses from the 2010 and 2011 testing is provided in Table 13. The static stress increase values used in the ratio were the maximum measured stress increase values summarized in Table 12. Results showed that the stress ratios varied from about 0.8 to 1.2, with an average of about 1.0, which indicate that there is no significant change in ground stresses between dynamic and static loading.

Also shown in Figure 83 are increase in vertical stresses under a 1000 bushel loaded semi-truck, a Ford F-750 utility truck, and a dual tandem axle loaded grain cart (Figure 84), that passed the bridge during the 10/29/2011 load testing. The increase in vertical stress under loaded semi truck was about 1.3 times higher than the increase in vertical stress under the loaded test truck. The increase in vertical stress under loaded grain cart was about 1.6 times higher than the increase in vertical stress under the loaded test truck.

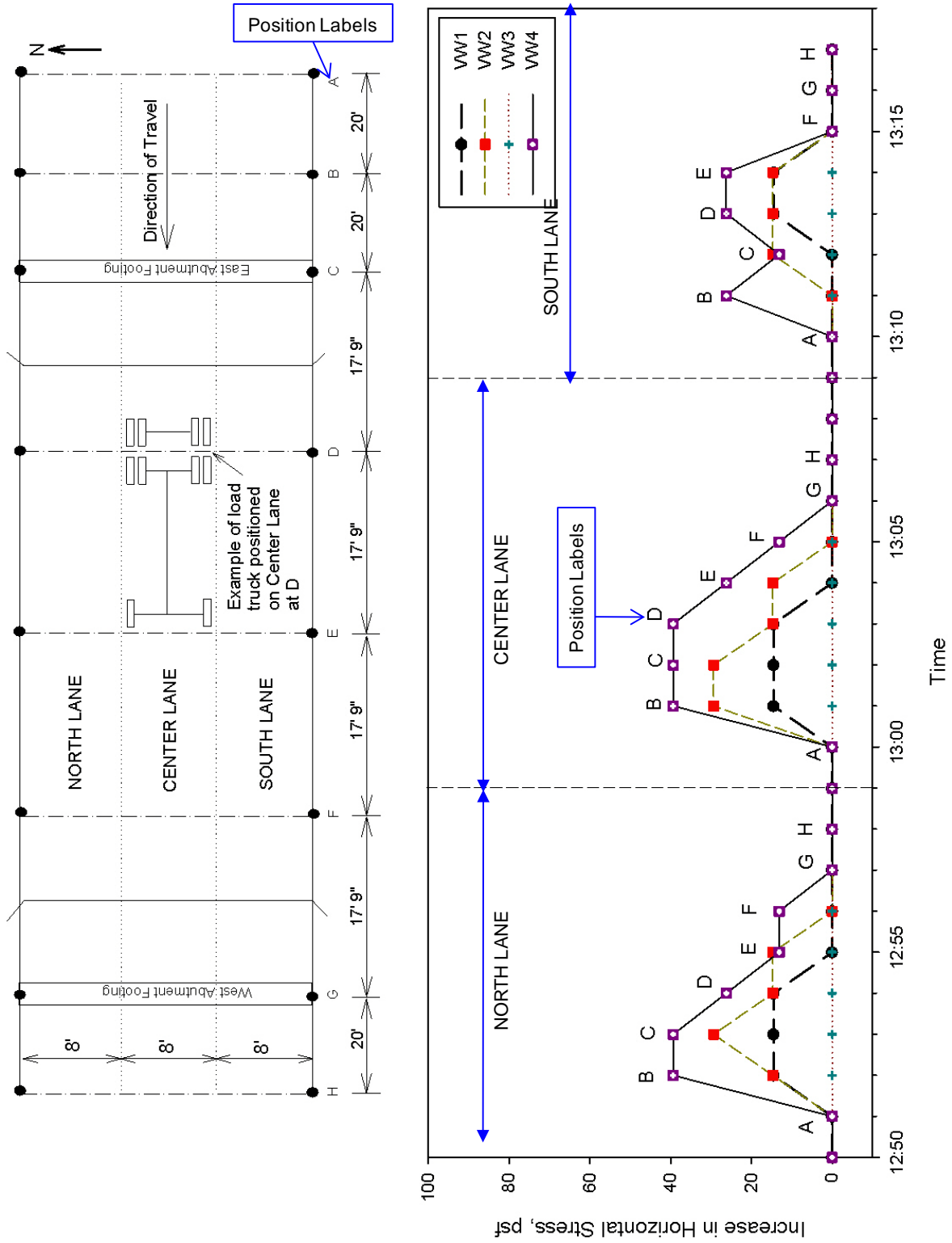


Figure 81. Bridge 2 — Increase in total horizontal stresses against the excavation walls during static load testing on north, center, and south lanes (10/20/2011)

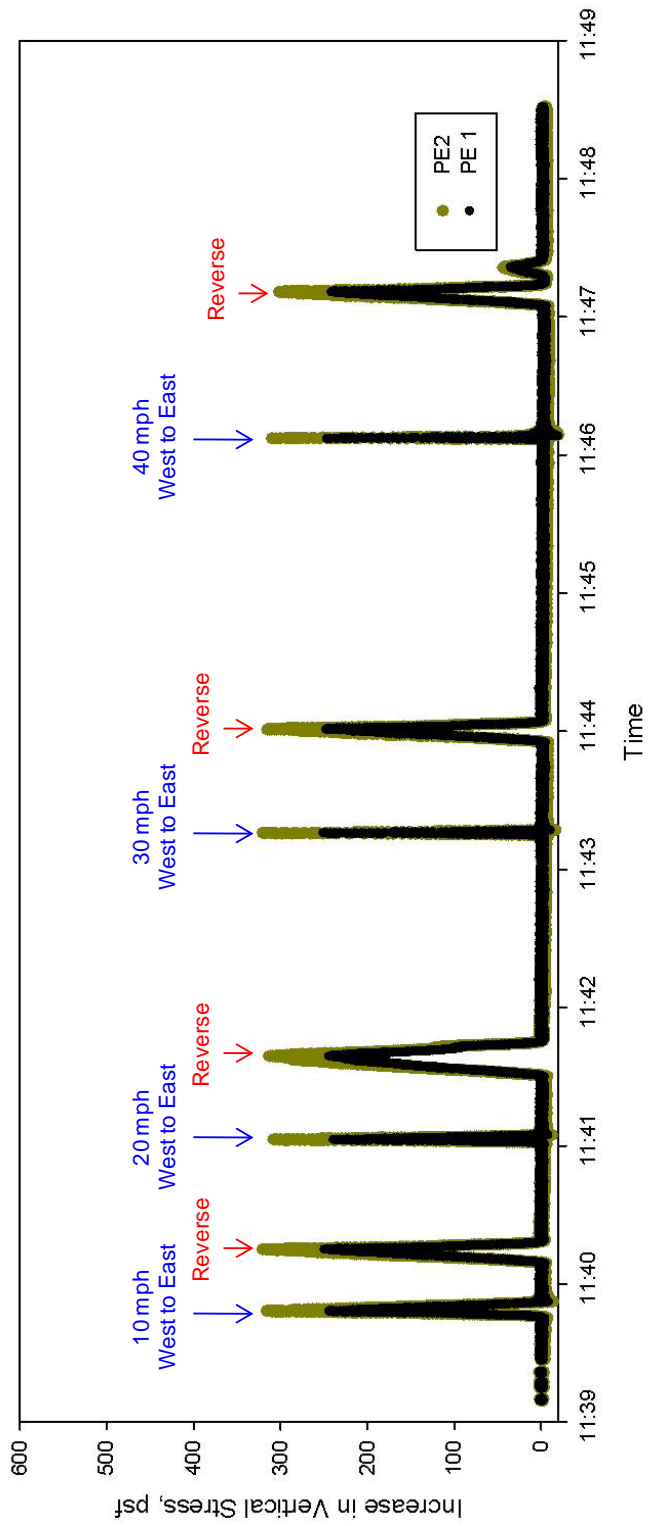


Figure 82. Bridge 2 — Increase in total vertical stresses in PE 1 (at the bottom of the excavation) and PE 2 (at about 2.2 ft below footing) during dynamic loading at 10 to 40 mph on center lane (10/29/2010)

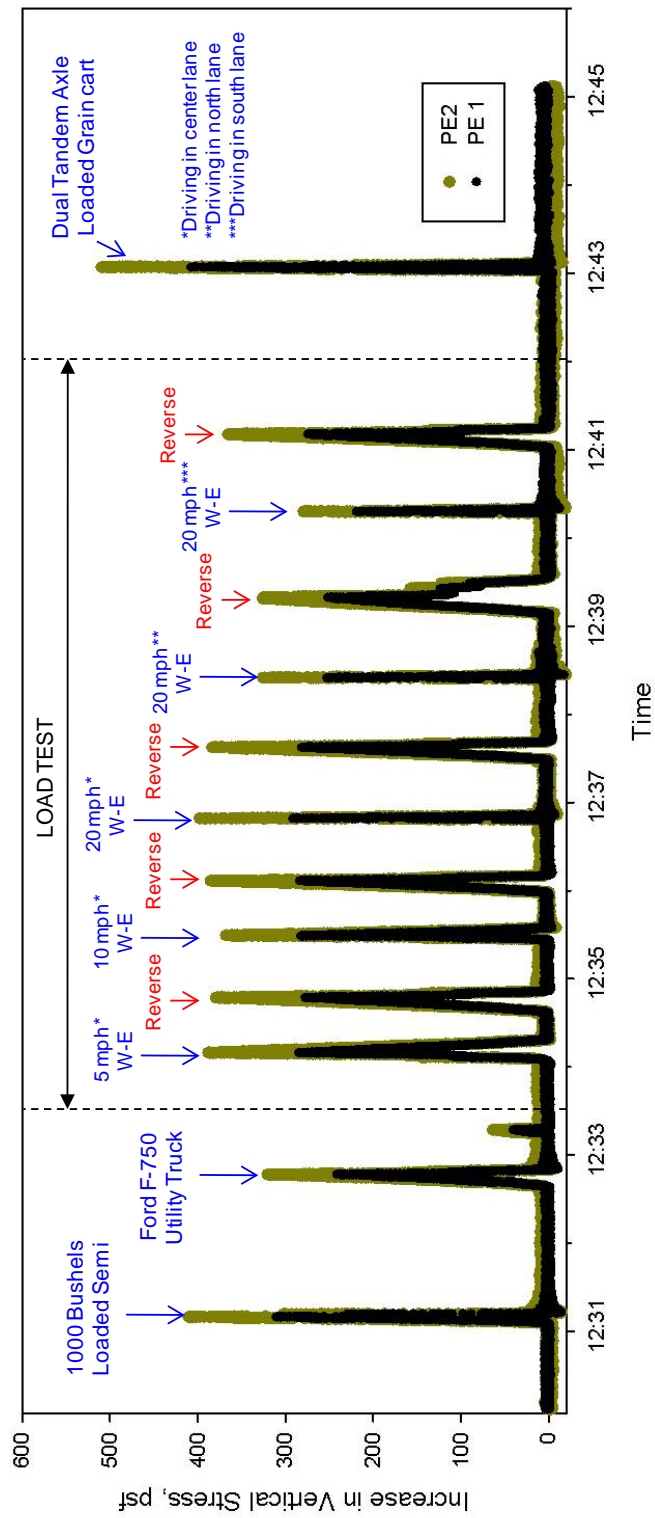


Figure 83. Bridge 2 — Increase in total vertical stresses in PE 1 (at the bottom of the excavation) and PE 2 (at about 2.2 ft below footing) during dynamic loading under husbandry traffic and load test vehicle (10/20/2011)

Table 13. Bridge 2 — Summary of maximum stresses measured in GRS fill material during dynamic loading and dynamic to static stress ratio

Sensor ID and Location	2010 Testing		2011 Testing	
	Dynamic stress (psf)	Dynamic to Static Stress Ratio	Dynamic stress (psf)	Dynamic to Static Stress Ratio
PE 1 – 3.8 ft below footing base				
5 mph (in center lane)	Not measured		279	1.18
10 mph (in center lane)	235	0.94	272	1.16
20 mph (in center lane)	237	0.95	287	1.22
30 mph (in center lane)	251	1.00	Not measured	
40 mph (in center lane)	242	0.97		
PE 2 – 2.2 ft below footing base				
5 mph (in center lane)			375	1.01
10 mph (in center lane)	310	0.79	363	0.98
20 mph (in center lane)	305	0.78	397	1.08
30 mph (in center lane)	317	0.81	Not measured	
40 mph (in center lane)	309	0.79		



Figure 84. Bridge 2 — Dual tandem axle loaded grain cart passed over the bridge during 10/20/2011 load testing

Bearing Capacity Analysis

Three bearing capacity failure modes as illustrated in Figure 85 are evaluated in this study. Failure mode A illustrates failure in the foundation soil layer due to stresses at the bottom of the GRS fill material (Figure 85a). The ultimate bearing capacity of foundation soil for that case was determined using Terzaghi's bearing capacity solution for strip footings as shown in Eq. (11):

$$q_{ult} = c'N_c + qN_q + 0.5\gamma BN_\gamma \quad (11)$$

where, q_{ult} = ultimate bearing capacity, c' = effective cohesion of the foundation soil layer, q = surcharge stress due to existing fill above the excavation base, γ = effective unit weight of the foundation soil, B = width of the excavation, N_c , N_q , and N_γ = Terzaghi's bearing capacity factors determined based on foundation soils ϕ' , ϕ' = effective angle of shearing resistance. According to Adams et al. (2011b), the minimum factor of safety for this condition $FS_{\text{bearing}} = 2.5$.

Failure mode B illustrates failure within the GRS fill material (Figure 85b). The ultimate bearing capacity of the GRS fill material was determined following the analytical approach recommended by Adams et al. (2011b) using Eq. (1) as described in the Background chapter of this report. The ultimate tensile strength $T_f = 1200$ lbs/ft and $\phi'_r = 41.9^\circ$ was used in the calculations. According to Adams et al. (2011b), the minimum factor of safety for this condition $FS_{\text{GRSbearing}} = 3.5$.

Failure mode C illustrates a punching shear failure of the footing through the GRS fill material and a bearing capacity failure in the foundation soil layer (Figure 85c). The ultimate bearing capacity for this case was determined using Meyerhof and Hanna's (1978) solution shown in Eq. (12):

$$q_{ult} = q_b + \frac{2c'_a H}{B} + \gamma_1 H^2 \left(1 + \frac{2D_f}{H} \right) \frac{K_s \tan \phi'_r}{B} - \gamma_1 H \quad (12)$$

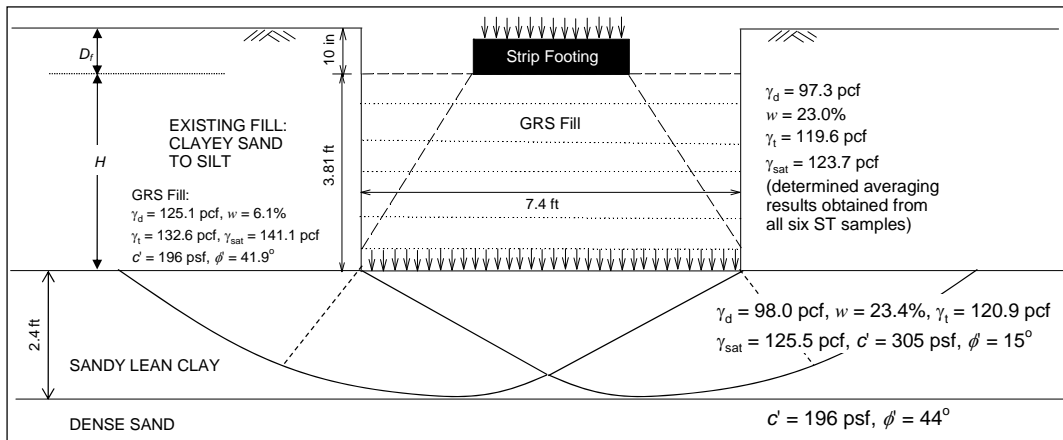
where, q_b = bearing capacity of the underlying foundation soil assuming the footing is placed directly over the foundation soil layer, c'_a = Meyerhof and Hanna's adhesion factor which is a function of the ratio of bearing capacity of the foundation soil and GRS fill material, H = thickness of GRS fill material, γ_1 = effective unit weight of the GRS fill material, D_f = footing embedment depth, K_s = Meyerhof and Hanna's punching shear coefficient which is a function of the ratio of bearing capacity of the foundation soil and GRS fill material and ϕ'_r , ϕ'_r = effective angle of shearing resistance of GRS fill material (with geosynthetic). The K_s and c'_a values were obtained from graphical solutions provided in Das (2004). A modification to Eq. (12) is provided by Sharma et al. (2009) as shown in Eq. (13), to account for the effect of reinforcement in the GRS fill material:

$$q_{ult} = q_b + \frac{2C'_a H}{B} + \gamma_1 H^2 \left(1 + \frac{2D_f}{H} \right) \frac{K_s \tan \phi'}{B} - \gamma_1 H + \frac{2 \sum_{i=1}^n T_i \tan \delta}{B} \quad (13)$$

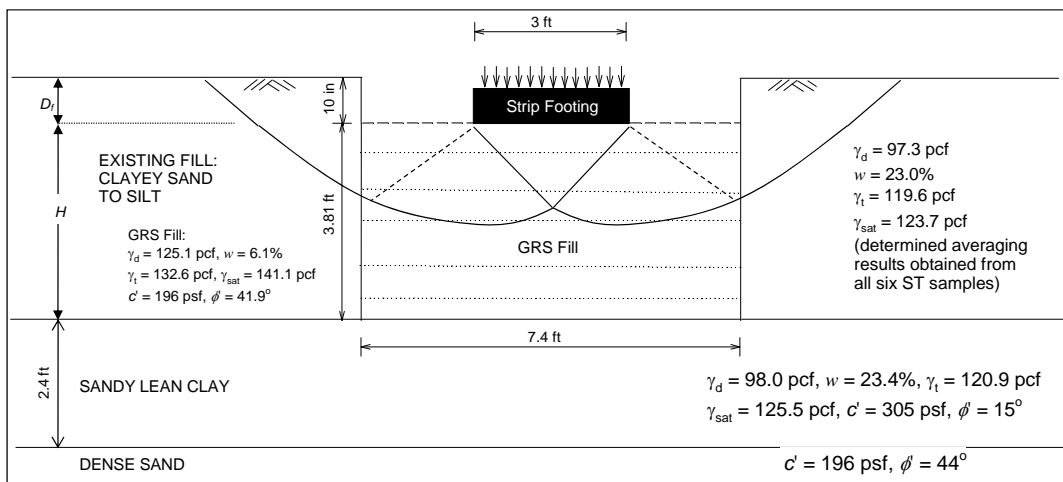
Where, T_i = tensile force in the i_{th} layer of reinforcement and δ = mobilized friction angle along two sides. The T_i and δ values are hard to estimate, so Eq. (13) was not used in the calculations. Nevertheless, the effect of reinforcement in the GRS fill material is accounted for in Eq. (12) by using the effective angle of shearing resistance, ϕ'_r , which was determined from laboratory testing on reinforced granular fill samples. As failure in this condition occurs in the foundation soil, the minimum factor of safety for this condition $FS_{bearing} = 2.5$.

q_{ult} values determined for the three failure models are summarized in Table 14. Calculations were made assuming water table at three different locations: (a) Case I – water table at the bottom of the sandy lean clay layer, (b) Case II – water table at the bottom of the GRS fill material, and (c) Case III – water table at the surface. The applied stress values (q_{app}) for the three cases were determined for three different loading conditions as shown Table 14: DL – dead loads only, DD + LL – dead load plus live loads from test truck and grain cart. The applied stress values measured from EPCs were used in these calculations. Detailed calculations are provided in Appendix B. Factor of safety (FS) was determined as the ratio of q_{ult} and q_{app} . A summary of the FS values for each condition are also provided in Table 14.

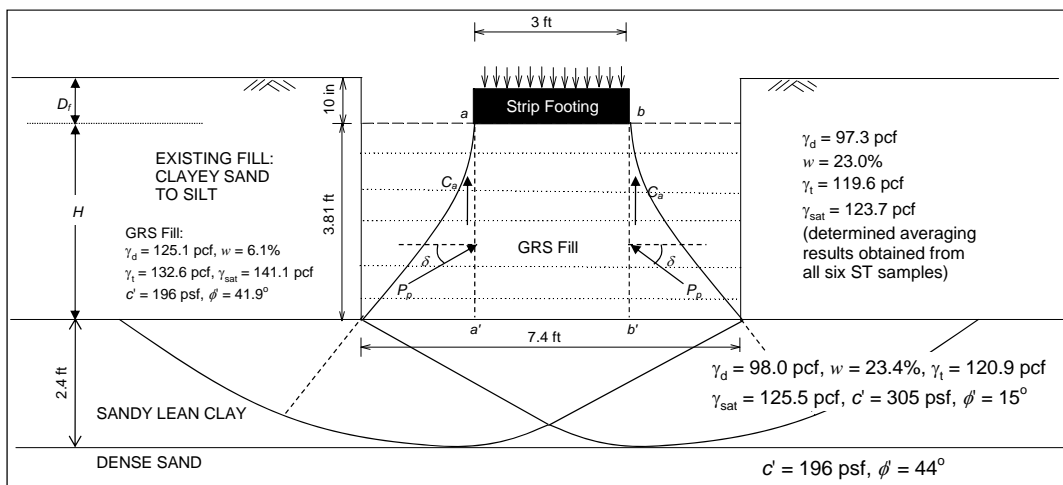
Bearing capacity analysis results summarized in Table 14 indicate that failure mode B (failure within the GRS fill material) showed the lowest FS values and were lower than the minimum recommended value ($FS_{GRSBearing} \geq 3.5$) by Adams et al. (2011b). For failure modes A and C, which are failures in the foundation soils, Case III with water table at the surface of the GRS fill material showed the lowest FS values with values lower than the recommended value ($FS_{Bearing} \geq 2.5$) Adams et al. (2011b) in case of DL+LL.



(a)



(b)



(c)

Figure 85. Bridge 2 — Bearing capacity failure modes: (a) failure in foundation soil due to stresses at the base of GRS fill material, (b) failure within GRS fill material, and (c) punching shear failure through the GRS fill material and bearing capacity failure in the foundation soil

Table 14. Bridge 2 — Summary of bearing capacity analysis results for different failure modes

Loading Condition	Failure Mode A			Failure Mode B			Failure Mode C		
	q_{ult} (psf)	q_{app} (psf)	F.S	q_{ult} (psf)	q_{app} (psf)	F.S	q_{ult} (psf)	q_{app} (psf)	F.S
<i>Case I: Water table at the base of the sandy lean clay layer</i>									
DL	7112	2200	3.2	5603	2120	2.6	9100	2120	4.3
DL + LL ¹		2600	2.7		2760	2.0		2760	3.3
DL + LL ²		2840	2.5		3144	1.8		3144	2.9
<i>Case II: Water table at the base of the GRS fill material</i>									
DL	6939	2200	3.2	5603	2120	2.6	8795	2120	4.1
DL + LL ¹		2600	2.7		2760	2.0		2760	3.2
DL + LL ²		2840	2.4		3144	1.8		3144	2.8
<i>Case III: Water table at the surface</i>									
DL	5759	2200	2.6	5603	2120	2.6	6802	2120	3.2
DL + LL ¹		2600	2.2		2760	2.0		2760	2.5
DL + LL ²		2840	2.0		3144	1.8		3144	2.2

¹From test truck loads; ²From grain cart loads; Highlighted in gray indicates not meeting the FS requirements per Adams et al. (2011b)

Slope Stability Analysis

The global stability of the new bridge abutment structure was assessed using SLOPE/W slope stability analysis software to determine the location and shape of the critical failure slip surface and the associated minimum FS. The stability was analyzed using non-circular failure slip surfaces using Bishop simplified, Janbu simplified, and Morgenstern-Price limit equilibrium analysis methods (Duncan and Wright 2005). The cross-section of the bridge foundation structure with different foundation soil layers and the soil shear strength parameters used in the analysis are shown in Figure 86. Undrained shear strength parameters were used for cohesive foundation layer (lean clay layer) and existing fill layer soils using a $\phi = 0$ model. The sandy foundation soils and GRS fill material are considered “free-draining” and therefore drained shear strength properties were used to model their behavior using Mohr-coulomb model. A footing contact pressure of 2,120 psf was applied to simulate DL surcharge over the GRS fill material. The concrete abutment retaining wall was modeled using an artificially high shear strength value ($\phi = 80^\circ$) so that the failure surface does not pass through the retaining wall. Water table was considered at three locations in the analysis: (1) Case A – water table near the base of the excavation, (2) Case B – water table during flooding, (3) Case C – water table in a rapid draw down condition where the water is rapidly drawn down in the stream and water is still present in the abutment backfill soils. The results of stability analysis with critical failure surface for the three water table conditions are presented in Figure 87. A summary of the FS values associated with each limit equilibrium method are shown in Table 15.

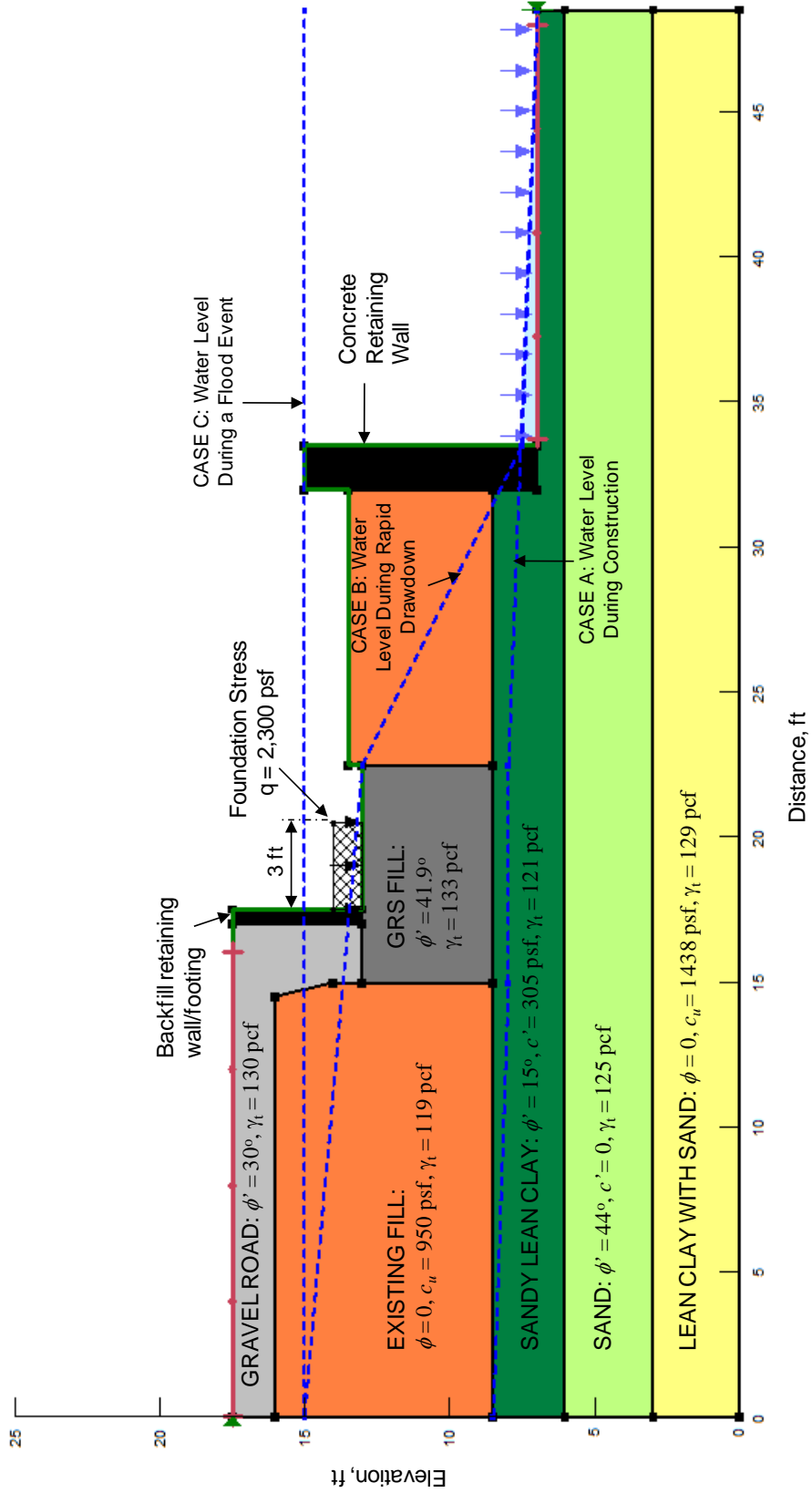


Figure 86. Bridge 2 — Cross-section setup for slope stability analysis

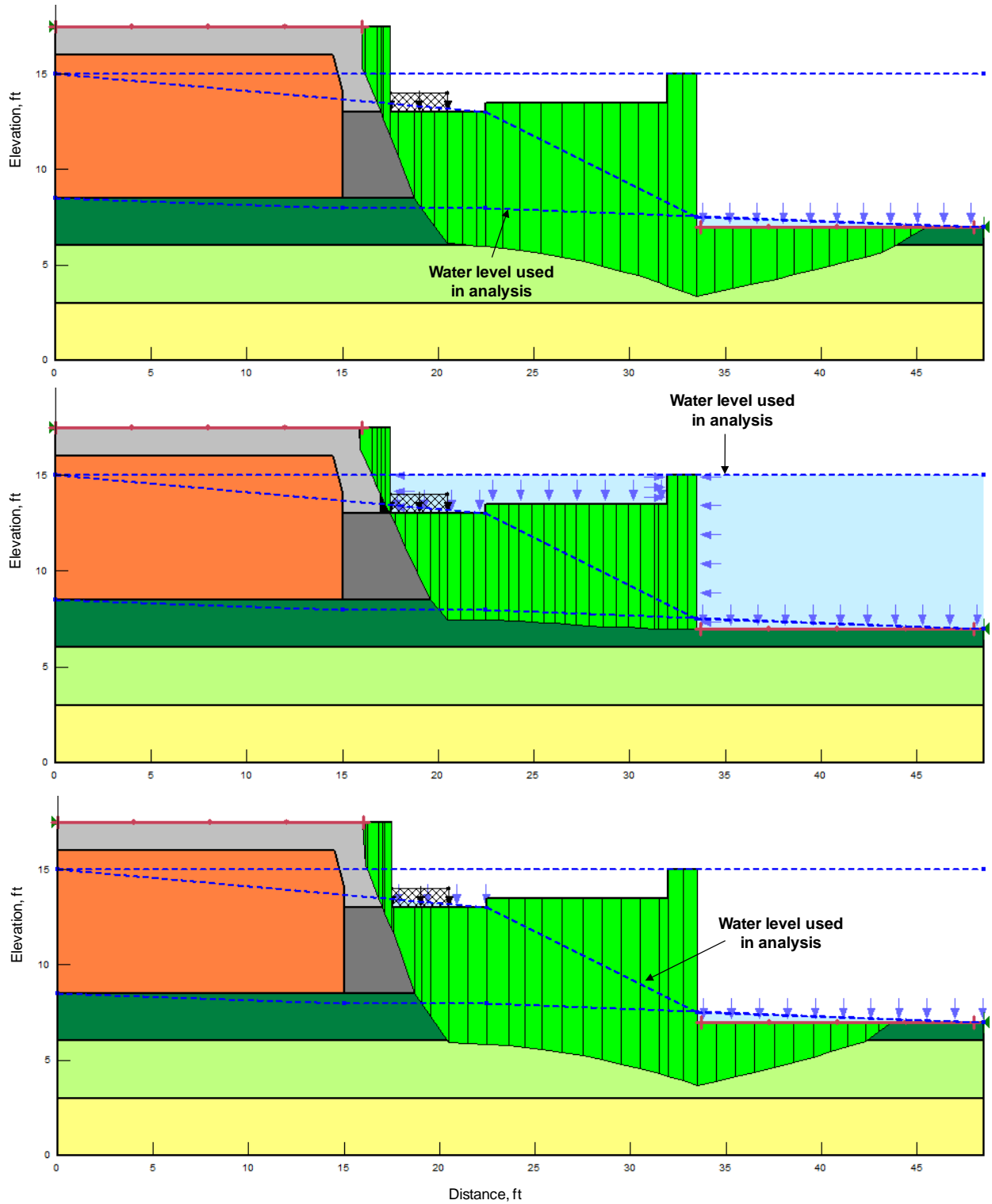


Figure 87. Bridge 2 — Global stability analysis for three different water level conditions

Table 15. Bridge 2 — Summary of FS results from slope stability analysis

Water table condition	Bishop Simplified Method	Janbu Simplified Method	Morgenstern-Price Method
Water table at the base of the excavation as measured during construction	1.60	1.38	1.65
Water table during flooding	1.40	1.24	1.37
Rapid draw down condition	1.34	1.16	1.38

All three limit equilibrium methods showed similar critical failure surfaces with failure occurring due to GRS fill material sliding through the underlying weaker sandy lean clay layer. Janbu modified method showed the lower FS compared to the other two methods. Morgenstern-Price and Bishop modified method showed similar FS values. Rapid draw down cases showed the lowest FS values. The FS values for both rapid draw down and flooding cases were lower than the FHWA minimum recommended $FS_{\text{Stability}}$ (1.5).

Recommendations for Future GRS Bridge Construction Projects

Based on a review of the construction procedures followed on the two demonstration bridge projects, results from in situ testing, analysis of the test results and in ground instrumentation data, the following recommendations are provided for consideration on future projects to help improve the stability and performance of GRS bridge abutment systems:

Selection of Geosynthetic Material

The ultimate reinforcement strength, T_f of the geosynthetic product used in this study was about 1200 lbs/ft, which is lower than the recommended minimum $T_f = 4,800$ lbs/ft. The T_f value plays a critical role in the ultimate bearing capacity of the foundations supported over GRS fill material. The bearing capacity analysis results indicated that the FS of GRS fill material (Failure mode B) ranged from about 1.8 to 2.6 (depending on the loading conditions), which is lower than the recommended minimum $FS_{\text{Bearing}} = 3.5$. Typically, geosynthetic manufacturers provide the T_f values as part of the product technical data sheets (for e.g., see Appendix A). Consideration must also be given to selecting a geosynthetic product that has good infiltration capacity so that the GRS fill material is easily drained during flooding. As an example, Mirafi® HP570 woven geosynthetic or higher grade has $T_f \geq 4,800$ lbs/ft and also has good permeability (30 gal/min/ft²).

Construction Considerations

Bridge 1 construction involved installation of rock fill for erosion protection at the toe of the GRS abutment slopes. The installation of rock fill material at that project site was performed by excavating a trench *after* the fill slopes were constructed. Excavation at the toe of slopes can potentially cause a global stability failure and must be avoided. Any excavations at the toe of the slope must be performed *before* the fill layers are constructed.

Both bridges evaluated in this study did not include a drainage design. Field observations indicated that flood water levels reached nearly up to the bottom of the bridge at Bridge 2 location. As indicated earlier, draining the water entered into the GRS fill materials is critical to the long term performance of these structures as it helps reducing lateral pressures behind abutment walls, erosion of fill materials, and excess pore pressures within the GRS fill material. Perforated drain tiles can be used within the GRS fill at critical areas which includes: behind the wall, base of the wall and locations where a fill slope meets a wall face. Drainage system also helps avoid a rapid draw down condition which was found to be the worst case scenario for global stability on the Bridge 2 abutment.

The slope stability analysis on the Bridge 2 abutment indicated potential failure surfaces at the interface of the GRS fill material and the underlying weaker foundation layer. Obtaining subsurface soil information prior to bridge construction is recommended, so that excavation depths to determine any weak foundation layers can be accurately determined. If soil boring information is not available, at least testing at the bottom of excavation must be conducted to determine if the foundation layers are stable. Such testing may include conducting a dynamic cone penetrometer (DCP) which involves dropping a 17.6 lb pound sliding hammer over an anvil and measuring the penetration depth of the driving rod attached to the anvil. The test procedure is described in ASTM D6951, and the penetration resistance measurements obtained from this test can be empirically correlated to undrained shear strength properties (e.g., White et al. 2009) or California Bearing Ratio (CBR).

KEY FINDINGS, CONCLUSIONS, AND RECOMMENDATIONS

A review of literature on GRS abutment systems along with material specifications, FHWA-recommended design methodology and construction considerations, and results from two field demonstration projects are presented in this report. The two projects included GRS abutment substructures and RRFC bridge superstructures. A woven geosynthetic material was used as the geosynthetic reinforcement in the fill material on both projects. The total construction costs of the two bridges were about \$43k and \$49k. These construction costs were about 50% to 60% lower than the estimated construction costs for building a conventional bridge structure with reinforced concrete abutments, piling, and concrete superstructure. The cost reductions using GRS substructures with RRFC superstructures are realized with the ease in construction, shortened construction time (one abutment per day), and reduced material and labor costs. A summary of project conditions and key findings and conclusions from each project site are provided below.

Bridge 1 – Olympic Avenue, Buchanan County, Iowa

Bridge 1 involved replacing an existing timber back wall abutment with a GRS bridge abutment with flexible wrapped geosynthetic grouted riprap facing to support a 73 ft RRFC bridge on a reinforced concrete spread footing. No instrumentation or testing was performed by the ISU research team on that project. The research team's assessment on project conditions based on review of photos, field visits, and bridge abutment settlement data are as follows:

- Field observations indicated that the grouted riprap installed over the wrapped geosynthetic facing for erosion protection was intact after about one year following construction. Flood waters at the bridge reached about 6 ft below the road elevation which is about the mid height of the GRS abutment.
- GRS abutment construction at this project site included installation of rock fill for erosion protection at the toe of the GRS abutment slopes. The installation of rock fill material at that project site was performed by excavating a trench after the fill slopes were constructed. Excavation at the toe of slopes can contribute to slope instability and must be avoided. Any excavations at the toe of the slope must be performed before the fill layers are constructed, and the excavations must be properly backfilled and compacted.
- Bridge elevation monitoring indicated maximum settlements at the north and south abutments of about 0.7 in. and 0.4 in., with no transverse differential settlement at both abutments at the conclusion of the monitoring phase.
- A drainage design was not included at this site. Drainage is critical to the long term performance of these structures.

Bridge 2 — 250th Street, Buchanan County, Iowa

Bridge 2 involved replacing a 90+ year old steel bridge supported on concrete abutment with a RRFC bridge supported on reinforced concrete spread footings founded on GRS fill material. The new bridge was longer than the old bridge, so taking advantage of the longer span, the

existing concrete bridge abutments along with some existing fill were left in place as GRS facing. The existing soil under the proposed new footing location was excavated and replaced with GRS fill material. Sheet piling was installed on the excavation sides as scour protection for GRS fill material. Soil borings, in situ testing, laboratory testing to characterize the foundation soils and GRS fill material, and instrumentation installation was conducted at this bridge site. The instrumentation included installing inclinometers and piezometers in the ground, and semiconductor and vibrating wire EPCs in the GRS fill material and under the footing. In situ tests involved conducting nuclear density tests and LWD tests on GRS fill materials, bridge LL tests with a loaded test truck monitoring bridge deflections and stresses in the GRS fill material, and bridge abutment settlement monitoring. Laboratory tests were conducted on the GRS fill material to characterize its shear strength properties using direct shear and CD triaxial tests on material with and without geosynthetic reinforcement. In addition, repeated load cyclic triaxial tests were conducted on material with and without geosynthetic reinforcement to evaluate differences in their permanent deformation characteristics. Key findings and conclusions from laboratory testing on GRS fill material, field testing and in ground instrumentation, and analysis of the test results and instrumentation data are as follows:

Laboratory Test Results:

CD triaxial tests on granular material with and without geosynthetic reinforcement indicated higher shear stresses at failure in sample with geosynthetic at all confining pressures (5 to 20 psi). Furthermore, the failure strains for the samples with geosynthetic were higher than the samples without geosynthetic. Tests results indicated the ϕ' increased from 34.4° to 41.9° with geosynthetic reinforcement in the sample. Cyclic triaxial tests were conducted on granular fill material with and without geosynthetic reinforcement with constant confining stress (3 psi) and by increasing cyclic deviator stresses (3 to 40 psi) every 10,000 cycles. Permanent strain was about the same for both samples ($< 0.5\%$) up to 50,000 cycles (with cyclic deviator stress of 20 psi), but was greater in the sample without geosynthetic, when the cyclic deviator stresses were increased to 30 and 40 psi. The permanent strain at the end of the test in the sample with geosynthetic was about 3% and without geosynthetic was about 8%. The reduced permanent strain and improved shear strength properties of the reinforced sample is due to the lateral restraint effect at the soil-geosynthetic interface.

Field Test Results and In-Ground Instrumentation:

NG dry unit weight and moisture content measurements obtained during compaction of GRS fill material indicated that the fill material was compacted to an average density of about 94% of the standard Proctor density, which is slightly lower than the recommended minimum 95% standard Proctor density by Adams et al. (2011b). LWD modulus measurements obtained during compaction of GRS fill material indicated that the modulus increased from about 1690 psi (~12 MPa) in lift 1 to over 7200 psi (50 MPa) on lifts 3, 5, and 6. This indicates that the bottom of the excavation was relatively soft, and the reinforced fill layers aided in bridging the soft underlying foundation layer.

Inclinometer results at a boring located closer (about 1 ft) to the excavation indicated more lateral ground movements than the other one installed about 3 ft away from the excavation. Lateral ground movements monitored during the 1 year monitoring period showed minimal movements.

The estimated DL stress under footing was about 2,120 psf. Vertical stresses measured using EPCs in GRS fill material at about 2.2 ft and 3.8 ft below the footing indicated that the vertical stresses applied under the footing are almost fully transferred down to the bottom of the GRS fill. This is an important observation and must be considered when bearing capacity of the underlying foundation layer is analyzed. The horizontal stresses against the excavation walls were about 600 psf (4 psi) or less. The horizontal to vertical stress ratio was low (< 0.25), thus indicating low lateral stress on the soil surrounding the GRS fill material.

Bridge elevation monitoring since completion of construction to about 1 year after construction indicated an average settlement of about 0.4 in. with a transverse maximum differential settlement of about 0.2 in. The readings indicated that most of the settlement was finished within the first two months after completion of construction.

A maximum deflection of about 0.9 in. was measured during static LL testing. The maximum measured deflection was close to but less than the AASHTO (1996) allowable deflection. However, it must be noted that the AASHTO (1996) allowable limits are based on a HS-20 three axle test truck weighing 72 kips while the test truck used in this study weighed about 52 to 53 kips. Static LL tests indicated non-uniform deflections transversely across the bridge at the center span (with a differential deflection of up to 0.8 in.) when the truck was positioned along the edges. This suggests poor load transfer across the RRFCs.

Peak increase in vertical stresses in the GRS fill material was observed when the test truck was positioned directly above the footing, as expected. Peak increase in horizontal stresses in the excavation at the GRS/existing soil interface was observed when the test truck was positioned either directly above or within 20 ft of the footing. The estimated vertical stress increase under LL using elastic solutions compared well with the measured vertical stress increase values from EPCs. The horizontal stress increase under LL were lower than the estimated values from elastic solutions, as the elastic solutions used do not account for the lateral restraint effect in the reinforced soil layers, which causes a reduction in the horizontal stresses.

EPC results indicated that the ratio of vertical stress increase in the GRS fill due to dynamic (with test truck traveling from 5 to 40 mph) and static loading varied from about 0.8 to 1.2, with an average of about 1.0. The increase in vertical stresses in the GRS fill material under a 1,000 bushel load semi-truck and a loaded grain cart was about 1.3 and 1.6 times higher than the increase in vertical stresses under the loaded test truck, respectively.

Bearing capacity analysis was conducted for three potential failure modes: A – bearing capacity failure within the foundation soil, B – bearing capacity failure within the GRS fill material, and C – punching shear failure through the GRS fill material and bearing capacity failure in the foundation soil. Analysis results indicated lowest factor of safety (FS) values (1.8 to 2.6) for

failure mode B and they were lower than the minimum recommended value ($FS_{GRSBearing} \geq 3.5$) by the FHWA. For failure modes A and C, a case with the water table at the surface of the GRS fill material showed the lowest FS values in case of DL+LL and were lower than the recommended value ($FS_{Bearing} \geq 2.5$) by the FHWA.

The ultimate strength of geosynthetic reinforcement, T_f , plays a critical role in determining the ultimate bearing capacity of the foundations over GRS fill material. The T_f of the geosynthetic product used in this study was about 1,200 lbs/ft, which is lower than the FHWA recommended minimum $T_f = 4,800$ lbs/ft. This resulted in lower FS values than recommended, as indicated above (failure mode B). For future projects, the T_f of geosynthetic reinforcement must be selected to meet the minimum FHWA requirements to improve the FS against bearing capacity failure. Typically, the T_f values are provided by the manufacturer as part of the product technical data sheets. Consideration must also be given to selecting a geosynthetic product that has good infiltration capacity so that the GRS fill material is easily drained during flooding. As an example, according to the manufacturer, Mirafi[®] HP570 woven geosynthetic or higher grade has $T_f \geq 4,800$ lbs/ft and also has good permeability (30 gal/min/ft²).

Global stability analysis was conducted using three water table scenarios: A – water level at the base of the GRS fill material, B – water level during flooding, and C – water levels in a rapid draw down condition. The analysis indicated that the FS values for both rapid draw down and flooding cases (1.2 to 1.4) were lower than the recommended minimum ($FS_{Stability} = 1.5$) by the FHWA. The potential failure surfaces were at the interface of the GRS fill material and the underlying weaker foundation layer. For future projects, obtaining subsurface soil information prior to bridge construction is recommended, so that excavation depths to remove weak foundation layers can be determined prior to construction. If soil boring information is not available, at least testing at the bottom of excavation must be conducted to determine if the foundation layers are stable.

Recommendations for Future Research

GRS bridge abutments were constructed using existing abutment wall and grouted riprap as facing elements in this research study. In situ test results from the two demonstration projects in this study indicated that the bridges performed well within the monitoring phase of the project. Performance of these structures over a long period must be investigated. Long-term performance of GRS abutments with different facing elements (e.g., sheet piles, concrete masonry units, and timber-faced walls), must be evaluated. Future research should also include an experimental study to evaluate the bearing capacity of GRS fill materials with different granular fill materials used commonly in Iowa and geosynthetic materials (woven and non woven) with varying ultimate strengths. The bearing capacity evaluations must include performance test evaluation with full-scale field testing to failure, to determine the ultimate bearing capacities.

REFERENCES

- AASHTO (1996). *AASHTO LRFD Bridge Design Specifications*, Second Edition, Customary US Units. Washington, D.C.
- AASHTO (1999). “Standard method of test for determining the resilient modulus of soils and aggregate materials – AASHTO T307” American Association of State Highway and Transportation Officials (AASHTO), Washington, D.C.
- AASHTO (2010). *LRFD Bridge Design Specifications*, Fifth Edition, American Association of State Highway and Transportation Officials, Washington, DC.
- Adams, M.T., Collin, J.G. (1997). “Large Model Spread Footing Load Tests on Geosynthetic Reinforced Soil Foundations.” *J. of Geotechnical and Geoenvironmental Engineering*, 123(1), 66-72.
- Adams, M.T., Lillis, C.P., Wu, J.T.H., and Ketchart, K. (2002). “Vegas Mini Pier Experiment and Postulate of Zero Volume Change.” *Proceedings, Seventh International Conference on Geosynthetics*, pp. 389–394, Nice, France.
- Adams, M.T., Nicks, J.E., Stabile, T., Wu, J.T.H., Schlatter, W., and Hartmann, J. (2011a). “Geosynthetic Reinforced Soil Integrated Bridge System—Synthesis Report.” Report No. FHWA-HRT-11-027, Federal Highway Administration, McLean, VA.
- Adams, M., Nicks, J., Stabile, T., Wu, J., Schlatter, W., and Hartmann, J. (2011b). “Geosynthetic Reinforced Soil Integrated Bridge System—Interim Implementation Guide.” Report No. FHWA-HRT-11-026, Federal Highway Administration, McLean, VA.
- Adams, M.T., Schlatter, W. and Stabile, T. (2007). “Geosynthetic reinforced soil integrated abutments at the Bowman Road Bridge in Defiance County, Ohio. *In Proceedings of Geo-Denver 2007*, ASCE, Denver.
- Bowles, J.E. (1996). *Foundation Analysis and Design*, 5th Edition, McGraw-Hill Publishers.
- Berg, R., Christopher, B., and Samtani, N. (2009). “Design of Mechanically Stabilized Earth Walls and Reinforced Soil Slopes—Volume 1.” Report No. FHWA-NHI-10-024, National Highway Institute, Federal Highway Administration, Arlington, VA.
- Duncan, J.M., Wright, S.G. (2005). *Shear Strength and Slope Stability*, John Wiley and Sons, Inc., New Jersey.
- Evans, R., White, D.J., Klaiber, W. (2012). “Modified Sheet Pile Abutments for Low Volume Road Bridges.” Iowa DOT Project TR-568, Iowa Department of Transportation, Ames, Iowa, January.
- FHWA. (2008). *National Bridge Inventory: Deficient Bridges by State and Highway System*. Office of Bridge Technology. Federal Highway Administration, U.S. Department of Transportation. <http://www.fhwa.dot.gov/bridge/deficient.cfm>, Accessed June 10, 2010.
- Geokon (2010). Instruction Manual – Models 4800, 4810, 4815, 4820, and 4830 VW Earth Pressure Cells, Geokon, Inc, Lebanon, NH.
- Geokon (2009). Instruction Manual – Model 4500 Series Vibrating Wire Piezometers, Geokon, Inc, Lebanon, NH.

- Geokon (2007). Instruction Manual – Models 3500, 3510, 3515, 3600 Earth Pressure Cells, Geokon, Inc, Lebanon, NH.
- Guido, V. A., Knueppel, J. D., and Sweeny, M. A. (1986). “Plate load tests on geogrid-reinforced earth slabs.” *Proc. of Geosynthetics '87*, IFAI, St. Paul, MN, 216-225.
- Huang, C. C., and Tatsuoka, F. (1990). “Bearing capacity of reinforced horizontal sandy ground.” *Geotextiles and Geomembranes*, Vol. 9, 51-82.
- Klaiber, F. W., Wipf, T.J., Nahra, M.J, Ingersoll, J. S., Sardo, A. G., and X. Qin. (2001). “Field and Laboratory Evaluation of Precast Concrete Bridges”, Final Report, Iowa DOT Project TR-440, Iowa Department of Transportation, Ames, Iowa, November.
- Klaiber, F. W., White, D.J., Wipf, T.J. Phares, B., and Robbins, V. (2004). “Development of Abutment Design Standards for Local Bridge Designs: Volume 1 – Development of Design Methodology, Volume 2 – Design Manual, Volume 3 – Verification of Design Methodology.” Final Report, Iowa DOT TR-486 Project, Iowa Department of Transportation, Ames, Iowa, August.
- Milligan, G. W. E., and Love, J. P. (1984). "Model testing of geogrids under an aggregate layer in soft ground." *Proc., Symp. on Polymer Grid Reinforcement in Civ. Engrg.*, ICI. London, England.
- Omar. M. T., Das, B. M., Puri, V. K., Yen, S. C., and Cook, E. E. (1994). “Bearing capacity of foundations on geogrid-reinforced sand.” *Proc. XI/Int. Conf. on Soil Mech. and Found. Engrg.*, Vol. 3, A. A. Balkema, Rotterdam, The Netherlands, 1279-1282.
- Poulos, H.G., Davis, E.H. (1994). *Elastic Solutions for Soil and Rock Mechanics*, John Wiley and Sons, New York.
- Qian, Y., Han, J., and Pokharel, S.K., and Parsons, R.L. (2011). Stress analysis on triangular aperture geogrid-reinforced bases over weak subgrade under cyclic loading - an experimental study. *Journal of the Transportation Research Board*, No. 2204, *Low-Volume Roads*, Vol. 2, 83-91.
- Sharma, R., Chen, Q., Abu-Farsakh, M., Yoon, S. (2009). “Analytical modeling of geogrid reinforced soil foundation.” *Geotextiles and Geomembranes*, Vol. 27, 63-72.
- Tateyama, M., Murata, O., Watanabe, K., and Tatsuoka, F. (1994). “Geosynthetic-Reinforced Retaining Walls for Bullet Train Yard in Nagoya.” Recent Case Histories of Permanent Geosynthetic- Reinforced Soil Retaining Wall (Tatsuoka and Leshchinsky, editors) A. A. Balkema Publishers, Rotterdam, The Netherlands, pp. 141–150.
- Tatsuoka, F., Uchimura, T., Tateyama, M., and Koseki, J. (1997). “Geosynthetic- Reinforcement Soil Retaining Walls as Important Permanent Structures.” Mechanically Stabilized Backfill (Wu, editor) A. A. Balkema Publishers, Rotterdam, The Netherlands, pp. 3–24.
- Vennapusa, P., and White, D.J. (2009). “Comparison of Light Weight Deflectometer Measurements for Pavement Foundation Materials”. *Geotechnical Testing Journal*, 32(3), pp. 239-251.

- White, D.J., Mekkawy, M., Klaiber, F. W., Wipf, T. J. (2007). “Investigation of Steel-Stringer Bridges: Substructure and Superstructure, Volume II.” Final Report, Iowa DOT Project TR-522, Iowa Department of Transportation, Ames, Iowa, October.
- White, D.J., Vennapusa, P., Gieselman, H., Johanson, L., Siekmeier, J. (2009). “Alternatives to heavy test rolling for cohesive subgrade assessment,” *Eighth Intl. Conf. on the Bearing Capacity of Raods, Railways, and Airfields (BCR2A'09)*, June 29 – July 2, Champaign, Illinois.
- Wipf, T. J., Klaiber, F. W., Prabhakaran, A. (1994). “Evaluation of Bridge Replacement Alternatives for the County Bridge System”, Final Report, Iowa DOT Project HR-365, Iowa Department of Transportation, Ames, Iowa, August.
- Wipf, T. J., Klaiber, F. W., Phares, B. M., Reid, J. R., and Peterson, M. J. (1997). “Investigation of Two Bridge Alternatives for Low Volume Roads: Volume 1: Precast Steel Beam Units, Volume 2: Beam on Slab Bridge, Final Report, Engineering Research Institute, HR-382, Iowa Department of Transportation, Ames, Iowa.
- Wipf, T. J., Klaiber, F. W., Threadgold, T. L. (1999). “Use of Railroad Flat Cars for Low-Volume Road Bridges.” Iowa DOT Project TR-421, Iowa Department of Transportation, Ames, Iowa, August.
- Wipf, T. J., Klaiber, F. W., Witt, J. D., and Doornink, J. D. (2003). “Demonstration Project Using Railroad Flatcars for Low-Volume Bridges”, Iowa DOT Project TR-444, Iowa Department of Transportation, Ames, Iowa, February.
- Wipf, T. J., F. W. Klaiber, Brehm, L. W. and Konda, T. F. (2004). “Investigation of the Modified Beam-in-Slab Bridge System: Volume 1 – Technical Report, Volume 2 – Design Manual, Volume 3 – Design Guide.” Final Report, Iowa DOT Project TR-467, Iowa Department of Transportation, Ames, Iowa, November.
- Wipf, T.J., Klaiber, F.W., Boomsma, H.A., Palmer, K.S., Keierleber, B., Witt, J. (2007a). “Field Testing of Railroad Flatcar Bridges – Volume I: Single Spans, Volume II: Multiple Spans.” Iowa DOT Project TR-498, Iowa Department of Transportation, Ames, Iowa, August.
- Wipf, T. J., Klaiber, F.W., White, D.J., Koskie, J. (2007). “Investigation of Steel-Stringer Bridges: Substructure and Superstructure, Volume I.” Final Report, Iowa DOT Project TR-522, Iowa Department of Transportation, Ames, Iowa, October.
- Wu, J.T.H. (1994). “Design and Construction of Low Cost Retaining Walls: The Next Generation in Technology.” Report No. CTI-UCD-1-94, Colorado Transportation Institute, Denver, CO.
- Wu, J.T., Lee, K., Helwany, S., Ketchart, K. (2006). “Design and construction guidelines for geosynthetic-reinforced soil bridge abutments with a flexible facing”, NCHRP Report 556, Transportation Research board, Washington, D.C.
- Zorn, G. (2003). *Operating manual: Light drop-weight tester ZFG2000*, Zorn Stendal, Germany.

APPENDIX A: MIRAFI® 500X TECHNICAL DATA SHEET

MIRAFI® _____ *TECHNICAL DATA SHEET*

Mirafi® 500X

Mirafi® 500X is composed of high-tenacity polypropylene yarns, which are woven into a stable network such that the yarns retain their relative position. 500X is inert to biological degradation and resistant to naturally encountered chemicals, alkalis, and acids.

Mechanical Properties	Test Method	Unit	Minimum Average Roll Value	
			MD	CD
Wide Width Tensile Strength	ASTM D 4595	kN/m (lbs/in)	17.6 (100)	21.0 (120)
Grab Tensile Strength	ASTM D 4632	kN (lbs)	0.9 (200)	0.9 (200)
Grab Tensile Elongation	ASTM D 4632	%	15	10
Trapezoid Tear Strength	ASTM D 4533	kN (lbs)	0.33 (75)	0.33 (75)
Mullen Burst Strength	ASTM D 3786	kPa (psi)	2756 (400)	
Puncture Strength	ASTM D 4833	kN (lbs)	0.4 (90)	
Percent Open Area	COE-02215-86	%	1	
Apparent Opening Size (AOS)	ASTM D 4751	mm (U.S. Sieve)	0.300 (50)	
Permittivity	ASTM D 4491	sec ⁻¹	0.05	
Flow Rate	ASTM D 4491	l/min/m ² (gal/min/ft ²)	200 (5.0)	
UV Resistance (at 500 hours)	ASTM D 4355	% strength retained	70	

Physical Properties	Test Method	Unit	Typical Value	
Weight	ASTM D 5261	g/m ² (oz/yd ²)	136 (4.0)	
Thickness	ASTM D 5199	mm (mils)	0.51 (20)	
Roll Dimensions (width x length)	--	m (ft)	3.8 x 132 (12.5 x 432)	5.3 x 94.2 (17.5 x 309)
Roll Area	--	m ² (yd ²)	502 (600)	
Estimated Roll Weight	--	kg (lb)	95 (210)	

Disclaimer: MIRAFI® Construction Products assumes no liability for the accuracy or completeness of this information or for the ultimate use by the purchaser. MIRAFI® disclaims any and all express, implied, or statutory standards, warranties or guarantees, including without limitation any implied warranty as to merchantability or fitness for a particular purpose or arising from a course of dealing or usage of trade as to any equipment, materials, or information furnished herewith. This document should not be construed as engineering advice.



CJPS000002
ETQR2

APPENDIX B: VIBRATING WIRE EARTH PRESSURE READINGS FROM UNDER THE FOOTING – BRIDGE 2

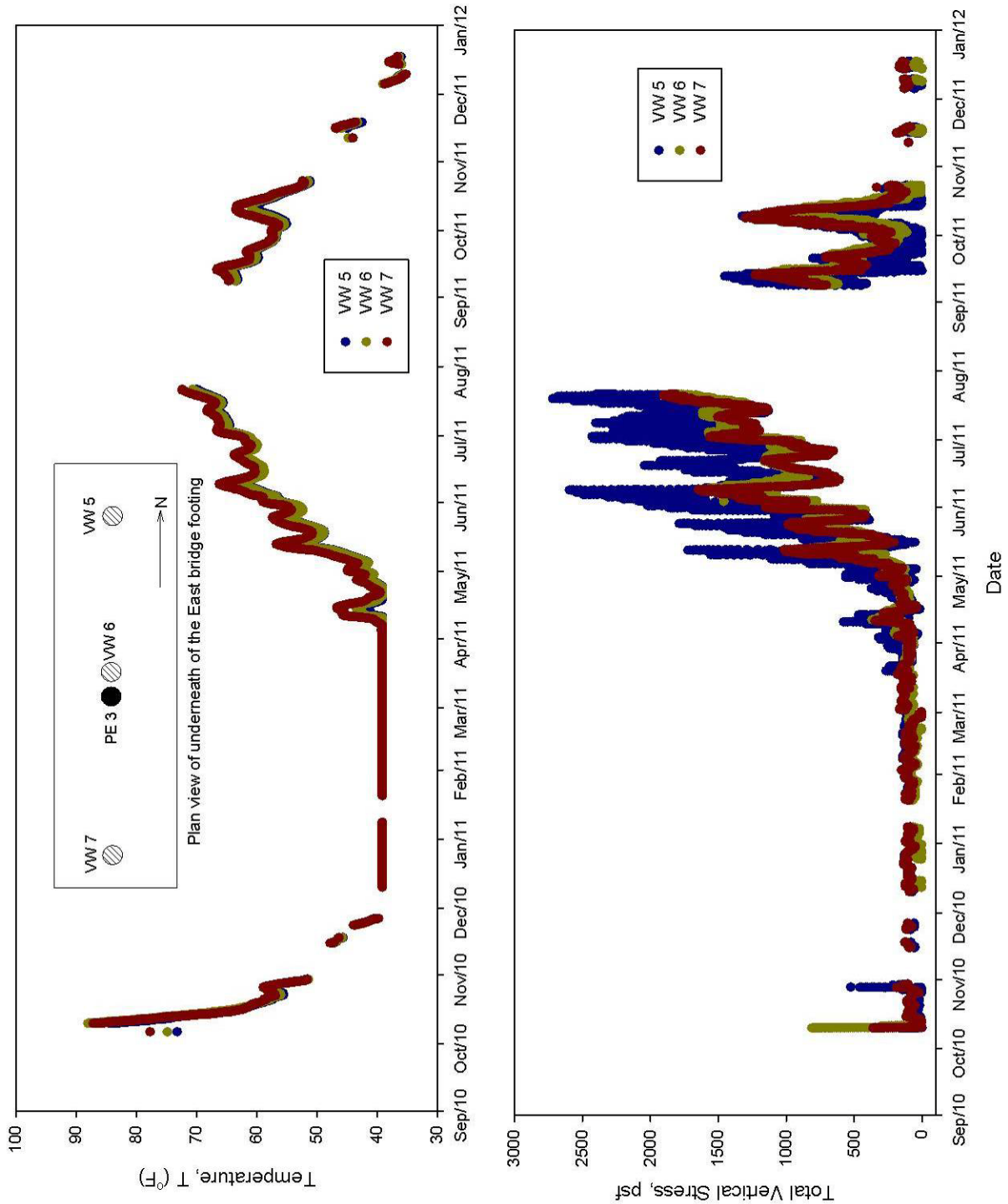


Figure B.1: Bridge 2 — Vertical stresses and temperature readings in vibrating wire EPCs installed under the footing